THREE DIMENSIONAL OSCILLATING FOIL PROPULSION

PENGFEI LIU, B.Eng.

Three Dimensional Oscillating Foil Propulsion

by

©Pengfei Liu, B. Eng.

A thesis submitted to the School of Graduate

Studies in partial fulfillment of the

requirements for the degree of

Master of Engineering

Faculty of Engineering and Applied Science

Memorial University of Newfoundland

March 1991

St. John's Newfoundland Canada

ISBN 0-315-68235-3

Canada

Abstract

An unsteady numerical method, called the quasi-vortex-lattice method (QVLM), to calculate aerodynamic forces on oscillating wings is investigated and applied to the problem of oscillating foil propulsion. It is based on the vortex-lattice-method (VLM). The method was formulated for prediction of aerodynamical characteristics of a non-planar wing with arbitrary shape in unsteady harmonic motion. Based on three dimensional $(3-D)$ unsteady lifting surface theory, the method has been designed to handle irregular wing shapes of both planar and non-planar wings and to work with low aspect ratio foils. A computer program was written for the prediction of propulsion features of a harmonically oscillating hydrofoil. This computer program was checked by comparing present results with existing published results for some given planforms. The computer program is capable of solving unsteady three dimensional, non-planar rigid foil propulsion problems.

Convergence of the QVLM implemented computer program and CPU time are discussed. The advantages and disadvantages of the unsteady QVLM method, and the improvement of the numerical approximation in the integration of the unsteady kernel function were investigated.

Propulsive features of three fast swimming animals were investigated. Three cetacean's flukes were studied by use of calculations of the propulsive efficiency and mean total thrust coefficient. These three fast swimmers were: fin whale (*Balaenoptera physalus*); white-sided dolphin (*Lagenorhynchus acutus*); and white whale (*Delphinapterus leucas*). Fin whale's flukes have the highest aspect ratio (6.1) and moderate sweep angle (31^0); white-sided dolphin's flukes have the highest leading edge sweep angle (47^0) and lowest aspect ratio (2.72); and white whale's flukes have

moderate aspect ratio (3.25) and the lowest sweep angle (28.3^0).

Calculation and comparisons were made for three cases: predictions of propulsive efficiency and thrust coefficient of the planforms of three cetaceans versus an advance ratio, J; the effects of changes in pitching axis positions and in phase angle (pitch leading heave) on those predictions; relations between the leading edge thrust coefficient and mean total thrust coefficient of the flukes.

It was found that fin whale's flukes had the highest propulsive efficiency in all cases, when the heave amplitude h was taken as the corresponding to these flukes' root chord length. The propulsive efficiency from white-sided dolphin's flukes was higher than that from white whale's, though the planform of the white-sided dolphin had a lower aspect ratio. Over the complete range of the phase angle from 0^0 to 360^0, only the fin whale's flukes predicted positive thrust. The flukes of white-sided dolphin and white whale produced negative thrust for phase angle between $190^0 \sim 270^0$ and $140^0 \sim 340^0$ at the reduced frequency $k = 0.75$ respectively; and $175^0 \sim 340^0$ at the reduced frequency $k = 0.15$ only for the flukes of white-side dolphin. When the root chord length was to be taken as reference length and the reduced frequency k was small, it was found that the variations of the efficiency and thrust were small. It was also found that the best propulsive efficiency and smallest thrust coefficient occurred at about same phase angle position, and vice versa. The best propulsive efficiency was found when the pitching axis was placed at 0.6, 0.7, 0.8 root chord position for the flukes of white whale, fin whale and white-sided dolphin respectively.

The recommended shape of man-made oscillating propeller in marine engineering applications was also discussed.

Acknowledgement

First of all, I would like to thank my supervisor Dr. Neil Bose, for suggesting and supporting the research presented in this thesis, and for being an inexhaustible source of ideas and encouragement throughout its duration. It was my pleasure to work under his guidance. Dr. Bose was more than a supervisor, he was a friend. The hospitality and friendship that I enjoyed from him at Memorial University of Newfoundland made my stay in St. John's a truly memorable experience.

I take great pleasure in acknowledging the instructions I received from Professor C. E. Lan, the originator of the method. His patient advice was promptly received from the Department of Aerospace Engineering, the University of Kansas. His valuable suggestions allowed my work to be conducted more efficiently and effectively.

I am grateful to Professor M. R. Haddara, for his strict training in the course in structural dynamics and for encouragement to me during my study at MUN.

Professor R. E. Baddour provided a great deal of encouragement to me during my study at MUN. I regard his course in advanced fluid mechanics as one of the highlights of my graduate studies.

I am grateful to Professor Xiuheng Wu, and Professor Shimo Li at Wuhan University of Water Transportation Engineering, China, for their encouragement during my graduate study in Canada. Their timely recommendations made my study at MUN possible. For these, I am deeply indebted to them.

I thank Dr. Min hu in the Department of Mathematics at MUN for valuable discussions and help with mathematical problems.

I am grateful to the School of Graduate Studies and the Faculty of Engineering and Applied Science for providing me with financial support in the form of a Graduate Student Fellowship, a fellowship supplement and Graduate Assistantship.

Thanks are also due to the staff of Center for Computer Aided Engineering and Professor G. Sabin for their kind help which made the research possible.

Last but not least, I would like to thank my mother Xiuqing Jiang, and my wife Lihua for the encouragement and love that I received from them throughout my graduate studies. Especially, I am indebted to my son Ming for his love, and for putting up with my long hours of work, which towards the end, often seemed to be never-ending.

Contents

List of Figures

List of Tables

Nomenclature

S	$\cdots$	area of the wing
B	$\cdots$	span of the wing
A	$\cdots$	aspect ratio of the wing, $A = B^2/S$
V_∞	$\cdots$	undisturbed velocity
M_∞	$\cdots$	Mach number
B_r	$\cdots$	reference length
k	$\cdots$	reduced frequency, $k = \omega B_r/V_\infty$
h	$\cdots$	heave amplitude
J	$\cdots$	advance ratio, $J = \pi V_\infty/\omega h = \pi B_r/2kh = \theta\pi/\alpha$
θ	$\cdots$	feathering parameter, $\theta = \alpha V_\infty/\omega h$
α	$\cdots$	angular amplitude of pitch
ω	$\cdots$	radian velocity of the oscillation
Φ_{ph}	$\cdots$	phase angle (pitch leading heave)
C_r	$\cdots$	root chord length
x, y, z	$\cdots$	cartesian coordinates moving with the wing
ξ	$\cdots$	coordinate of an elemental doublet in x direction
η	$\cdots$	coordinate of an elemental doublet in y direction
ζ	$\cdots$	coordinate of an elemental doublet in z direction
$\bar{T}$	$\cdots$	mean thrust force of an oscillating foil
$\bar{IP}$	$\cdots$	mean thrust input power
w_z	$\cdots$	downwash
ρ	$\cdots$	density of fluid
$\gamma(x)$	$\cdots$	circulation at x
$\Gamma(x)$	$\cdots$	sectional or total circulation
Φ	$\cdots$	doublet velocity potential
Φ'	$\cdots$	disturbed doublet velocity potential
ΔC_p	$\cdots$	the pressure difference across an elemental doublet on the wing's surface
C_l	$\cdots$	lift coefficient
C_m	$\cdots$	pitching moment coefficient
C_t	$\cdots$	total mean thrust coefficient, $C_t = \bar{T}/[\frac{1}{2}\rho S V_\infty^2]$
C_{tl}	$\cdots$	leading-edge thrust coefficient
η	$\cdots$	propulsive efficiency, $\eta = \bar{T}V_\infty^2/\bar{IP}$
N_c	$\cdots$	number of chordwise control points
N_s	$\cdots$	number of spanwise control points on the half span
N_i	$\cdots$	number of stations of a planform offsets

Chapter 1

Introduction

1.1 The Motive and Origin of Oscillating Propulsion

As a main implement of propulsion of nautical vehicles, the propeller has over a two hundred year history. With the development of the technology, propulsive efficiency has gradually improved. However, the efficiency of many propellers is around fifty to sixty percent and few propellers can achieve an efficiency as high as seventy percent. Since 1974, in which year the first crude oil crisis started, energy prices have become a concern. People have been trying to find ways to retard energy consumption. Improvements in the performance of an ordinary propeller is not a unique solution to this problem any more, because propulsive efficiency will not increase greatly without changing the mode of propulsion. Therefore, the study of flying and swimming in nature has attracted people's attention.

Hydrodynamically, the study of the swimming motion of large aquatic animals is of interest. Newman and Wu (1974) described their interest in fish and cetacean swimming as "Their impressive performance is too difficult for human beings to

emulate, either with our bodies or with our machines, and we can only marvel at the ability of these creatures in the sea to attain high maximum speeds, efficiency of transportation, or special maneuvering capabilities". Theoretically, study of aquatic animal propulsion is divided into two parts: the drag of a streamlined body caused by viscous shear stresses in the thin boundary layer; and the propulsive efficiency and thrust found from ideal potential flow analyses without the effect of the boundary layer. The objective of this thesis is to find the propulsive efficiency and the thrust forces of an oscillating foil of arbitrary planform, which is employed to simulate aquatic animal propulsion as a prelude to the design of man-made oscillating propellers.

1.2 Definition of the Problem

Studies in bio-mechanical engineering (Hertel (1963)) show that fish propulsion is accomplished by body and tail fin "strokes", defined as "active stroke", "natural stroke" and "passive stroke". In the active mode, a fish does work to generate the thrust which is equivalent to the resistance it encounters at its forward velocity. In the natural mode, the surface of the fish body and fin is tangential to the flow, the angle of incidence is zero; no lift is created or thrust force is generated, but a drag force exists. In the passive mode, the tail stroke is driven by a current or wave; energy is transferred to the movements by the flow in such a way that the fish extracts energy and transfers it into thrust. Many fast swimming animals are cetaceans, such as whales and dolphins (Newman and Wu (1974), Bose and Lien

(1989)).

Hertel (1963) studied the propulsive features of whales and dolphins. His results revealed that these animals have a high (side view) and narrow (top view) tail which carries a fin. The height is for providing powerful muscles to power the tail-fin stroke. Measurements of a sei whale are tabulated in table 1.1. The propulsion of swimming mammals was concluded to be made up of three combined oscillations: a vertical stroke with special use of the tail fin; the horizontal sweep (side slip) using the high lateral surface of the tail, and the twisting (rotating) about the longitudinal axis for manoeuvre. The study showed that the vertical fin stroke is active and the coupled up-and-down stroke is accomplished by a twisting oscillation (pitching and heaving) of the fin around a transverse axis and shifted in phase by 90^0 (pitching leads heaving).

	area m^2	lever arm m	moment m^3
flukes	3.3	5.8	19
tail column	4.5	1.9	8.5
top view	7.8		27.5
side view	9.5	2.9	27.5

Table 1.1: A comparison of striking areas and moments of the sei whale,*by H. Hertel (1963)*

Engineering simulation of a tail fin might be done by an oscillating foil, which could be either a rigid or elastic wing. Unsteady two-dimensional theory is well developed for large aspect ratio tail fins (Lighthill (1970)). However, this theory is not appropriate to estimate the hydrodynamics of lower aspect ratio wings and wings with a large sweep angle, such as the lunate tails possessed by most fast

swimming animals, such as whales, dolphins, sailfish and swordfish. Therefore, the objective of this thesis is to simulate cetacean propulsion by employing unsteady 3-D thin wing or lifting-surface theory.

1.3 Proposed Method

Numerical methods in 3-D unsteady thin wing theory are roughly divided into two families: lifting-line theory and lifting-surface theory. Numerical simulations based on lifting-line theory are accurate for larger aspect ratio wings. For low aspect ratio wings, lifting-surface theory is a better choice. Analytical solutions for unsteady lifting surface theory are limited to a few wing shapes such as elliptical,circular and rectangular wings. Solutions for arbitrary wing shapes are obtained by numerical methods. The main numerical methods to solve lifting-surface problems are the vortex-lattice-method (VLM) (DeYong, 1976); the kernel-function method of Multhopp (1950) or some methods based on the kernel-function method such as Davies' (1963); the doublet-lattice method (DLM) developed by Albano and Rodden (1969); quasi-vortex-lattice method (QVLM) developed by Lan (1974 and 1979).

The VLM is common in engineering applications because of its simplicity and accuracy. However, many studies have shown that the VLM is accurate only to get overall loading coefficients (Lan (1974)). Its shortcomings are unrealistic pressure distributions (too high at the trailing-edge and too low at the leading-edge); low predicted distributions of the leading-edge suction; and slow convergence (large mesh number is required for an accurate solution). Hence the VLM is not a good choice for

oscillating propulsion problems where the leading-edge suction force is important.

The kernel-function method, such as Davies' (1965) derivation, is difficult to apply to general configurations and as for the VLM the prediction of the leading edge suction is not reliable. The latter, especially, varies with the number and arrangement of the collocation points in the discretization as evidenced by Lan and Lamar (1977). The DLM can be applied to general configurations (arbitrary shape), but again the predicted unsteady leading-edge suction is not accurate (Lan (1979); Kálmán et al. (1970)). Lan (1974) developed the QVLM based on the VLM and first applied it to predict all aerodynamic characteristics of several planforms in steady flow. The results show that the QVLM was as easy to use as the VLM, but that it could predict the loading coefficients accurately, especially the lift distribution on the leading-edge and hence the leading-edge suction. Further, Lan (1979) extended the steady QVLM to the unsteady case and showed that the method was easily applied to general configurations such as low aspect ratio, swept wings with good accuracy.

In the present work, the QVLM, both for the steady and unsteady cases, is investigated and applied to simulate the propulsion of lunate planform foils (see chapter 4 for details). These foils are used by fast-swimming cetaceans and mammals and could be used for oscillating propellers. Computations were made to verify that the QVLM in its present form was in accordance with that developed by Lan. The program was checked by the calculation of the lift distribution of a circular wing in pure pitching motion. It was then used to predict the propulsive efficiency and thrust coefficient of the $A1$ and $B2$ wings defined in Chopra and Kambe's study (1977) and these results were compared with those found by Chopra and Kambe

(1977). Then the method was applied to compute the propulsion of three species of cetaceans' flukes in terms of their propulsive efficiency and thrust coefficient with respect to changes in pitching axis positions and phase angle values (pitch leading heave).

Chapter 2

Literature Survey

2.1 Unsteady Two-dimensional Aerofoil Propulsion

By the 1920s, the study of two dimensional wing theory was well developed. However, the variable motion of an aerofoil existed in practical applications; in unsteady flow the circulation and aerodynamic characteristics of a moving foil change from instant to instant. In predicting the aerodynamics of a wing in unsteady motion, the theory of unsteady aerodynamics needed to be developed.

The initiation of unsteady thin wing theory may be traced back as far as the 1920s. The pioneers in this field include von Kármán and Burgers (1935), Theodorsen (1935), von Kármán and Sears (1938), Bisplinchoff et al.(1955)). Initially, the problem of an aerofoil in non-uniform motion arose in practical situations such as wing flutter and flying in gusts. In determining the boundary condition for an unsteady aerofoil, the downwash velocity w can be derived from the Navier-Stokes equations with constant density ρ in an ideal flow after neglecting the nonlinear terms (Bis-

plinghoff et al. (1955)), as

$$w_z = \frac{\partial z}{\partial t} + V_\infty \frac{\partial z}{\partial x}. \tag{2.1}$$

Applying Kutta's condition, i.e. finite, continuous velocity and pressure at the trailing edge, Eq. 2.1 can be used to solve Laplace's equation of the local disturbance velocity potential strength on the wing surface

$$\nabla^2 \Phi' = 0, \tag{2.2}$$

to obtain the relation between downwash and circulation. The conditions for the Eq. 2.2 are based on small-disturbance theory. Φ' is defined as the disturbance velocity potential; w_x, w_y and w_z are the disturbance velocities in the three coordinates.

The aerodynamical forces can be found by solving Eq. 2.2. Theodorsen (1935) solved the integration for the two dimensional case analytically. Theodorsen's method was based on Joukowski's conformal transformation and Kutta's hypothesis. Since three dimensional unsteady oscillating foil propulsion is the objective of the present study, of which a detailed formulation is given in Chapter 4, derivation of Theodorsen's theory, the solution to the two dimensional oscillating foil problem, is not given in detail.

Following Theodorsen, Bisplinghoff et al. (1955) proposed a different method to find the downwash w_z in figure 2.1. They considered a chordwise rigid aerofoil with a flap hinged at $x = bc$. In the motion, the aerofoil moved up and down with an amplitude of $h(t)$(heave) and rotated about an axis $x = ba$ through an angular amplitude $\alpha(t)$(pitch); the flap part of the wing flapped with an angular displacement $\beta(t)$ relative to the chordline of the foil. The positive directions were as shown in figure 2.1. Camber effects were neglected because of the assumptions of

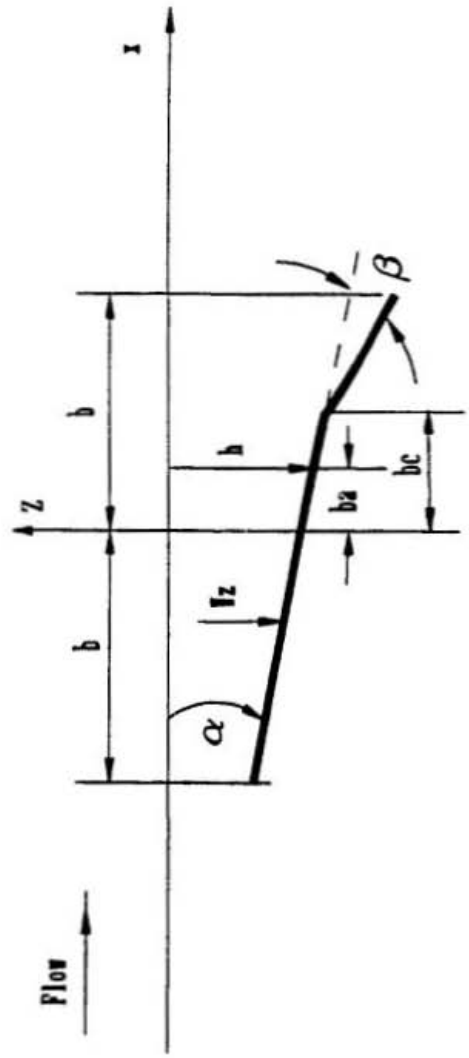

Figure 2.1: A Schematic representation of a 2-D Oscillating Foil with Flap

a thin wing and linear-small amplitude oscillations. In the motion, the foil rotates around its pitching axis and vibrates up-and-down at the same radian speed ω. The equation governing the motion superposes these two motions, therefore the constant initial angle of attack was also omitted. Let $z(x,t)$ be the chordwise instantaneous small displacement which can be described as

$$z(x,t) = \begin{cases} -h - \alpha(x - ba); & \text{for } -b \le x \le bc \\ -h - \alpha(x - ba) - \beta(x - bc); & \text{for } bc \le x \le b. \end{cases} \tag{2.3}$$

Substituting the above equations into Eq. 2.1, $w_z(x,t)$ can be written as

$$w_z(x,t) = \begin{cases} -\dot{h} - V\alpha - \dot{\alpha}(x - ba); & \text{for } -b \le x \le bc \\ -\dot{h} - V\alpha - \dot{\alpha}(x - ba) - V\beta - \dot{\beta}(x - bc); & \text{for } bc \le x \le b, \end{cases} \tag{2.4}$$

where the dot denotes the derivative with respect to time t. From the downwash velocity $w_z(x,t)$, the lift and moment were found in a similar way to that used by Theodorsen (1935).

Probably, the study of Garrick (1936) was the first published proposal for the application of unsteady thin wing theory to oscillating propulsion. With the development of computing technology and numerical methods, numerical modelling of the oscillating wing problem has been possible since the early 1950s. Several papers were published in this period (see the last section of this chapter). Bio-mechanical engineering studies on swimming propulsion were started in the 1960s, such as those of Bainbrige (1958), Brett (1964), and Lighthill (1969). Wu (1971) proposed a 2-D flexible plate propulsion at variable speed in an inviscid fluid. In his study, Fourier synthesis was used to obtain linear effects such as pressure, lift and moment, and therefore of the thrust, kinetic energy and input power. The Fourier synthesis can

be presented by two functions:

$$g(x,t) = Re[\sum_n g_n(x)e^{i\omega_n t}], \tag{2.5}$$

$$f(x,t) = Re[\sum_n f_n(x)e^{i\omega_n t}], \tag{2.6}$$

where Re denotes the real part, the time average of gf is

$$\overline{gf} \equiv \lim_{T\to\infty} \frac{1}{T}\int_0^T g(x,t)f(x,t)dt = \frac{1}{2}Re[\sum_n g_n(x)\bar{f}_n(x,t)], \tag{2.7}$$

where Re denotes the real part and $\bar{f}_n$ is the complex conjugate of f.

Lighthill (1969 and 1970) studied the hydromechanical efficiency of aquatic animal propulsion. These studies were conducted by use of 2-D analysis. Again, Lighthill (1970) analysed the swimming propulsion of the carangiform mode of fish swimming, or lunate-tail propulsion. In carangiform swimming most of the animal's locomotion is created by its tail rather than its body; most of these oscillating tails are lunate-shaped. In Lighthill's (1970) 2-D formulation, the propulsive efficiency and thrust coefficient of an oscillating foil with infinite span was computed for different pitching axis positions; this led to the conclusion that the pitching axis of an oscillating foil should be set near to the trailing-edge for both the best thrust and efficiency considerations.

Some numerical methods on oscillating propulsion were published in the 1970s, including those of Chopra (1974), Chopra and Kambe (1977), and Lan (1979). The efficiency and thrust computation for an actual swimming animal's tail was described by Bose and Lien (1989). They measured the fluke's geometry of an immature fin whale, proposed a finite-span correction based on the results from Chopra and Kambe's (1977) calculations, and then used the correction method to find the propulsive efficiency and thrust coefficient of the flukes of the fin whale.

Practically, the use of two dimensional unsteady theory in predicting the propulsion of a 3-D oscillating foil with low aspect ratio is limited to a qualitative analysis. In order to predict realistic thrust coefficient and propulsive efficiency of a low aspect ratio, irregular shaped hydrofoil with perhaps large sweep angle, the use of 3-D unsteady thin wing theory is necessary.

2.2 Steady 3-D Thin Wing Aerodynamics

Flow past a finite span aerofoil is different from that of an infinite span wing. In the establishment of 3-D thin wing theory, a vortex system is assumed to model the thin wing. This is called the Lanchester-Prandtl theory and it was established by Lanchester and subsequently developed by Prandtl in the early part of this century (see von Kármán and Burgers (1935) and Houghton and Brock (1960)). This theory is perhaps a milestone in the history of aeronautical science. The establishment of the Lanchester-Prandtl vortex theory made the prediction of the aerodynamic characteristics of a wing of arbitrary planform possible.

In Lanchester's vortex theory, a system of vortices replaces the lifting foil. The vortex system is divided into three parts: the bound vortex (parallel to the span direction and bound to the wing), the starting vortex (left at the position of the wing when the motion started), and the trailing vortices (these trail behind the foil and connect the bound vortex to the starting vortex, in steady flow they effectively trail downstream to infinity). The bound vortex and trailing vortex systems form a complete vortex ring called a horseshoe vortex (shown in figure 2.2 a).

For a finite span wing, the magnitude of circulation at midspan is maximum and at the tips is zero. Hence the spanwise circulation distribution for a 3-D wing is

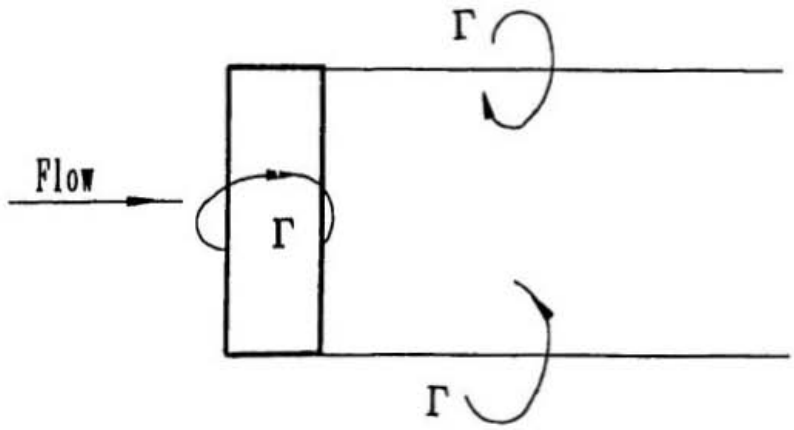

a.

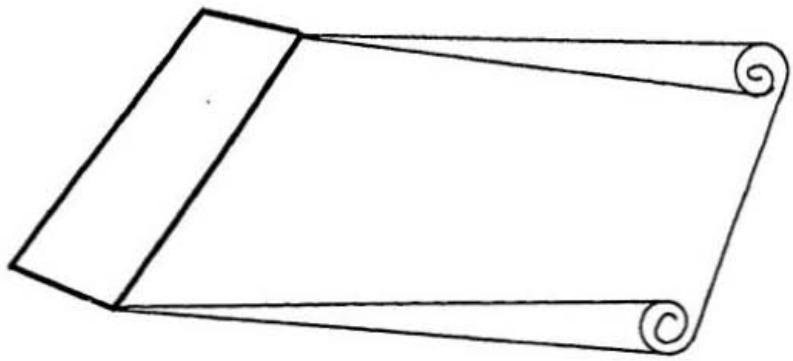

b.

Figure 2.2: a. The horseshoe vortex formation. b. Vortex distortion into vortex sheet

not constant. Therefore, between any sections, the circulation Γ_i and Γ_{i+1}, have a difference of strength of $\Gamma_i - \Gamma_{i+1}$. As the circulation changes along the span, a trailing vortex sheet is formed and extends downstream from the foil. Meanwhile, the sheet will roll up at a certain distance downstream. A trailing vortex sheet and its distortion of a steady foil is shown in figure 2.2 b.

A law that relates the intensity of magnetic field generated by a conductor through which an electric current flows, was introduced to aerodynamics to determine the downwash due to a vortex filament. The law is called the Biot-Savart law. From figure 2.3, it is noted that the induced velocity at point P due to the vortex element of length δs and with strength Γ is

$$\delta v = \frac{\Gamma}{4\pi r^2} \sin\theta \delta s, \tag{2.8}$$

where δv is normal to the plane APB. Taking the limits of the integration as

$$\begin{aligned} \Phi_A &= -(\frac{\pi}{2} - \alpha) \\ \Phi_B &= (\frac{\pi}{2} - \beta), \end{aligned} \tag{2.9}$$

the induced velocity v at P by vortex AB becomes

$$\begin{aligned} v &= \int_{(\frac{\pi}{2}-\alpha}^{(\frac{\pi}{2}-\beta} \frac{\Gamma}{4\pi h} \cos(\Phi) d\Phi \\ &= \frac{\Gamma}{4\pi h}[\sin(\frac{\pi}{2} - \beta) + sin(\frac{\pi}{2} - \alpha)] \\ &= \frac{\Gamma}{4\pi h}[\cos(\alpha) + \cos(\beta)], \end{aligned} \tag{2.10}$$

as described by Houghton and Brock (1960).

Solutions to the 3-D steady aerodynamics of an aerofoil vary with the vortex filament arrangement chosen to represent the wing. A rectangular wing replaced by

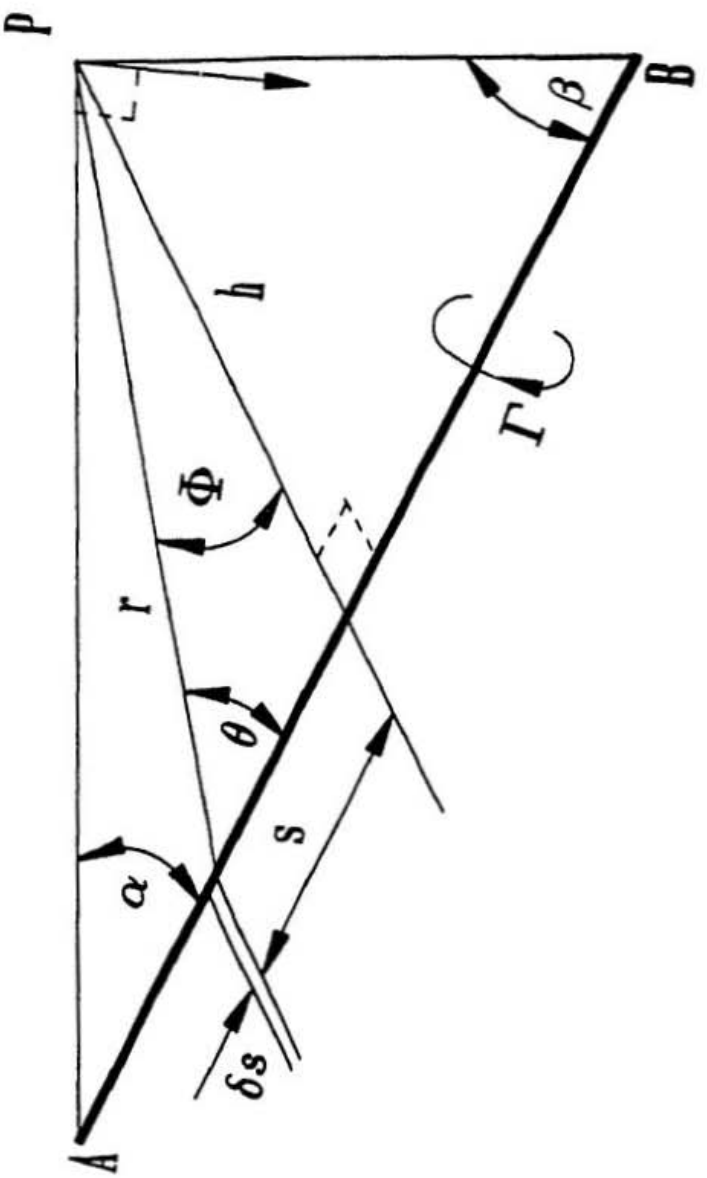

Figure 2.3: Induced velocity by an element vortex filament, Biot-Savart law

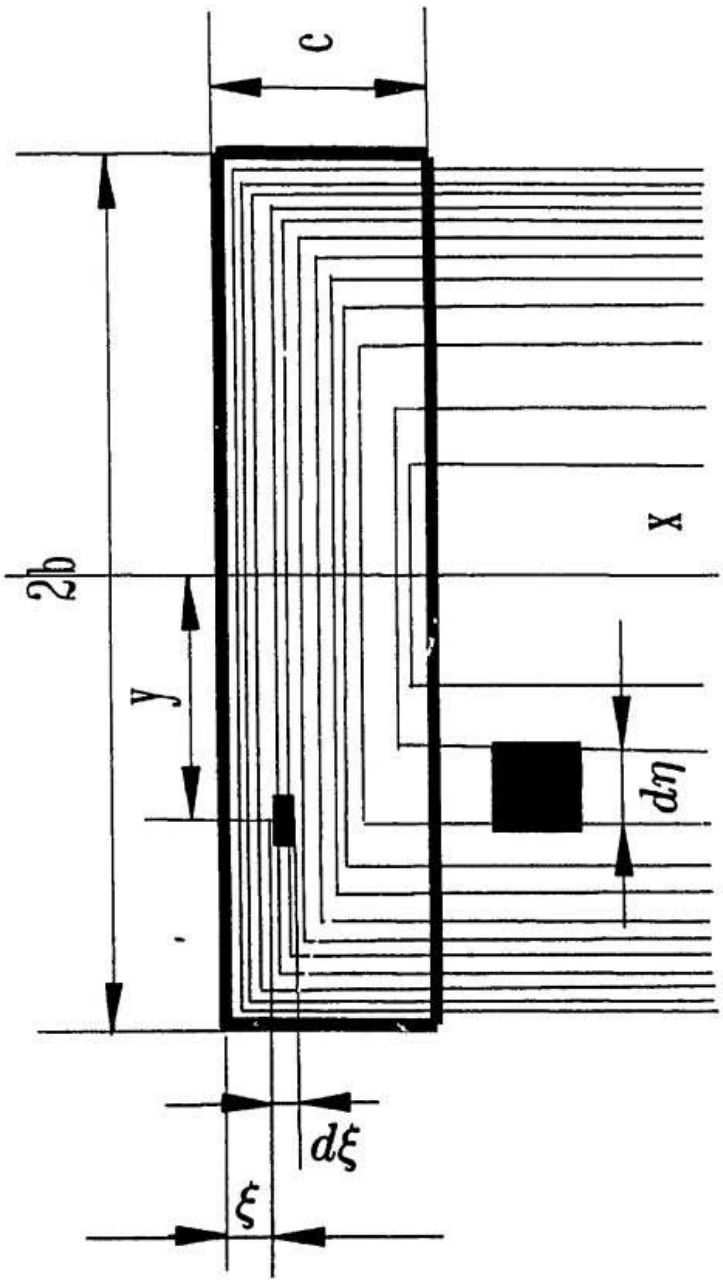

Figure 2.4: Lifting line approach of a vortex system replaces a rectangular wing

lifting lines is shown in figure 2.4 after von Kármán and Burgers (1935). The lifting line theory assumes that the dimensions of chord c are small compared with the span $B = 2b$. Therefore, in calculation, one or a number of vortex lines will replace the airfoil. The downwash w_z at (x, y) by all vortices on the wing is defined as

$$w_z = \frac{1}{\rho V_\infty}\left[\int_{-b}^{+b} \frac{\frac{dl_s}{d\eta}}{4\pi(y-\eta)} d\eta + \int_0^c \frac{\Gamma^*}{2\pi(x-\xi)} d\xi\right], \tag{2.11}$$

where Γ^* is the circulation or the force per unit area, because the pressure difference Δp on the wing surface per unit area has a relation of $\Delta p = 2\Gamma^*$ (see Lan 1974). l_s is the spanwise sectional lift, and ξ and η are dummy variables of x and y respectively.

A lifting surface arrangement is shown in figure 2.5 also after von Kármán and Burgers (1935). Figure 2.5 shows one of a number of lifting surfaces that replace the foil planform. For small aspect ratio wings, the downwash velocity at any point (x, y) on the wing is contributed by the points in the boxes on the wing in the form

$$w_z = \frac{1}{\rho V_\infty} \int\int \Gamma^* \frac{z^2 r - [(r-x-\xi)[(x-\xi)^2 + (y-\eta)^2]}{4\pi r^3 (r-x-\xi)^2} d\xi d\eta, \tag{2.12}$$

where Γ^* is also the force per unit span; z is the doublet position in z direction; $r = \sqrt{x^2 + y^2 + z^2}$, the distance of the doublet to the origin; (ξ, η), doublet location; and ρ and V_∞ are the fluid density and undisturbed velocity respectively.

The analytical solutions for the equations based on lifting line theory and lifting surface theory are limited to special cases such as elliptical and circular wings, and these exact solution only available in the case that an orthorganal coordinate system was placed on a foil (Küessener (1953), Harry, et al. (1957)). For arbitrary wing configurations, the aerodynamic loads have to be obtained by numerical methods.

In 1925, Blenk (von Kármán and Burgers (1935)) proposed a theory based on lifting surface theory which was applied to a rectangular foil of respect ratio 6

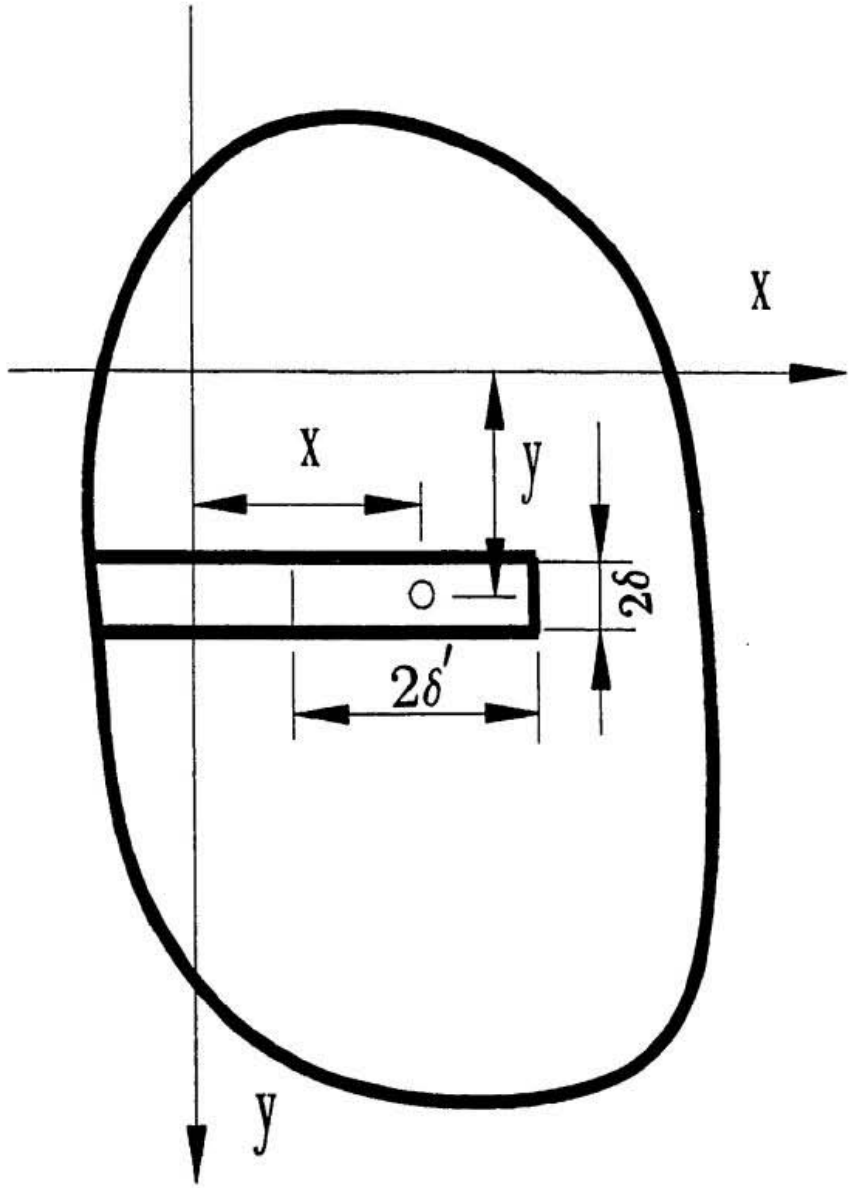

Figure 2.5: An irregular shaped planform replaced by lifting surfaces

and the system of equations was solved analytically. His later studies also concentrated on parallelogram wings and swept wings, but the values were not reliable. Falkner (1943) summarized Prandtl, Betz, Munk and others (1918-1919) spanwise continuous loading methods, and in the aerodynamic computation, he chose the one-quarter chord point as the loading point and three-quarter chord point as the downwash point. This was called the $1/4 - 3/4$ rule, a concept which was put forward by Pistolesi in 1937 (Deyong (1976)). Falkner (1943) was probably the first to use the term vortex-lattice theory to describe a method to treat wings of arbitrary shapes. Later in 1947 (Deyong (1976)), he conducted an intensive study on the vortex-lattice method to determine its accuracy; its use in the treatment of delta wings; the loading of pointed tips and determination of the slope of the loading curves.

The vortex-lattice-method (VLM) has been used extensively for aerodynamic computations. A variety of researchers have improved the VLM in terms of lattice arrangements, wing geometries and better mathematical modeling of the flow. There are also some new methods developed based on the VLM, such as the doublet-lattice-method (DLM) and the quasi-vortex-lattice-method (QVLM) as mentioned in the introduction in the foregoing chapter.

2.3 Unsteady 3-D Lifting Surface and Propulsion Problems

The study of wings with finite span in unsteady motion was started in the late 1930s. A variety of proposals were put forward in this period. The studies of Jones (1940) were based on an 'operational' method to predict the lift of a 3-D wing undergoing

a change in angle of attack; a sharp edged gust and a continuous oscillation. The operational method provides correction factors for the aerodynamic inertia and the angle of attack of an aerofoil with infinite span in order to obtain the results for a finite span aerofoil.

A study by Dengler and Goland (1952) obtained the lift distribution for an oscillating rectangular wing with aspect ratio 5. However, this lift distribution was found for only pure pitching or pure heaving motions, instead of for the combined motion. Hence it is not applicable to propulsion problems. Moreover, the lifting line techniques used in their method are limited to large aspect ratio aerofoils. An analytically based method by Küessner (1953) attempted to solve lifting problems involving arbitrary geometry and downwash distribution. The lifting surface in this method had to be defined as a number of orthogonal surfaces on orthogonal coordinates. This definition is not good for a tapered wing, also the orthogonal coordinates made the computation complicated. To obtain a solution by this method, a numerical method had to be applied. In this study, there was no discussion of the accuracy of the method nor were there any comparisons with previous results.

Meanwhile, a numerical method to solve the aerodynamical problems of oscillating low aspect ratio wings was proposed by Lawrence and Gerber (1952). The studied geometries were rectangular and triangular wings. Based on lifting surface theory, the integral equation of downwash was approximated as a single-variable integral equation. The results were believed reliable, but these results were good only when the trailing-edge of the wings were straight and the aspect ratios less than 4. A similar method was also developed by Merbt and Landahl (1953). In this method, the wings were defined to have very low aspect ratios, 0.5 or 1.0. The

x-derivatives (referred to the chordwise direction) were neglected in the linearized potential equation which thus led to the 2-D wave equation. The flow was assumed 2-D in cross-sections perpendicular to the free stream direction. The solution involved the use of Mathieu functions. The method is only suitable for application to very low aspect ratio wings. A summary of many of these methods has been given by Bisplinghoff et al.(1955).

Falkner's (1943) concept of lifting-surface theory, the initial form of the VLM, and Multhopp's (1950) kernel function method made great contributions to computational aerodynamics. Many authors extended Multhopp's kernel function method to the unsteady case. Among others, Richardson (1955) derived an integral equation in terms of the velocity potential (and hence the downwash) and lift by using the doublet method. One part of this integral equation was called the unsteady kernel K. In solving the equation, both the loading function (under the integral sign) and the downwash were expressed as a finite series as Multhopp had done before. Richardson's method was able to deal with wings of any planform in both unsteady subsonic and supersonic cases.

A mathematical study of the kernel function was made by Watkins, et al. (1955). The scheme they applied to treat $y_0 = y - \eta = 0$ (where η is the doublet position in the y direction and y is the downwash position in the y direction), in which situation the kernel function becomes singular, was to utilize polar coordinates and the expansion of infinite series. In this method, the forms of the kernel function under the integral sign were given in the sonic case, steady case and incompressible case respectively. Also the first four terms of an infinite series were chosen to represent the kernel function $K(x_0, y_0)$ and it was believed that the error of the results was within

two percent. Runyan and Woolston (1957), Watkins, et al.(1959), Davies (1963) also studied the use of the kernel function. Most of these authors used and revised Multhopp's kernel function theory. In Multhopp's derivation of the solution to the kernel function, he compromised the accuracy and the labour of the calculation, because at that time all the calculations had to be done by hand. Therefore the results were not good in accuracy. In the past two decades, equipped with higher speed computers, many authors have revised Multhopp's procedure to search for highly accurate solutions.

A formulation of the kernel function in the non-planar case was done by Yates (1966), and then by Landahl (1966). Landahl's derivation gave a simple form. However, the kernel function could not be expressed in terms of known functions and it needed to be evaluated numerically.

The solution to the kernel function is one of the most difficult problems in 3-D oscillating lifting surface theory. The treatments for its solution are divided into two parts: first, utilizing mathematical manipulation to separate the integral and expanding the downwash function and loading function into series; second, searching for an optimized control surface arrangement to reduce the singularities. The authors involved in this study include Watkins, et al.(1955), Richardson (1955), Hsu (1957), Davies (1963), Ashley (1968), and Albano and Rodden (1969).

There are many numerical methods available to solve unsteady 3-D lifting surface problems. Perhaps the VLM is the most popular. The collocation of the downwash and loading points are chosen by the $1/4 - 3/4$ rule. This chordwise rule is applied to each panel on the chord of a wing. In the early 1950s, the accuracy of the results from the VLM was doubtful because of the capacity of computers. In the 1970s, the

Chopra (1976) extended the 2-D theory of lunate tail propulsion to motions of arbitrary and finite amplitude. Unsteady 3-D wing theory utilized in animal propulsion was first done by Chopra and Kambe (1977). They used Davies' (1963) computer program, the model which was similar to Multhopp's kernel method of the lifting surface theory. Chopra's and Kambe's (1977) results for propulsive efficiency tended to be unrealistically high compared with those for the 2-D case and the thrust coefficient disagreed with that found by Lan (1979) for a rectangular wing in the high reduced frequency range. As there are neither experimental results nor analytical solutions available for propulsive efficiency and thrust coefficient, it is difficult to judge which method is more accurate.

An asymptotic theory based on lifting line theory was developed by Cheng and Murillo (1984). The sectional lift distribution was compared with that from Albano and Rodden's DLM. The agreement was good. However, no comparisons were made between the propulsive efficiency and thrust coefficient from the two methods.

Some experiments on oscillating foil propulsion were done by Lai et al. (1989). Their study was concerned with the simulation of a foil propeller driven by a flexible bar. The structural dynamics of the flexible bar were also studied.

In order to verify numerical simulations, the theory of unsteady 3-D oscillating propulsion needs further development in both numerical improvement and experimental practice. The theoretical study in this field has continued over a whole century, but some problems such as the accurate integration of the kernel function, still remain. A reliable, accurate, simple, CPU economical, numerical model is still required.

application of this method reached its peak. The high demand for accurate results and realistic loading distributions, meant that the VLM received much improvement both mathematically and collocationally. These improvements included the mathematical interpretation of the kernel function and numerous lattice arrangement suggestions .

A doublet-lattice method (DLM) presented by Albano and Rodden (1969) improved the loading distribution compared with the VLM. However, the DLM cannot predict the leading edge suction accurately. In Albano's and Rodden's study, the integration of $\int_0^\infty \frac{t}{(1+t^2)^{\frac{1}{2}}} dt$ was expressed by a four-term series, hence the accuracy is not as good as the expression of Jordan's (1976).

A quasi continuous method or quasi-vortex-lattice method developed by Lan (1974) considered all singularities such as the square-root and Cauchy singularities in the integration. These singularities were not considered in the development of the VLM. Lan (1979) extended the QVLM to unsteady flow and utilized the QVLM to study animal carangiform propulsion problems. The integration involved in the kernel were separated, approximated as parabolic equations and then integrated analytically.

The use of unsteady aerofoil theory for the oscillating propulsion problem was initiated around 1970. The study was lead by Lighthill (1969, 1970), Wu (1971) etc. Most of Lighthill's studies were two dimensional analyses as mentioned in the second section of this chapter. Chopra (1974) used a correction method based on two dimensional unsteady lifting line theory and computed a solution for an oscillating foil with aspect ratio 4 and 6. The efficiency trends of these wings with changing pitching axis position agreed qualitatively with Lighthill's (1970) 2-D study. Again,

Chapter 3

Numerical Solutions for Steady Three Dimensional Thin Wing Problems

3.1 Background to the Methods

In about a century's development of aerodynamical calculations, large amounts of research work have been done on the establishment of theory and numerical modeling. The theory to solve aerodynamical force problems can be mainly divided into lifting line theory and lifting surface theory. Lifting line theory is suitable for the calculation of large aspect ratio planforms, over an aspect ratio of about 6. One advantage of lifting line theory is the reduced amount of calculation labour needed. However, at the present time, the amount of computing labour is no longer the main problem; accuracy of the results after long numerical calculations is required. Therefore, many computations for aerodynamical characteristics employ lifting surface theory. The vortex-lattice method (VLM) is one of the most popular methods in the application of lifting surface theory. In the VLM method, the lifting surface is divided into a number of panels, or vortex lattices. One arrangement of a vortex

lattice is shown in figure 3.1.

In the subsonic VLM method, the loading point is set at the quarter-chord of each panel and the downwash point or control point is set at the three-quarter chord point of each panel. This quarter-chord and three-quarter-chord arrangement is known as 'quarter-and-three-quarter' rule. This rule can be proved and extended from the subsonic case to the supersonic case (Richardson (1955)). At the control point, the downwash induced by the vortices includes both the self-induced downwash from the vortex in the element corresponding to the control point and that from all other vortices on the lifting surface, as well as their trailing vortices. These downwash's are located in their panels at the quarter-chord positions. Both density of lift and downwash values are constant at this point (may be a complex constant in the unsteady case). The expressions for the downwash form a linear system of equations in terms of the distribution of circulation. The unknown density of nondimensional circulation $\gamma(x, y)$ at each panel is obtained by solving the linear system of equations simultaneously. The advantages of the VLM are: it gives an accurate calculation of overall aerodynamic characteristics; it can be applied to arbitrary planforms; and it is easy to use. However, the VLM is not accurate in calculating the distribution of lift and the leading-edge suction (Lan (1974)). The accurate prediction of leading-edge suction is important for the calculation of propulsive efficiency and thrust coefficient, for an oscillating wing.

3.2 The QVLM for Lifting Surface Theory

As mentioned in foregoing chapters, the development of the quasi-vortex-lattice method (QVLM) was based on the VLM. Lan (1974) reviewed the VLM method

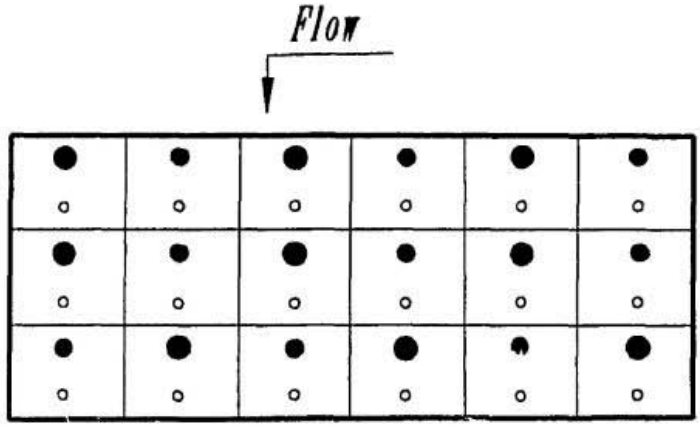

Figure 3.1: A vortex lattice arrangement of the vortex-lattice method, according to the "one-quarter and three-quarter rule". •, loading point; o, control point.

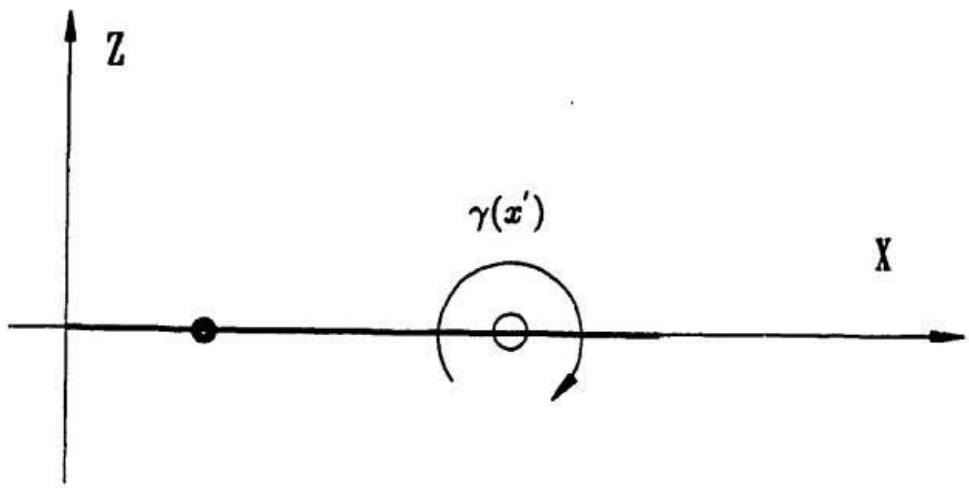

Figure 3.2: Lay out of the locations of the circulation and downwash for a two dimensional thin wing

and improved the accuracy of the results from the VLM by solving the singularities problem in the equations for the integration of downwash.

Consider the induced velocity $w(x)$ at a point x on a two dimensional wing (Glauert (1926),*p.*88) in figure 3.2, from the circulation at a density of $\gamma(x')$ located at x',

$$w(x) = \int_0^1 \frac{\gamma(x')dx'}{2\pi(x-x')}, \tag{3.1}$$

where the integration limits 0 and 1 denote the leading edge and trailing edge respectively. From Lan (1974, equation (4)), when $w(x) = 1.0$,

$$\gamma(x) = 2(1-x)^{\frac{1}{2}}x^{-\frac{1}{2}}. \tag{3.2}$$

When $x = x'$, a Cauchy singularity appears in the denominator of the integrand at $x = 1$ and $x = 0$ (at the trailing edge and leading edge), a square-root singularity occurs at $x = 0$ in the numerator of the integrand. In the VLM method, the integral is described by (Lan 1974, equations (2) and (3))

$$2\pi w_i = \sum_j a_{ij}\gamma_j, \tag{3.3}$$

where

$$\begin{aligned} a_{ij} &= \frac{\Delta x}{(x_i - x_j)} = \frac{1}{\frac{1}{2}+i-j}, \\ & i = 1,2,\cdots,NC; \\ & j = 1.2,\cdots,NS, \end{aligned}$$

where NC, NS are the number of chordwise and spanwise control points respectively. In Eq. 3.3, $a_{ij} \simeq \frac{dx}{x-x'}$, the matrix of calculation coefficients. The i and j stand for the ith control point and the jth loading point, or vortex location respectively. As $x_i - x_j \neq 0$ and $x \neq 0$ on any panel on the wing, Cauchy and

square-root singularities do not appear in the approximate integration. The effects of the singularities on the result of the integration are neglected.

In order to evaluate the integral accurately, Lan (1974) considered both singularities in the QVLM. In the QVLM, the lifting surface is divided into a number of control points and downwash points according to a semi-circle arrangement. The transformation from the x-coordinate ($0 \leq x \leq 1$) to a θ-coordinate ($0 \leq \theta \leq \pi$) is done by the relation

$$x = (1 - \cos\theta)/2. \tag{3.4}$$

Therefore, Eq. 3.1 can be written as

$$w(\theta) = -\frac{1}{2\pi}\int_0^\pi \frac{\gamma(\theta')\sin\theta' d\theta'}{\cos\theta - \cos\theta'} \tag{3.5}$$

In order to eliminate both singularities, in Lan's (1974) derivation, a function

$$g(\theta) = \gamma(\theta)\sin\theta \tag{3.6}$$

was introduced. The square-root singularity is then eliminated because of the factor of $\sin\theta$. When $\theta' = \theta$,

$$-\frac{g(\theta)}{2\pi}\int_0^\pi \frac{d\theta'}{\cos\theta - \cos\theta'} = 0. \tag{3.7}$$

Therefore, the Cauchy singularity is also eliminated. Lan did not give full derivations of many of his equations. For completeness and to help readers and future users, derivations are given in appendices; the derivation of Eq. 3.7 is given in Appendix A.

By applying the mid-point trapezoidal rule (see full derivations in Appendix B), Eq. 3.5 can be written as

$$w(\theta) = -\frac{1}{2\pi}\int_0^\pi \frac{g(\theta') - g(\theta)}{\cos\theta - \cos\theta'} d\theta'$$

$$\begin{aligned} &\simeq -\frac{\Delta\theta'}{2\pi}\sum_{k=1}^{N}\frac{g[(2k-1)\Delta\theta'/2]-g(\theta)}{\cos\theta-\cos[(2k-1)\Delta\theta'/2]} \\ &= \frac{-1}{2N}\sum_{k=1}^{N}\left[\frac{g((2k-1)\pi/2N)}{\cos\theta-\cos[(2k-1)\pi/(2N)]}\right. \\ &\quad \left.-\frac{g(\theta)}{\cos\theta-\cos[(2k-1)\pi/(2N)]}\right] \end{aligned} \tag{3.8}$$

which is similar to Eq. (10) in Lan (1974). For computational convenience, Lan eliminated the last term of Eq. 3.8 by employing Chebychev polynomials (the full derivation is given in Appendix C). From the results of Appendix C , the variables λ_k and λ_i in the Chebychev polynomials are found to be

$$\lambda_k = \cos\theta_k = \cos[(2k-1)\pi/(2N)], K = 1, 2, ...N \tag{3.9}$$

and

$$\lambda_i = \cos\theta_i = \cos[i\pi/(2N)], K = 1, 2, ...N-1. \tag{3.10}$$

Eq. 3.9 and 3.10 define the positions of the control points and loading points. The arrangement of downwash and loading point of the QVLM is shown in figure 3.3.

As the unknown function $\gamma(\theta)$, the density of circulation of each vortex lattice, has a square-root singularity at $\theta = 0$, a parameter C is set where

$$\gamma(\theta) = C(1-x)^{\frac{1}{2}}x^{-\frac{1}{2}}$$

instead of

$$\gamma(\theta) = 2(1-x)^{\frac{1}{2}}x^{-\frac{1}{2}}$$

in the exact solution, and then take the limit

$$\begin{aligned} \lim_{\theta\to 0} g(\theta) &= \lim_{\theta\to 0}\gamma(\theta)\sin\theta \\ &= \lim_{\theta\to 0} C(1-x)^{\frac{1}{2}}x^{-\frac{1}{2}}\cdot 2x^{\frac{1}{2}}(1-x)^{\frac{1}{2}} \\ &= 2C. \end{aligned} \tag{3.11}$$

where $2x^{1/2}(1-x)^{1/2}$ is equivalent to $\sin\theta$ under the θ-coordinate (see equation 3.4). The parameter C is defined at the singularity point. In two dimensional thin wing theory, the velocity in the x direction is $u(x) = \gamma(x)/2$ on the surface of the wing (Newman (1977), *p.*180). It follows that the leading edge suction parameter C_s is found by

$$\begin{aligned} C_s &= \lim_{x\to 0} u(x)x^{\frac{1}{2}} = \lim_{x\to 0}\gamma(x)x^{\frac{1}{2}}/2 \\ &= \lim_{x\to 0} C(1-x)^{\frac{1}{2}}x^{-\frac{1}{2}}x^{\frac{1}{2}}/2 = C/2. \end{aligned} \tag{3.12}$$

Therefore, when C is known, C_s is known. As

$$\begin{aligned} \lim_{\theta\to 0}\sum_{k=1}^{N}\frac{1}{\cos\theta - \cos[(2k-1)\pi/(2N)]} &= \lim_{\theta\to 0}\sum_{k=1}^{N}\frac{1}{\lambda-\lambda_k} \\ &= \lim_{\theta\to 0}\frac{T_N'(\lambda)}{T_N(\lambda)} = -N^2, \end{aligned} \tag{3.13}$$

as a result, Eq. 3.8 can be written as

$$w(x_i) \simeq \frac{1}{2N}\sum_{k=1}^{N}\frac{\gamma_k x_k^{\frac{1}{2}}(1-x_k)^{\frac{1}{2}}}{x_i - x_k} + \begin{cases} NC, & \text{if } i=0 \\ 0, & \text{otherwise,} \end{cases} \tag{3.14}$$

where NC is the number of chrodwise control point. In the two dimensional case, the numerical results from the QVLM are the same as the exact solution (Lan (1974)).

As the difference between the QVLM and the VLM is only in the weighting scheme in the integration of Eq. 3.1 and the vortex strip and control point arrangement, Lan extended it to the three dimensional case in a similar manner. Consider a vortex segment as shown in figure 3.4. According to the Biot-Savart law, the influence of a free vortex line with strength Γ parallel to the direction of the undisturbed velocity (or trailing vortex) in linearized compressible flow was given by Ward (1955)

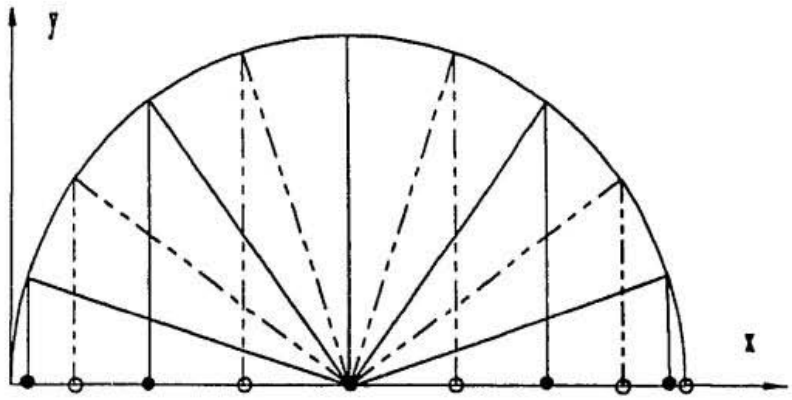

Figure 3.3: The collocation arrangement of the QVLM. •, loading point; o, control point.

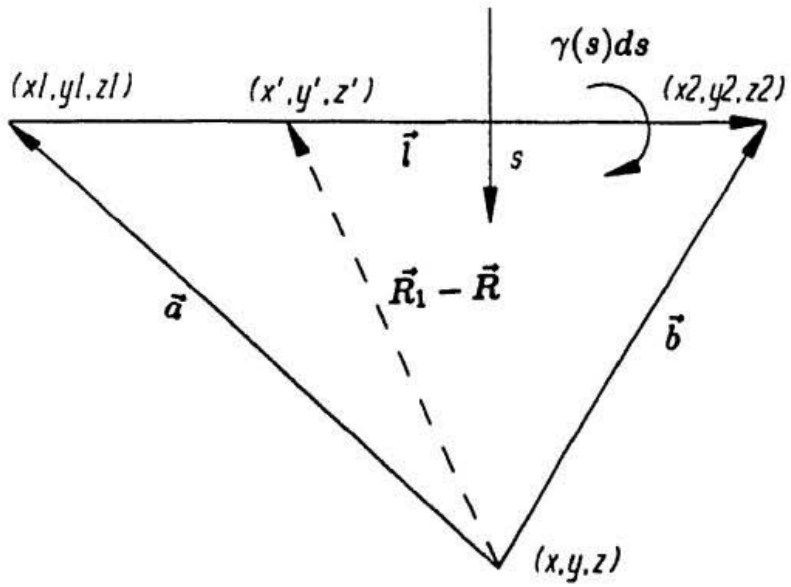

Figure 3.4: Schematic diagram of a vortex segment

in the form

$$\vec{V}_i(r) = \frac{\beta^2\Gamma}{4\pi}\int_l \frac{(\vec{R}_1 - \vec{R}) \times d\vec{l}}{R_\beta^3}. \tag{3.15}$$

In the three dimensional case, in which Γ is not constant along the span, the above equation becomes

$$\vec{V}_i(r) = \frac{\beta^2}{4\pi}\int_{x_l}^{x_t} \gamma(x')dx' \int_{x_l}^{\infty} \frac{(\vec{R}_1 - \vec{R}) \times d\vec{l}}{R_\beta^3}. \tag{3.16}$$

The influence of a bound vortex can be defined by Eq. 3.16 after some mathematical manipulations (see Lan (1974)). From results for the induced velocity from the bound and trailing vortices (see Appendix D), the induced downwash at a point $P_{l,m}$ for a steady 3-D thin wing in compressible flow can then be expressed as

$$\begin{aligned}\left(\frac{dz}{dx}\right)_{l,m} - \alpha_{l,m} \quad &= \sum_{j=1}^{NS}\sum_{k=1}^{NC} \\ &\cdot\Bigg\{\frac{(x_{2k}-x_{1k})(x_{2k}-x_i)+\beta^2(y_{2k}-y_{1k})(y_{2k}-y_i)}{[(x_{2k}-x_i)^2+\beta^2(y_{2k}-y_i)^2]^{\frac{1}{2}}[(x_{1k}-x_i)(y_{2k}-y_i)-(x_{2k}-x_{1k})(y_{1k}-y_i)]} \\ &-\frac{(x_{2k}-x_{1k})(x_{2k}-x_i)+\beta^2(y_{2k}-y_{1k})(y_{2k}-y_i)}{[(x_{1k}-x_i)^2+\beta^2(y_{1k}-y_i)^2]^{\frac{1}{2}}[(x_{1k}-x_i)(y_{2k}-y_i)-(x_{2k}-x_{1k})(y_{1k}-y_i)]} \\ &-\frac{1}{y_{1k}-y_i}\left[\left(1-\frac{x_{1k}-x_i}{[(x_{1k}-x_i)^2+\beta^2(y_{1k}-y_i)^2]^{\frac{1}{2}}}\right]+\frac{1}{y_{2k}-y_i}\right. \\ &\left.\left[1-\frac{x_{2k}-x_i}{[(x_{2k}-x_i)^2+\beta^2(y_{2k}-y_i)^2]^{\frac{1}{2}}}\right]\right\}\frac{c}{8N}\gamma_j(\theta_k)\sin(\theta_k)\end{aligned} \tag{3.17}$$

When $l = j, m = k$, the above equation is a linear system of $(j \times k) \times (j \times k)th$ order for $j \times k$ unknown γ_{kj}, the distribution of circulation at each loading point.

The suction parameter C_s in the three dimensional case can be obtained in a similar way as in the two dimensional case described above. Once $\gamma(x, y)$is known at each point, the lift and moment of a three dimensional wing are obtained by chordwise numerical integration for the sectional loading and then by the spanwise

numerical integration for total loading. In the present investigation, a program incorporating the QVLM was written and its results were verified against Lan's (1974) for, firstly, an infinite span aerofoil with 30% flap and 30^0 flap deflection; secondly, a rectangular wing with aspect ratio 2 at Mach number $M_\infty = 0$; and thirdly, a Warren 12 planform with aspect ratio $2(2)^{\frac{1}{2}}$ at $M_\infty = 0$. All results in the present investigation were the same as Lan's (1974).

As can be seen in the next chapter, the computer program incorporating the QVLM in the steady case is important in the extension from the the steady case to the unsteady case. The program for the unsteady case which was framed by Eq. 4.10 consists of a steady part and an unsteady part; when the oscillating frequency ω is zero, the program reduces to the steady case of computation. The theoretical analysis of the forces on the unsteady lifting-surface is discussed in Chapter 4.

Chapter 4

Numerical Method for a Three Dimensional Lifting Surface in Harmonic Motion

The method introduced in this chapter is the quasi-vortex-lattice method (QVLM); it is applied to the calculation of aerodynamic forces on an unsteady lifting-surface. From the wing flow tangency condition, the downwash of the lifting-surface is obtained. From the geometry conditions and flow conditions of the lifting surface, the non-dimensional velocity potential on a doublet is determined by the QVLM formulation. The downwash at one point induced by all oscillating vortices on the lifting surface can be obtained by differentiating the doublet velocity potential. Therefore, the downwash can be canceled and a system of linear equations is formed. By solving the system of linear equations simultaneously, the loading distribution of the unsteady lifting surface is obtained. Then the loading distribution is used to find the aerodynamic forces such as pitching moment coefficient, lift coefficient and induced drag.

4.1 Boundary Condition

For a three dimensional wing without a flap, the positive x axis is taken as lying along the root chord and points downstream, and the positive y axis points to the right and lies on the pitching axis as is shown in figure 4.1. When the foil heaves with a vertical displacement $\bar{h}(y,t)$ and pitches with an angular displacement $\bar{\alpha}(y,t)$ about the position $x = x_a$, the combined vertical displacement $z(x,y,t)$ at any point on the planform without flapping can be derived from Eq. 2.3

$$z(x,t) = \begin{cases} -h - \alpha(x - ba); & \text{for } -b \le x \le bc \\ -h - \alpha(x - ba) - \beta(x - bc); & \text{for } bc \le x \le b, \end{cases} \tag{4.1}$$

which is

$$z(x,y,t) = -\bar{h}(y,t) - \bar{\alpha}(y,t)(x - x_a). \tag{4.2}$$

Differentiating Eq. 4.1 with respect to t, the non-dimensional downwash is given by

$$\begin{aligned} \bar{w}(x,y,t) &= \frac{1}{V_\infty}\frac{Dz}{Dt} = \frac{1}{V_\infty}\frac{\partial z}{\partial t} + \frac{\partial z}{\partial x} \\ &= -\frac{1}{V_\infty}\dot{\bar{h}} - \frac{1}{V_\infty}\dot{\bar{\alpha}}(x - x_a) - \bar{\alpha}, \end{aligned} \tag{4.3}$$

which is Eq. 2.2 in Lan (1979). As the foil has a harmonic time variation of oscillation, the downwash can be written in another form

$$\bar{w}(x,y,t) = Re[w(x,y)e^{i\omega t}] \tag{4.4}$$

where Re denotes the real part, and ω denotes the oscillating frequency. Assuming $\bar{w} = Re[we^{i\omega t}]$, $\bar{\alpha} = Re[\alpha e^{i\omega t}]$, and $\bar{h} = Re[he^{i\omega t}]$, the downwash can be shown (see Eq. E.6 in Appendix E) as

$$w(x,y) = -i\frac{\omega}{V_\infty}h(y) - \alpha(y) - i\frac{\omega}{V_\infty}\alpha(y)(x - x_a). \tag{4.5}$$

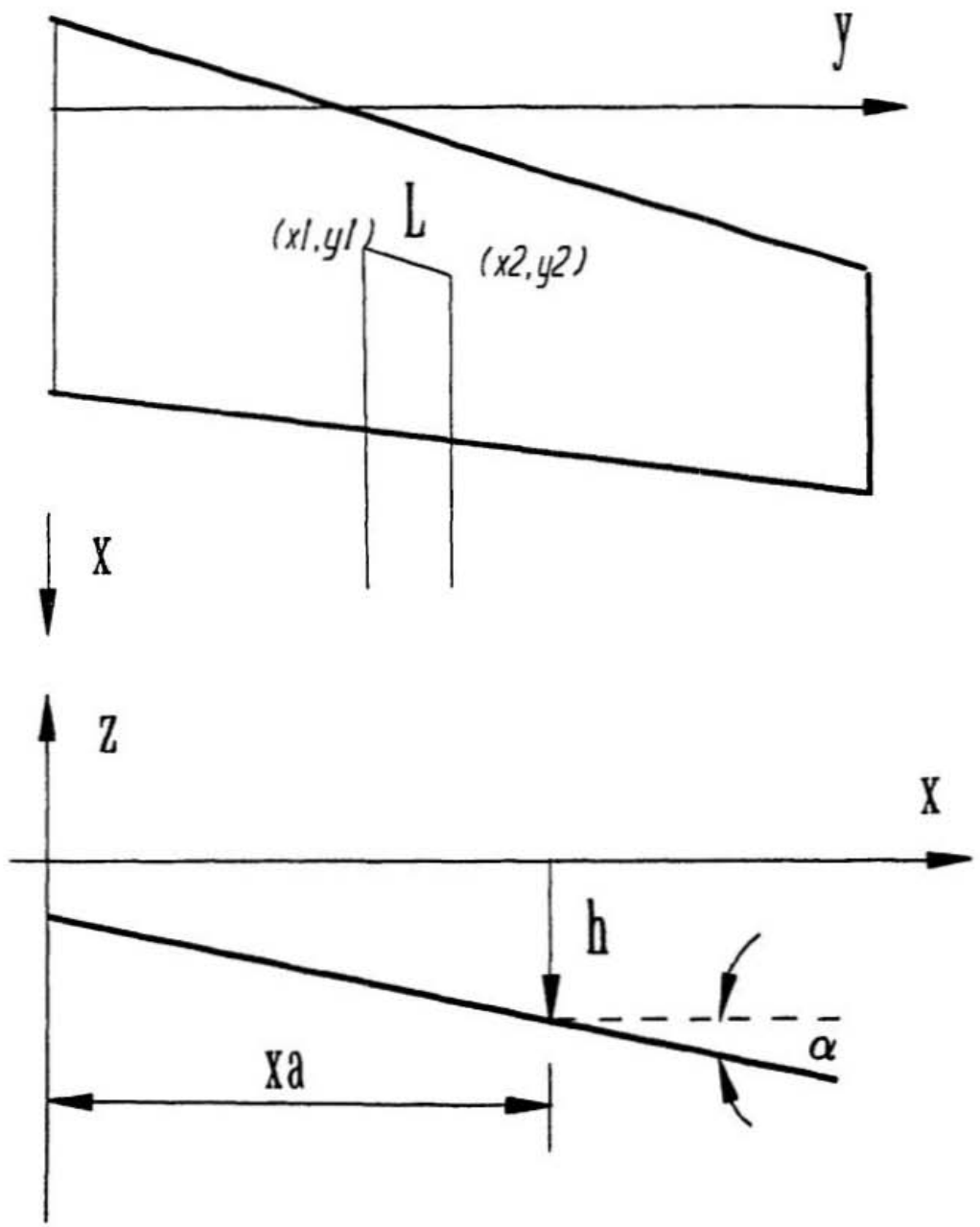

Figure 4.1: Coordinate system for an oscillating foil

A reduced frequency, k, is introduced where

$$k = \frac{\omega B_r}{V_\infty}, \tag{4.6}$$

where B_r is a reference length referred to the chord length and, V_∞ is the freestream velocity. Substituting Eq. 4.5 into Eq. 4.4 and considering a phase angle Φ_{ph} (pitch leading heave), it follows that

$$w(x,y) = -i\frac{k}{B_r}h(y) - \alpha(y)e^{i(\Phi-\pi)} - i\frac{k}{B_r}\alpha(y)e^{i(\Phi-\pi)}(x - x_a), \tag{4.7}$$

which is Eq. 2.3 in Lan (1979). When the wing is rigid, h, and α are constant along the span. The boundary condition of an oscillating surface is obtained from Eq. 4.7.

4.2 Mathematical Model of the Kernel Function

When a lifting surface is oscillating harmonically in a compressible subsonic flow at Mach number M_∞, the non-dimensional velocity potential can be determined as in Lan (1979) after Richardson (1955) in the form

$$\begin{aligned}\Phi(x,y,z) &= \frac{1}{8\pi}\int\int_s \Delta C_p(\xi,\eta)\left\{(\frac{1}{r^2} + \frac{x_0}{Rr_1^2})z_0 e^{-i\omega(u_1 r_1 + x_0)/V_\infty}\right. \\ &- \left. i\frac{\omega}{V_\infty}\frac{z_0}{r_1}e^{-i\omega x_0/V_\infty}\int_{u_1}^{\infty}[1 - \frac{\lambda}{(1+\lambda^2)^{1/2}}]e^{-i\omega r_1\lambda/V_\infty}d\lambda\right\}d\xi d\eta, \end{aligned} \tag{4.8}$$

where

1. s, wing area,

2. λ, intermediate variable,

3. $x_0 = x - \xi$,

4. $y_0 = y - \eta$,

5. $z_0 = z - \zeta$,

6. (ξ, η, ζ) are the coordinates of an element doublet,

7. $r_1^2 = (y_0^2 + z_0^2)$,

8. $R^2 = x_0^2 + (1 - M_\infty^2)(y_0^2 + z_0^2)$,

9. $u_1 r_1 = (-x_0 + MR)/(1 - M_\infty^2)$, and

10. ΔC_p is the dimensionless pressure difference across the wing surface, which will be the unknown values in the system of linear equations.

When the flow is incompressible, $M = 0$. The relation between downwash and Eq. 4.8 can be identified after integration and then differentiation to obtain $w(x, y) = \frac{\partial \Phi}{\partial z}$.

In Lan's (1979) discretization, the lift distribution is assumed stepwise constant along span (in the η direction). Therefore, the integration of Eq. 4.8 is first done in the spanwise direction. Then the relation between downwash and $\frac{\partial \Phi}{\partial z}$ can be found by differentiation of Eq. 4.8 with respect to z. Finally, the equation is integrated by the mid-point trapezoidal rule in the x direction. Some manipulations are necessary in the integration of

$$\int_L (\frac{1}{r^2} + \frac{x_0}{Rr^2}) z_0 d\eta, \tag{4.9}$$

where L is the vortex strip on which the lift is distributed stepwise. A complete solution for Eq. 4.9 is given in Appendix E. By using the results from Appendix E, the integrand, without ΔC_p of Eq. 4.8 which is denoted Φ_{in} can be expressed as

$$\Phi_{in} = \Phi_1 + \Phi_2$$

$$= \frac{1}{8\pi}\left\{\arctan(\frac{2a\tau+b}{z(y_2-y_1)z}) - \arctan(\frac{Qv-(x_2-x_1)z^2}{z(y_2-y_1)(A\tau^2+B\tau+C)^{1/2}})\right\}$$
$$-i\frac{\omega}{V_\infty}\frac{1}{8\pi}\left\{\arctan(\frac{2a\tau+b}{2(y_2-y_1)z})\int_{u_1 r_1}^{\infty}[1-\frac{\tau_1}{(\tau_1^2+r_1^2)^{1/2}}]e^{-i\omega(\tau_1+x_0)/V_\infty}d\tau_1|_L\right.$$
$$\left.-\int_L \arctan(\frac{2a\tau+b}{2(y_2-y_1)z})\frac{\partial I}{\partial\eta}d\eta\right\}. \qquad (4.10)$$

It is noted that the first term Φ_1 in Eq. 4.10 is a steady term and Φ_2 is an unsteady term. In the steady case, when $\omega = 0$, only the Φ_1 term exists, and this will lead to the solution in the steady case. After differentiating Φ_1 with respect to z, the result is the same as the expression of the downwash derived from the Biot-Savart law when mach number $M_\infty = 0$ (see the result of Appendix D). For the unsteady terms, differentiating these terms with respect to z (see Appendix F), leads to

$$\frac{\partial\Phi_2}{\partial z} = -i\frac{\omega}{V_\infty}\frac{1}{8\pi}[-\frac{y_2-y_1}{(y_2-y_1)+z^2}I_2 + \frac{y_1-y}{(y_1-y)+z^2}I_1$$
$$+ \arctan(\frac{y_2-y}{z})\frac{\partial I_2}{\partial z} - \arctan(\frac{y_1-y}{z})\frac{\partial I_1}{\partial z} + W_2 + W_3], \qquad (4.11)$$

where

$$I_1 = T_1(x, y, x_1, y_1), \qquad (4.12)$$

$$I_2 = T_1(x, y, x_2, y_2), \qquad (4.13)$$

and

$$T_1 = \int_{u_1 r_1}^{\infty}\left[1-\frac{\tau_1}{(\tau_1^2+r_1^2)^{1/2}}\right]e^{-i\omega(\tau_1+x_0)/V_\infty}d\tau_1. \qquad (4.14)$$

The last two terms W_2 and W_3 in Eq. 4.11 contain singularities when $y = \eta$ at $z = 0$. Therefore, the integration of W_2 and W_3 needs to be treated separately.

Consider

$$W_2 = \int_0^1 \frac{\eta-y}{(\eta-y)^2+z^2}\frac{\partial I}{\partial\eta}(y_2-y_1)d\tau, \qquad (4.15)$$

where $\frac{\partial I}{\partial \eta}$ from the result of Appendix G becomes

$$\begin{aligned}\frac{\partial I}{\partial \eta} &= \frac{\partial I}{\partial r_1}\frac{\partial r_1}{\partial \eta} + \frac{\partial I}{\partial x_0}\frac{\partial x_0}{\partial \eta} \\ &= -(y-\eta)\int_{u_1 r_1}^{\infty} \frac{\tau_1 e^{-i\omega(\tau_1+x_0)/V_\infty} d\tau_1}{(\tau_1^2+r_1^2)^{3/2}} \\ &+ i\frac{\omega}{V_\infty} I \frac{x_2-x_1}{y_2-y_1} - [1-\frac{u_1}{(1+u_1^2)}]\frac{x_2-x_1}{y_2-y_1}. \end{aligned} \tag{4.16}$$

There is no singularity term in Eq. 4.16. However, the integrand of Eq. 4.15 has a singularity when $y-\eta=0$ if $z=0$. To deal with this problem, Lan (1979 and 1990) used a scheme the same as that of Albano and Rodden (1969): the non-singular part $\frac{\partial I}{\partial \eta}$ was approximated by a quadratic function of τ, then Eq. 4.15 was integrated analytically. The solution to W_3 was done in a similar way. Approximated integrations of W_2 and W_3 are described in Appendix H. Although the error of the parabolic approximation is normally small (Albano and Rodden (1969)), the curves at boundaries ($\tau=0$, and $\tau=1.0$) have larger differences. In the present study, parabolic functions is used in the approximation. For more accurate results, appropriate higher order polynomials are required.

Another problem is the treatment of the integral

$$\int_a^{\infty} \frac{\lambda}{(1+\lambda^2)^{1/2}} d\lambda. \tag{4.17}$$

Albano and Rodden (1969) used the expression (Watkin et al. (1959))

$$\frac{\lambda}{(1+\lambda^2)^{1/2}} \simeq 1.0 - 0.101e^{-0.329\lambda} - 0.899e^{-1.4067\lambda} - 0.09480933e^{-2.90\lambda}\sin(\pi\lambda), \tag{4.18}$$

and Lan (1979) used a more accurate expression by Jordan (1976) as

$$\frac{\lambda}{(1+\lambda^2)^{1/2}} \simeq 1 - \sum_{n=1}^{10} a_n e^{-c_n\lambda}, \tag{4.19}$$

n	a_n	c_n	n	a_n	c_n
1	0.002907843	0.0625	6	0.5556069	2.0
2	0.002591528	0.125	7	0.748426	3.0
3	0.02667074	0.25	8	-0.7769790	4.0
4	0.070971	0.5	9	0.07004561	8.0
5	0.347837	1.0	10	-0.004557519	16.0

Table 4.1: The coefficient of Jordan approximation

where a_n and c_n are listed in table 4.1. However, both these expressions are only valid when $\lambda \geq 0$. Otherwise, the solution does not converge. This can be avoided by the mathematical manipulation in the integration (see Lan(1979)). This manipulation was to change the integration limit u_1 form negative to positive, by utilizing the odd and even function characteristics of the sine and cosine functions. These functions were used to express $exp\{-i\omega\lambda r_1/V_\infty\}$.

Once $\frac{\partial\Phi}{\partial z}$ is obtained, the spanwise sectional downwash can be identified as

$$\frac{\partial\Phi}{\partial z}(x,y,z) = \int_{x_l}^{x_t} \Delta C_p(\xi)(\frac{\partial\Phi_1}{\partial z} + \frac{\partial\Phi_2}{\partial z})d\xi, \tag{4.20}$$

where $\frac{\partial\Phi_1}{\partial z}$ is the steady part of the integrand, i.e. Eq. F.1. Eq. 4.20 can be integrated by the mid-point trapezoidal rule; the collocation points are positioned in a similar way was in the steady theory (see Chapter 3). Once the lift coefficient C_l at each point is obtained, the moment coefficient C_m, leading-edge suction C_s etc. can be obtained in a similar way as for a foil in steady flow. Applying Eq. 2.7 (see Appendix J), thrust coefficient and propulsive efficiency can be obtained.

Numerical interpretations of some terms in Eq. 4.8 in the program, are listed in Appendix I. The results of some terms were checked by using Macsyma, a package for analytical math derivation.

This method was assembled into a computer program written in FORTRAN. The procedure is described in the next chapter.

Chapter 5

Computing Procedure

5.1 Introduction

For computational convenience, the expressions of the exponential function terms in Eq. 4.8 were interpreted by sine and cosine functions (see Appendix I). The computing formulation in the program was based on the results in Appendix I. After all initial values were input, matrices of all elements in terms of the coefficients of the pressure differences at each element on the lifting surface were obtained. Then these matrices were arranged into one matrix according to the locations of the elements.

The loading distribution was obtained after solving a system of linear equations formed by the matrix. Meanwhile, the suction coefficient was obtained by considering only the elements of the first row (leading-edge) along the span. Pitching moment coefficient was obtained from the loading distribution. The thrust coefficient and propulsive efficiency were determined last.

5.2 Input Data of Initial Values

There are two kinds of initial values in the input procedure: the wing motions and the geometric values of the planform. For the foil motion, the given values are reduced frequency k, pitching axis x_a, reference length B_r, pitching amplitude α and heaving amplitude h. From these, the velocity ratio

$$\frac{\omega}{V_\infty} = \frac{k}{b_r}, \tag{5.1}$$

the feathering parameter

$$\theta = \alpha V_\infty / (h\omega), \tag{5.2}$$

and the wing flow condition $w(x, y, z)$ are found. The wing shape values are given in terms of the number of stations from the wing offsets record. N_i is used to denote the number of the intervals of the interpolation points. The program is designed to treat an asymmetric planform. For a symmetrical foil, input data is required only for the left half span. The number of chordwise vortex strips N_c and the number of spanwise vortex strips N_s can be selected in accordance with the demands of accuracy. Once the N_c, N_s, N_i and wing shape curves are defined, these values are sent to a subroutine GEOR. The locations of vortex strip points, the downwash control points, sectional sweep angles, aspect ratio, foil area, and wing curve properties (first and second derivatives of the curves) are obtained by the interpolation of spline functions.

5.3 Matrix Computation

All the elements of matrix $[\frac{\partial \Phi}{\partial z}]$ are complex values. These elements are obtained from Eq. 4.20 corresponding to the loading and control locations. For simplicity,

a planar planform discretized as $N_c = 3$, $N_s = 3$ is given as an example (see figure 5.1). In this case, $II = JJ = N_s = 3$, where II and JJ are the number of the chordwise and spanwise control point respectively. The element matrices are defined by $AA(II, JJ, KI, KJ)$ and are shown in table 5.1.

In the calculation of the values in $AA(II, JJ, KI, KJ)$, the following programmed complex functions were used:

$DPHI$ a function that summarizes all functions, including both steady and unsteady terms.

$DPHI1$ downwash induced by steady vortices, determined by Eq. F.1.

$DPHI2$ downwash induced by unsteady vortices, determined by Eq. F.2.

$T1E$ the integration of T_1, Eq. I.4 or Eq. I.13 depending on $u_1 < 0.0$ or $u_1 \geq 0.0$.

$T2$ the integration of T_2, Eq. I.7 or Eq. I.18 depending on $u_1 < 0.0$ or $u_1 \geq 0.0$.

$T3E$ the integration of T_3, Eq. I.10 or Eq. I.23 depending on $u_1 < 0.0$ or $u_1 \geq 0.0$.

$PW2$ the parabolic approximation of $\partial I/\partial \eta$, Eq. H.6.

$W2$ the integration of W_2, Eq. H.9.

$W3$ the integration of W_3, Eq. H.18.

$G1$ the parabolic approximation of the last two terms of $\partial^2 I/\partial \eta \partial z$, Eq. H.13.

$G2$ the parabolic approximation of the first term of $\partial^2 I/\partial \eta \partial z$ of Eq. H.12.

$T11$ numerical value of $I_1 = I(x, y, x_1, y_1)$ of Eq. 4.12

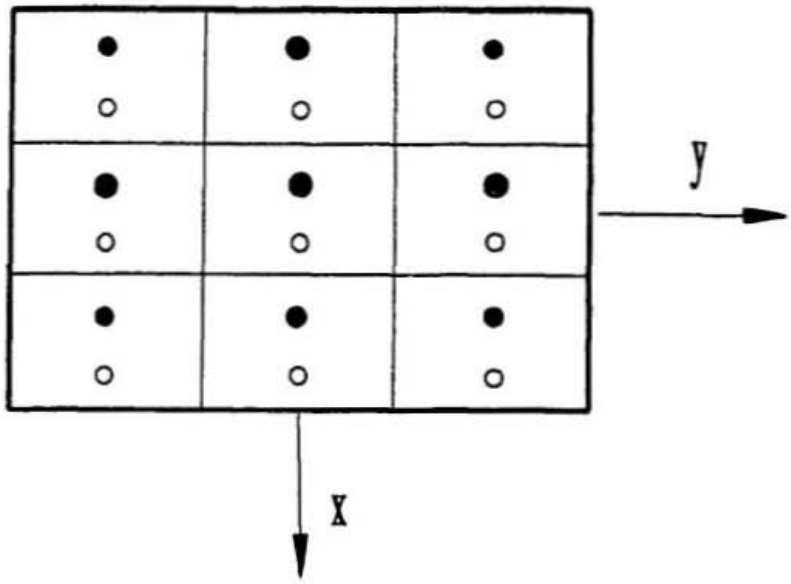

Figure 5.1: Computational matrix from a rectangular wing. •, loading point; ○, control point.

$II=1, jj=1$				$II=1, JJ=2$				$II=1, jj=3$			
$KI\backslash KJ$	I	II	III	$KI\backslash KJ$	I	II	III	$KI\backslash KJ$	I	II	III
I	*	2	3	I	1	2	3	I	1	2	3
II	4	5	6	II	*	5	6	II	4	5	6
III	7	8	9	III	7	8	9	II	*	8	9
$II=2, jj=1$				$II=2, JJ=2$				$II=2, jj=3$			
$KI\backslash KJ$	I	II	III	$KI\backslash KJ$	I	II	III	$KI\backslash KJ$	I	II	III
I	1	*	3	I	1	2	3	I	1	2	3
II	4	5	6	II	4	*	6	II	4	5	6
III	7	8	9	III	7	8	9	II	7	*	9
$II=3, jj=1$				$II=3, JJ=2$				$II=3, jj=3$			
$KI\backslash KJ$	I	II	III	$KI\backslash KJ$	I	II	III	$KI\backslash KJ$	I	II	III
I	1	2	*	I	1	2	3	I	1	2	3
II	4	5	6	II	4	5	*	II	4	5	6
III	7	8	9	III	7	8	9	II	7	8	*
where '' is self-induced element*											

Table 5.1: Matrices formed at each downwash point by all vortices on the wing

$T12$ numerical value of $I_2 = I(x, y, x_2, y_2)$ of Eq. 4.13

$T31$ numerical value of $\partial I_1/\partial z = T_3(x, y, x_1, y_1)$

$T32$ numerical value of $\partial I_2/\partial z = T_3(x, y, x_2, y_2)$

$ATOX$ the numerical integration of the integral $\int\{\arctan(\beta)/\beta\}d\beta$ of Eq. II.20.

In the steady case, only $DPHI1$ is to be used in the program.

Summarizing the downwash contributed by all elemental vortex strips to each vortex lattice, a linear system of equations with IDth or ICth order is formed by summarizing the downwash from all vortex lattices as shown in Table 5.2. A lin-

$IC\backslash ID$	I	II	III	IV	V	VI	VII	VIII	IX	$w(x,y)$
I	*	2	3	4	5	6	7	8	9	$w(1,1)$
II	1	*	3	4	5	6	7	8	9	$w(2,1)$
III	1	2	*	4	5	6	7	8	9	$w(3,1)$
IV	1	2	3	*	5	6	7	8	9	$w(1,2)$
V	1	2	3	4	*	6	7	8	9	$w(2,2)$
VI	1	2	3	4	5	*	7	8	9	$w(3,2)$
VII	1	2	3	4	5	6	*	8	9	$w(1,3)$
VIII	1	2	3	4	5	6	7	*	9	$w(2,3)$
IX	1	2	3	4	5	6	7	8	*	$w(3,3)$
where $IC = II + (JJ-1) * N_c$, $ID = KI + (KJ-1) * N_c$										
and $A(IC, ID) = AA(II, JJ, KI, KJ)$, $A(IC, N_s * N_c) = w(I, J)$										

Table 5.2: Loading Matrix Formulation

ear system solver will solve the complex matrix directly and give the circulation distribution on the lifting surface.

By solving the linear system of complex equations, the complex loading is known. By using the resulting lift distribution, sectional leading-edge suction coefficient $\bar{C}_{tl}$

and mean total thrust coefficient C_t, pitching moment coefficient C_m (complex) about the y axis ($y = 0$ being set to be pitching axis for computational convenience), and finally the thrust coefficient are obtained. The equations to calculate the leading-edge suction coefficient, total mean thrust coefficient, and propulsive efficiency are given in Appendix J.

A computer program of the propulsion problem for a 3-D lifting surface in harmonical oscillation (input data are for a rectangular wing) is given in Appendix K.

Chapter 6

Results and Discussion

6.1 Verification of the Computer Program

Prior to calculations of practical wing planforms, the computer program was checked in the following cases: the chordwise pressure distribution compared with the published results of a special planform, a circular wing from both numerical and analytical solutions; propulsive efficiency and thrust coefficient of a rectangular wing of aspect ratio 8; propulsive efficiency and thrust coefficient of a swept leading-edge, lunate-tail wing of aspect ratio 8 ($B2$ wing). These three planforms are shown in figure 6.1.

The pressure distribution of the circular wing from this program was compared with that from the numerical solution by Lan (1979) and an analytical solution by van Spiegle (Lan(1979)). The comparison of pressure distribution was at mid-semispan of the circular wing (see figure 6.2). The circular wing was assumed to be in pure pitching motion at a reduced frequency $k = 0.8$; the reference length B_r used is the half chord at mid-semispan. Curve C_1 denotes the real part and C_2 denotes the imaginary part of the pressure distribution function. The number of spanwise

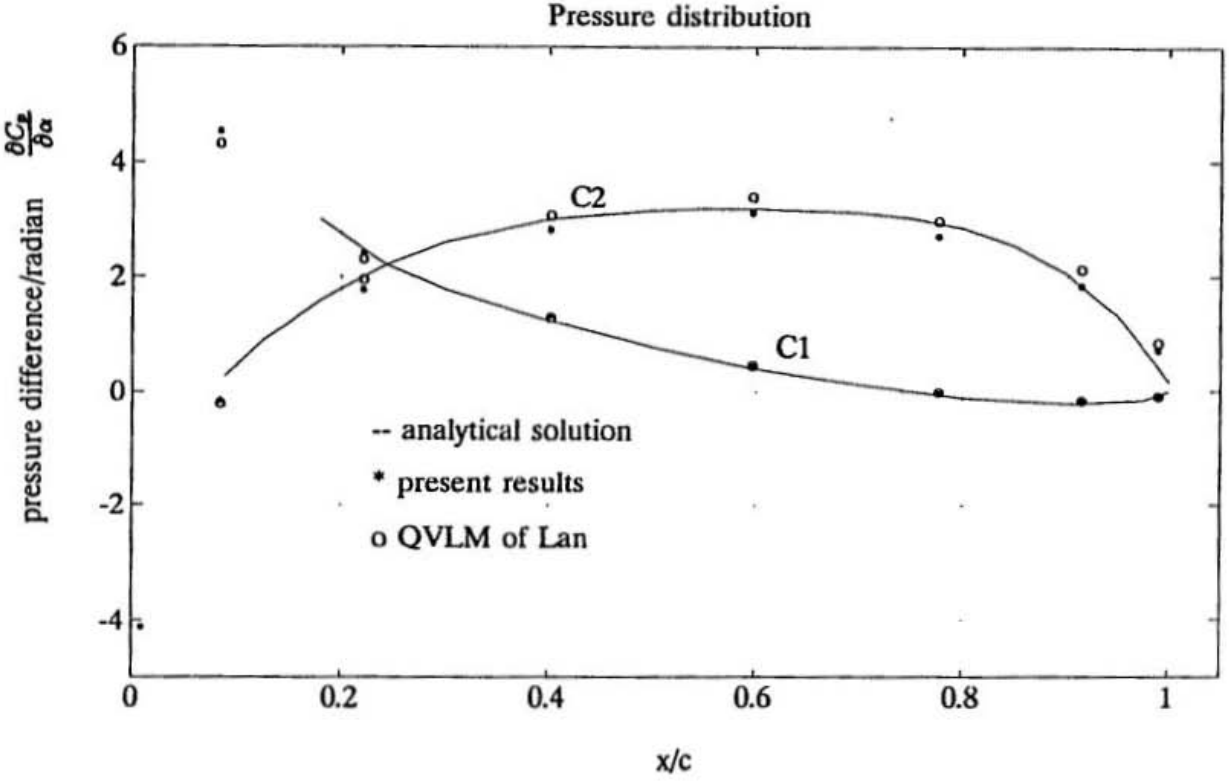

Figure 6.2: Pressure distribution at mid-semispan of a circular wing. $\frac{\partial C_p}{\partial \alpha}$ is the rate of change of pressure coefficient with angle of attack, x/c is the chordwise location.

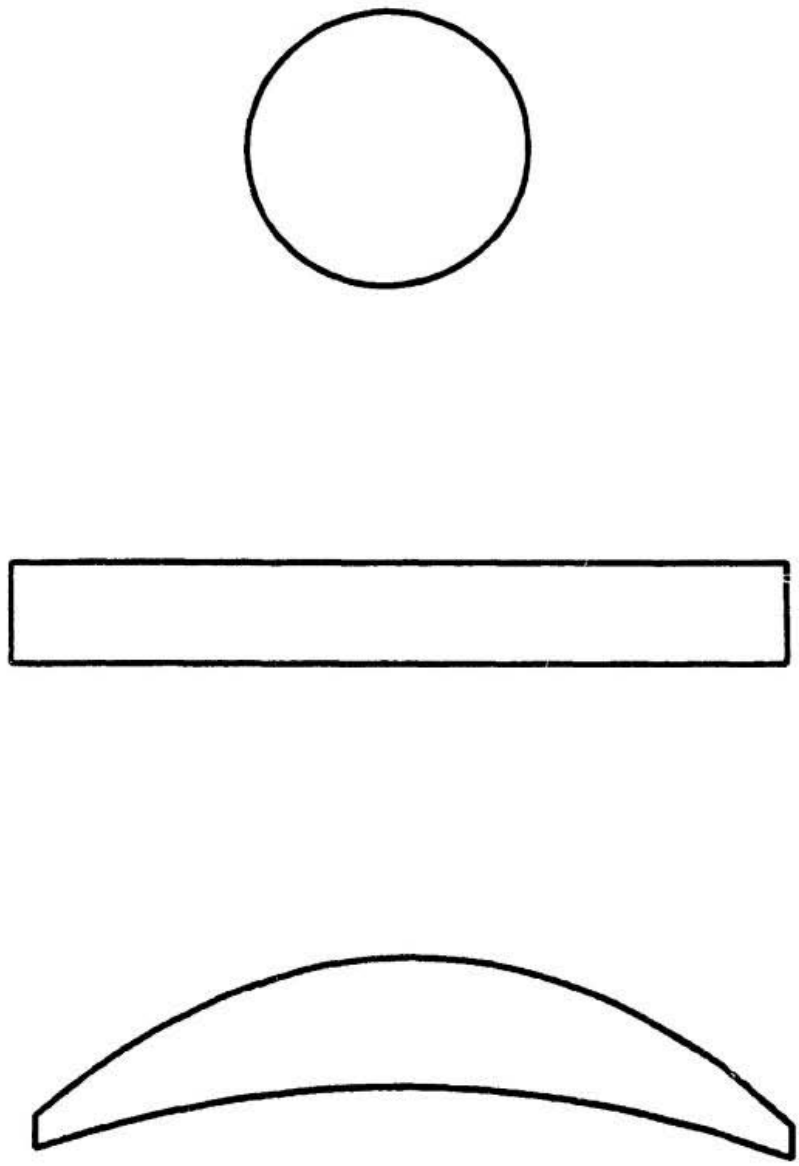

Figure 6.1: Planforms used in the computation for the computer program verification. Circular planform, rectangular foil, and lunate-tail wing ($B2$ wing).

control points on the half wing was $NS = 7$, and the number of chordwise control points was $NC = 8$. When the wing was in pure pitching motion, the amplitude of heave h was zero, the feathering parameter $\theta = \alpha V_\infty / \omega h = \infty$. Figure 6.2 shows that the QVLM implemented in the present program has good agreement with the analytical solution and the results of Lan (1979).

Analytical solutions to oscillating surfaces are only possible for the calculation of circular and elliptic planforms (Küessner (1953), Harry et al. (1957)). Predictions of thrust coefficient and propulsive efficiency, versus reduced frequency, k, for a rectangular wing of aspect ratio 8 are shown in figures 6.3 and 6.4. A comparison is shown between the present results and the method of Chopra and Kambe (1977). Results are presented for a feathering parameter $\theta = V_\infty \alpha_i' / (\omega h)$ of 0.0, 0.4, and 0.8; reference length $B_r = c$, (the chord length); phase angle (pitch leading heave) $\Phi_{ph} = \pi/2$; and for a pitching axis at the quarter chord position. Zero feathering parameter means that the angular amplitude of the pitch α, is zero. In this case, the wing is in pure heave motion. The computation mesh was taken as $NC \times NS = 10 \times 17$. The comparison of the thrust coefficient C_t and propulsive efficiency η in figures 6.3 and 6.4 show good agreement between the methods, although there are differences between the thrust coefficient predictions at high reduced frequency and feathering parameter.

Figures 6.5 and 6.6 show the results for the $B2$ wing by using the present method with two approaches: firstly, by only including the effect of steady wake vorticity in the computation of the leading-edge suction; and secondly, by including both steady and unsteady components of the wake vorticity in the computation of leading edge suction. In the first approach, good agreement can be seen between the methods for

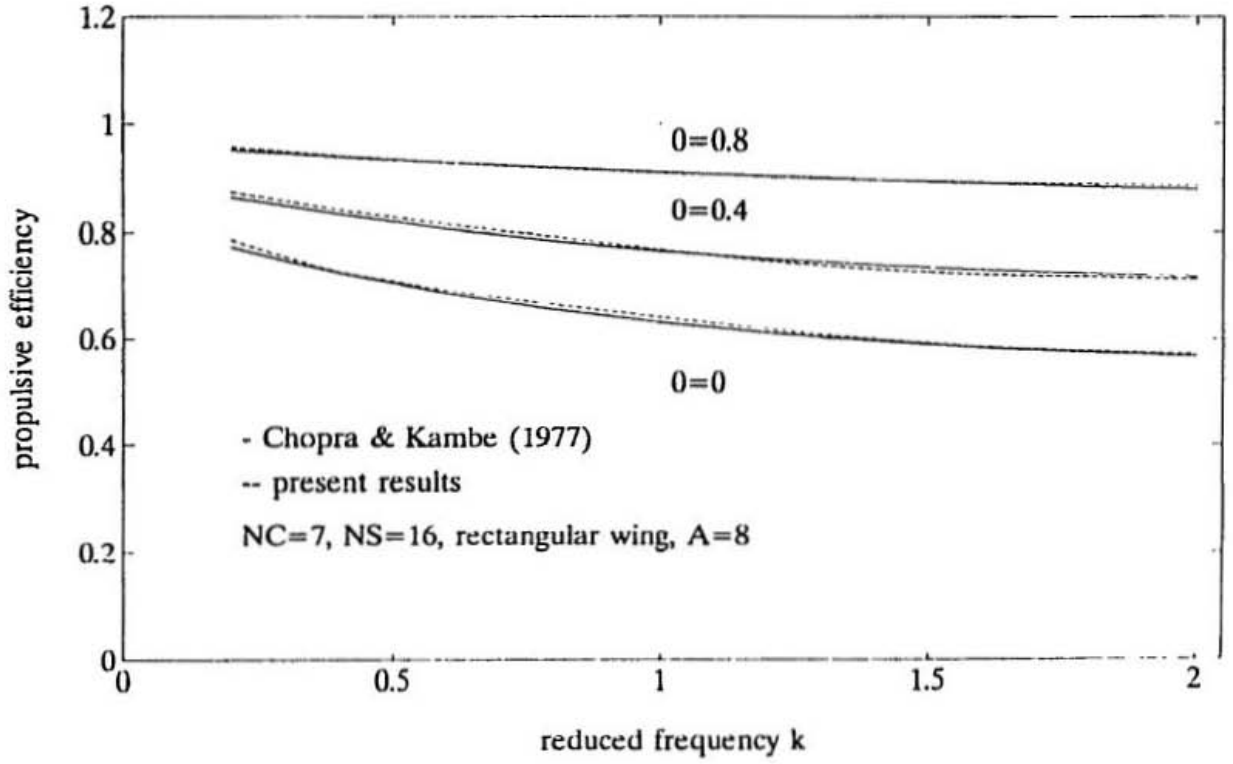

Figure 6.3: Propulsive efficiency vs reduced frequency k of a rectangular foil.

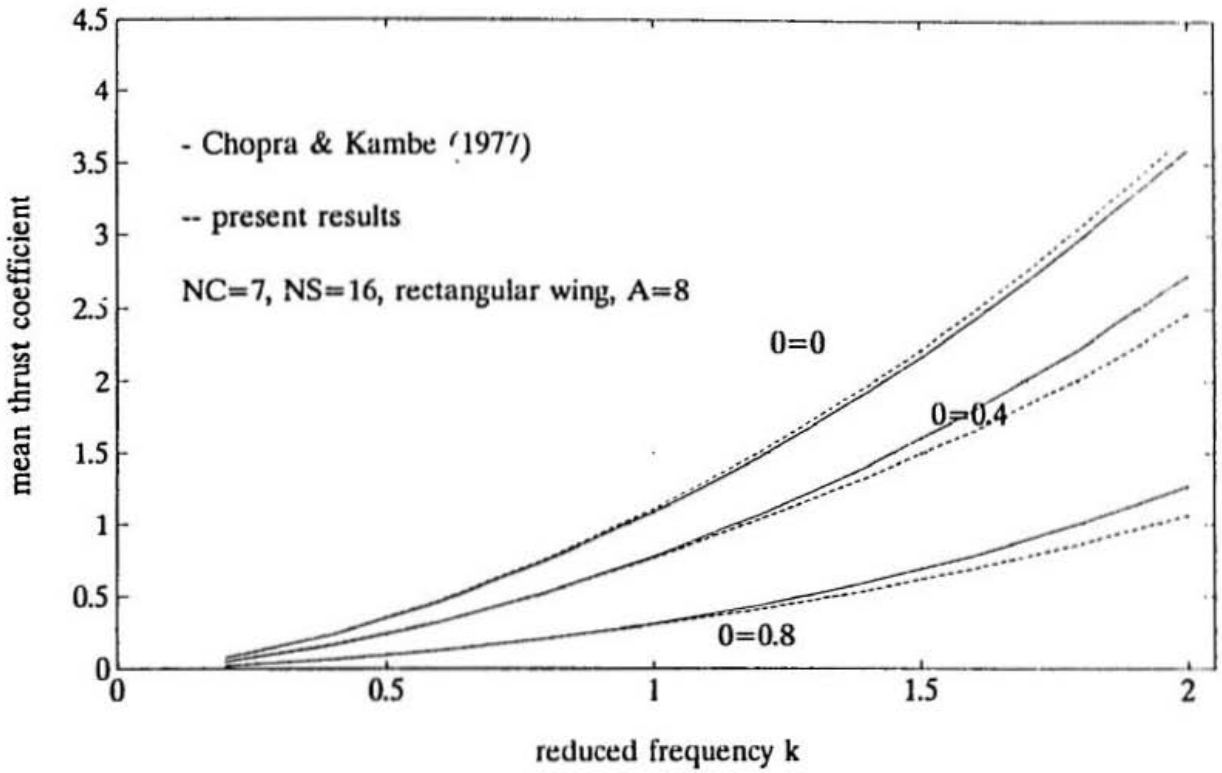

Figure 6.4: Mean total thrust coefficient vs reduced frequency k of a rectangular foil.

propulsive efficiency when $\theta \leq 0.4$. For thrust coefficient, discrepancies occur when k is large ($k \geq 1.5$). When the reduced frequency k and the feathering parameter θ are both large, agreement between results of efficiency is less good. In reality, in this situation, the angular amplitude of pitching may also be large; for example, when $k = 1.5, \theta = 0.8, h/B_r = 1, \alpha = \theta \cdot kh/B_r = 1.2rad = 68.7^0$. Small amplitude theory becomes inapplicable for high values of h/B_r. In the second approach, when the unsteady wake terms are included, efficiency and thrust coefficients of a swept wing are reduced from those found previously. These unsteady components were included in all the calculations which follow for the three cetacean flukes as it was felt that these terms should be included in a rigorous solution.

6.2 Discussion of the QVLM Method

From the foregoing section, the QVLM computer program was proved to be accurate and reliable in predicting the loading distribution for a circular planform configuration. Predictions of the leading-edge suction, the mean total thrust coefficient and the propulsive efficiency, for a rectangular wing, were also shown to be dependable, including either the unsteady terms or steady terms in the wake, based on the comparisons with the results of Lan (1979) and Chopra and Kambe (1977). However, as there are no comparable exact solutions or experimental data available, the reason for the differences compared with the predictions from other methods for swept wings, especially, for the curved trailing edge wings, cannot be explained. In the calculation of the leading-edge suction parameter, it is believed that all unsteady wake terms should be taken into account, as Lan (1979) did, because the computed upwash at each control point along the leading-edge has contributions

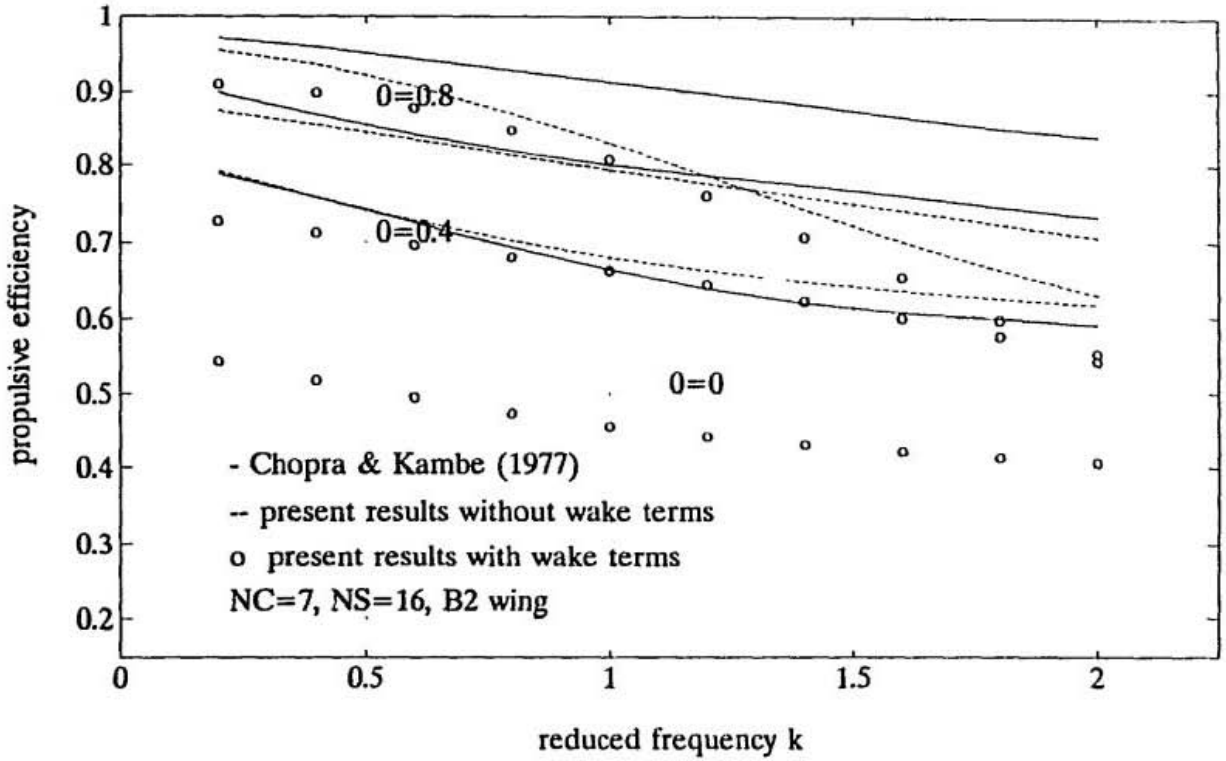

Figure 6.5: Comparison of predictions of propulsive efficiency η versus reduced frequency, k, for Chopra & Kambe's (1977) wing planform $B2$.

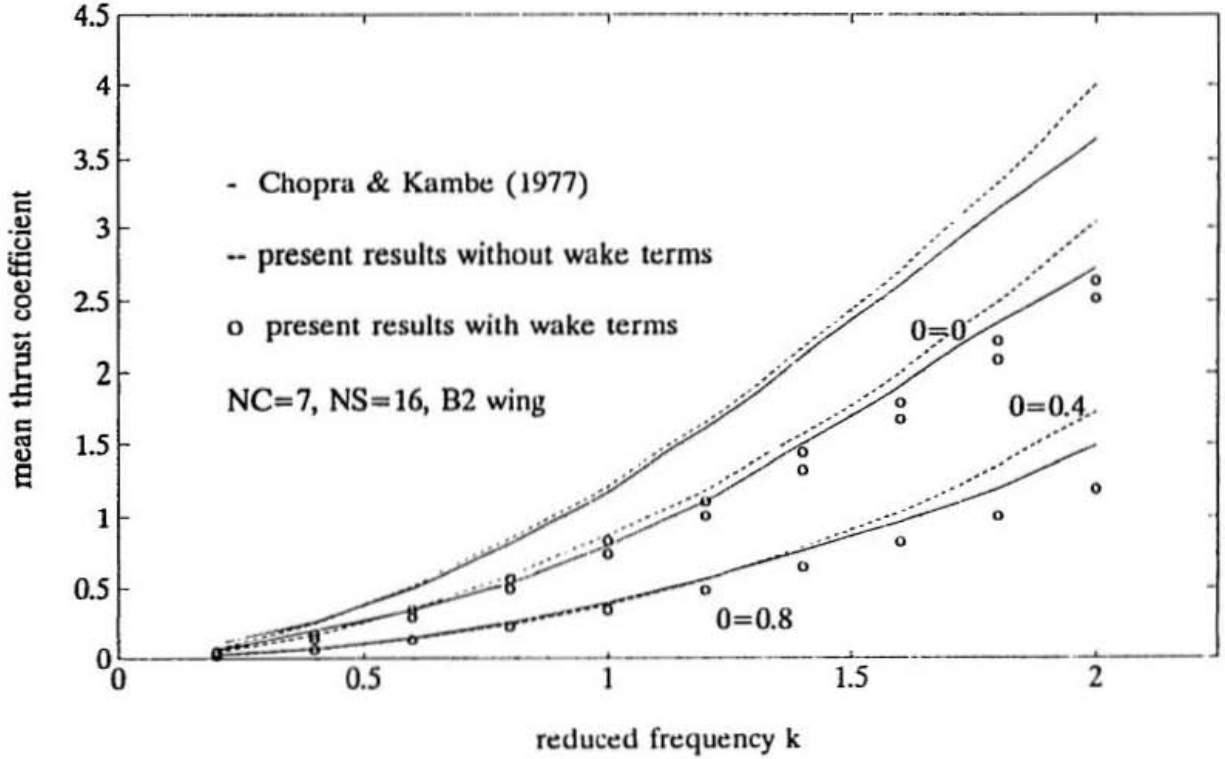

Figure 6.6: Comparison of predictions of total thrust coefficient C_t versus reduced frequency, k, for Chopra & Kambe's (1977) wing planform $B2$.

from all vortices on the lifting surface including self-induced vortices.

A theoretical deficiency in the QVLM development also exists: the Cauchy singularity problem is only solved in the chordwise direction, but a Cauchy singularity also exists in the spanwise direction. The tip singularity has the same importance as that at the leading-edge (Guermond, (1988)).

Collocationally, the vortex strip locations suggested by Lan (1974) cannot be accepted for certain wing shape configurations: for a circular wing, the first control point and the last control point of the vortex strips at wing tips are outside of the wing surface (Guermond (1988)).

Numerically, Lan's (1979) unsteady QVLM formulation consists of three approximations: the Jordan's approximation (Eq. 4.19); the integration of W_2 (Eq. 4.15); and when a non-planar wing is considered, the integration of W_3 (Eq. G.12). Jordan's approximation can be accepted in engineering applications because of its accuracy. In the approximation for W_2, it was found that the parabolic functions found from three points on the curve over the range of the integration used to approximate the integrand at the two boundaries of the curve at $\tau = 0$ and $\tau = 1$, where $\tau = 0$ and $\tau = 1$ are the integration limits along the doublet line from (x_1, y_1) to (x_2, y_2), had larger discrepancies compared with the curves calculated from a numerical integration that used using much closer interval spacings over the range of the integration. Plots showed that it was more appropriate to approximate the curves by higher even order polynomials such as fourth or sixth order functions for better accuracy. The quadratic function approximations lead to a limit in choosing the ratio of N_s/N_c (Albano and Rodden (1969)): to obtain best results, they suggested that the values of $2N_s/N_c$ should be taken as the same as the wing's aspect

ratio. For a non-planar wing, analytical integration needs to be done: the integrand can be approximated by a fourth order polynomial (the non-singular part); and the singular term.

Convergence of the results was rapid for the rectangular wing, as was also found by Lan (1979): for a rectangular wing, when $N_c \times N_s$ was taken as 48 and 80, the predicted propulsive efficiency had a difference of about 3% in the two cases (N_c is the number of the chordwise control points and N_s is the number of the spanwise control points on the half span). However, for wings with higher sweep angles or sharp tips, the number of the control points needs to be increased. The convergence of a method can be determined by the ratio of a near field induced drag to a far field induced drag of the same wing in the steady case (Lan (1974)). However, in the case of a wing in harmonic motion, the near field drag cannot be obtained because the value of angle of attack is not applicable.

The CPU time required for running the program was long: when N_c and N_s were taken as 10×16, the CPU time was about 30 minutes for a result at one reduced frequency and one feathering parameter when the calculation was done in a VAX 8530 computer; the CPU time was about 15 minutes in a DEC 3100 workstation, but the latter case is a single user system.

6.3 Propulsion of Three Cetaceans' Flukes

In the calculation and comparison for the thrust coefficient C_t and propulsive efficiency η of the flukes of three cetaceans, a parameter J, called the advance ratio, was used. This parameter was introduced by Bose and Lien (1989) and was defined

as

$$J = \pi V_\infty/(\omega h) = \pi B_r/(k \cdot h) = \theta\pi/\alpha. \tag{6.1}$$

For constant h and α, this advance ratio, J, increases when k decreases and increases when θ increases. In the following calculation of the flukes of three cetaceans, all computing mesh sizes were taken as $N_c \times N_s = 7 \times 16$. Figures 6.7 and 6.8 show the predictions for the $B2$ wing and a fin whale's flukes (*Balaenoptera physalus*) by using the present approach alongside a two-dimensional strip theory and the same strip theory with a 3D correction; the latter two results were presented by Bose and Lien (1989). The conditions are for a heave amplitude of $h = 1.5m$; a pitch amplitude $\alpha = 20^0$; the pitching axis is at the trailing edge of the root chord and the phase angle $\Phi_{ph} = \pi/2$. Results from the QVLM which models the three-dimensional effects of the flow show reduced levels of efficiency and thrust. The differences mainly due to the differences in aspect ratio, and at the lower values of advance ratio, i.e. below about 4, the practical angle of attack is large enough that separation would occur (Bose and Lien (1989)).

The geometric values for the three cetaceans' flukes were taken from measurements recorded by Bose and Lien (1989). The span of the planform is $S = 3.0m$, and the aspect ratio is 6.1. The oscillating parameters are $h = 1.5$, $\Phi_{ph} = \pi/2$, and $\alpha = 20^0$.

Comparisons of the predictions of propulsive efficiency η and thrust coefficient C_t versus advance ratio J, for the three cetaceans' flukes are shown in figures 6.9 and 6.10. The geometric values of the white whale's (*Delphinapterus leucas*) and white-sided dolphin's (*Lagenorhynchus acutus*) flukes were taken from Bose et al. (1990). The flukes of three cetaceans are shown in figure 6.11, and several parameters of

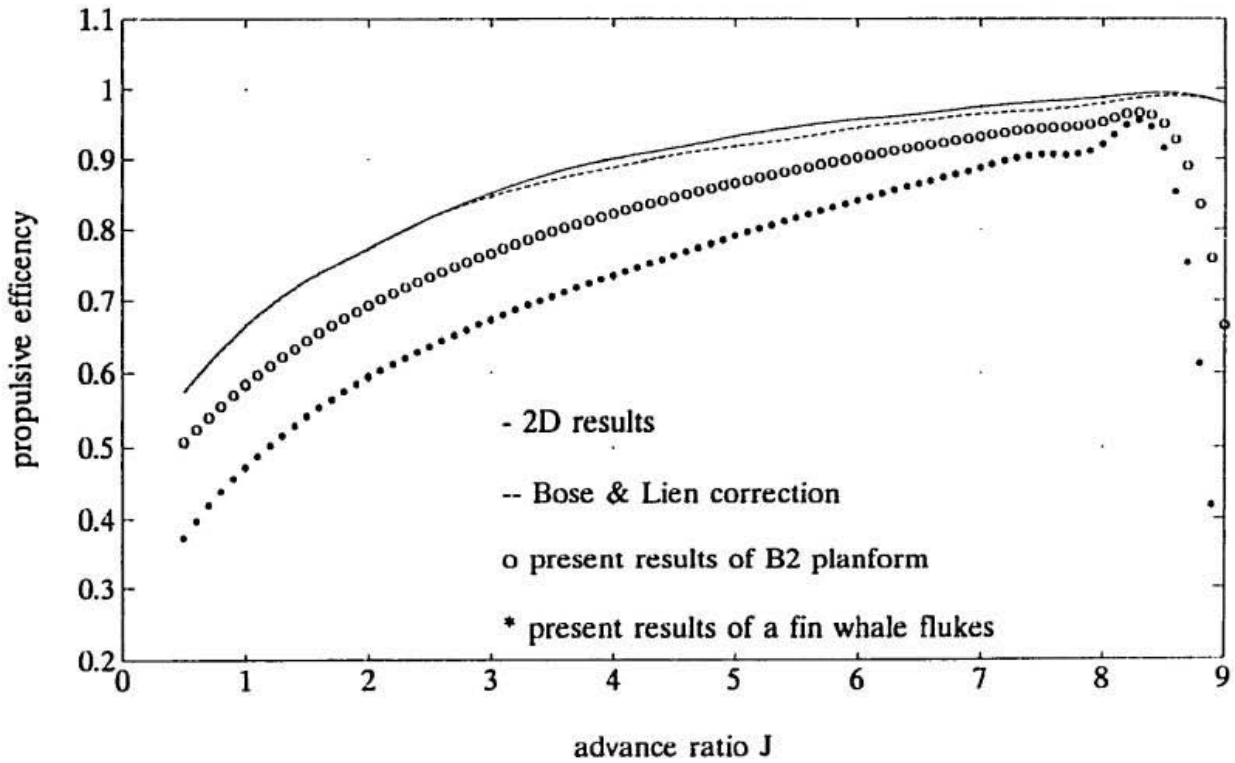

Figure 6.7: Predictions of propulsive efficiency vs advance ratio J for Chopra and Kambe's (1977) *B2* wing shown alongside a 2D strip theory and a 2D strip theory with a 3D correction from Bose and Lien (1989).

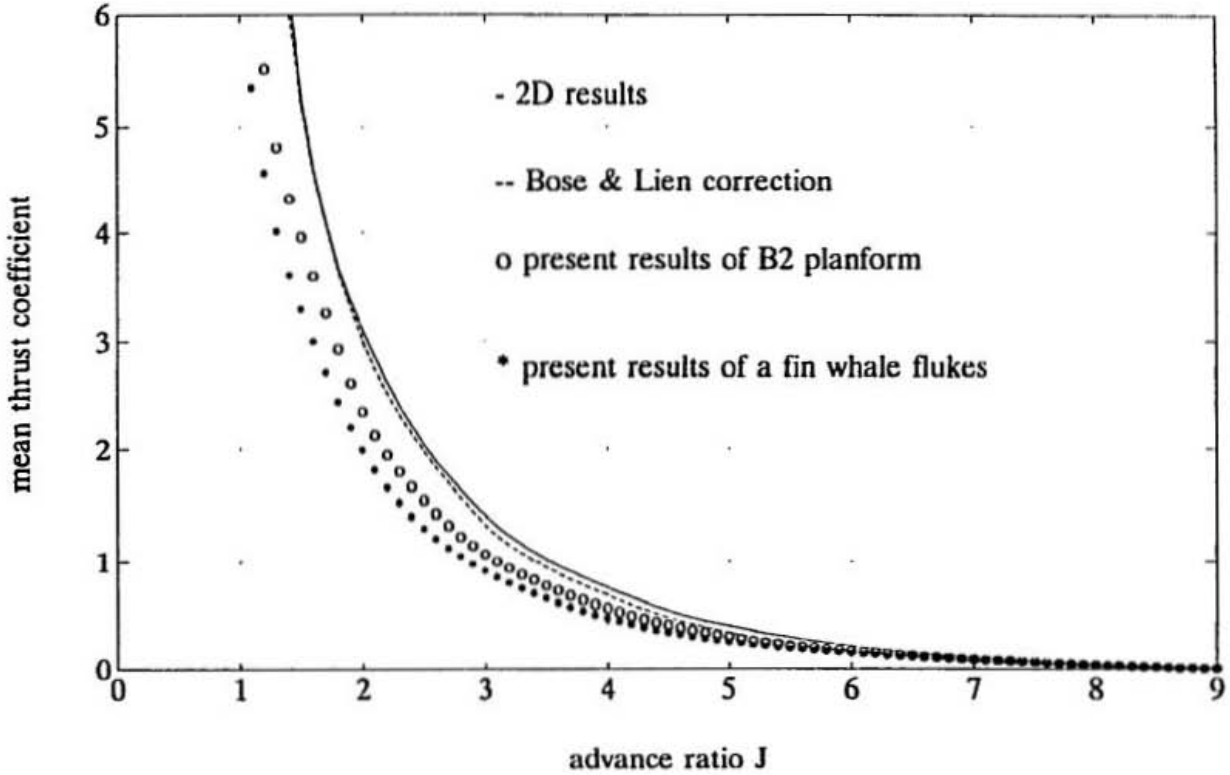

Figure 6.8: Predictions of thrust coefficient vs advance ratio J for Chopra and Kambe's (1977) $B2$ wing shown alongside a 2D strip theory and a 2D strip theory with a 3D correction from Bose and Lien (1989).

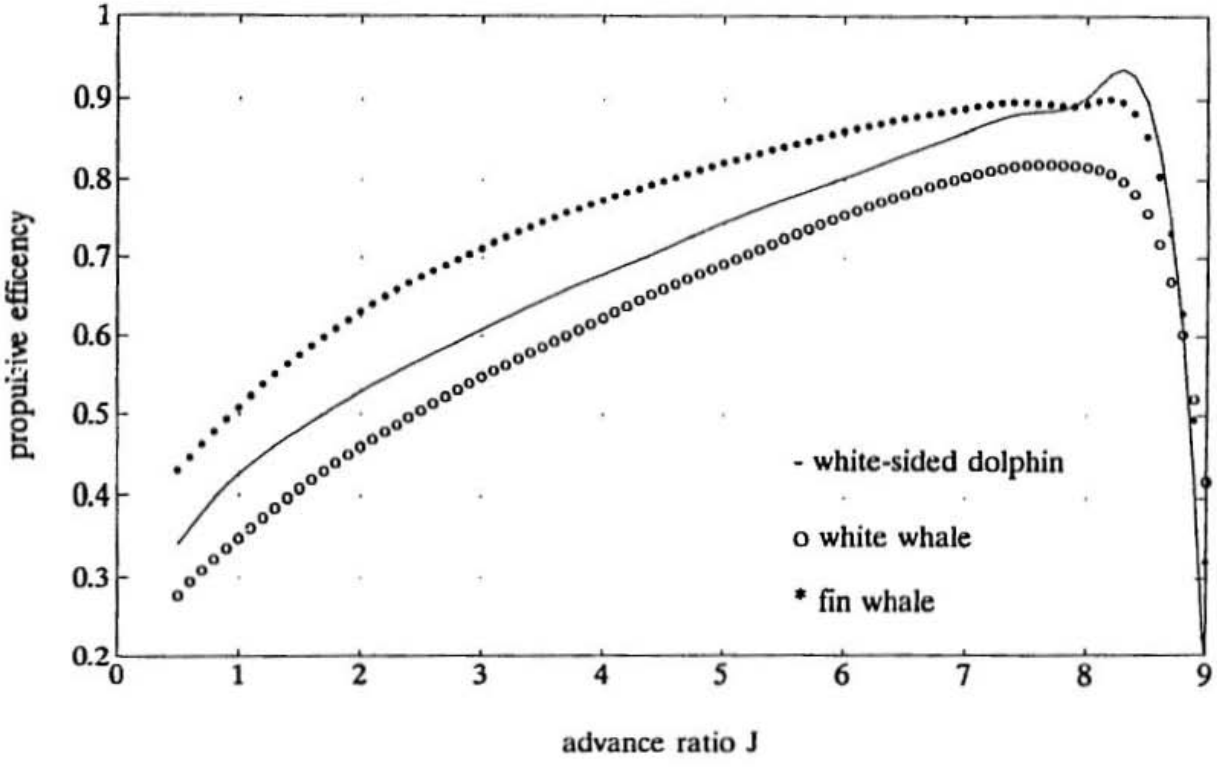

Figure 6.9: Comparison of propulsive efficiency versus advance ratio J of three cetaceans' flukes.

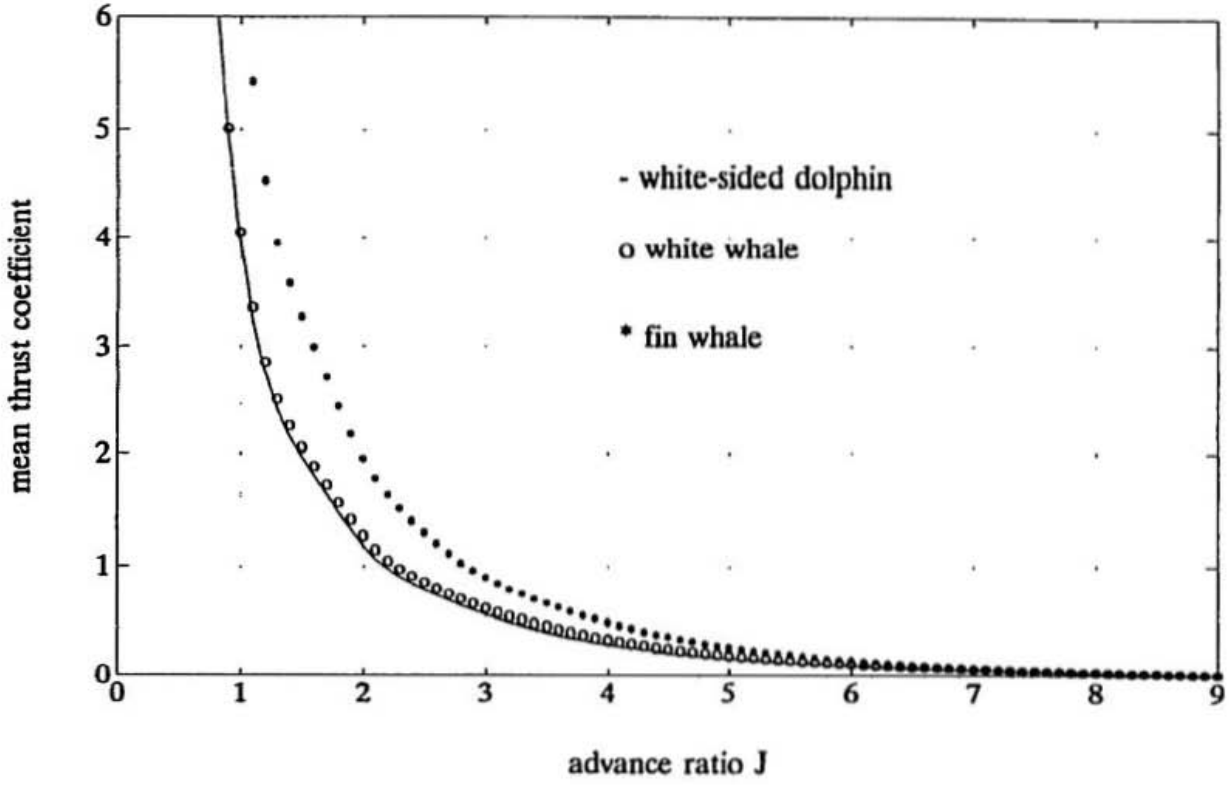

Figure 6.10. Comparison of mean thrust coefficient versus advance ratio J of three cetaceans' flukes.

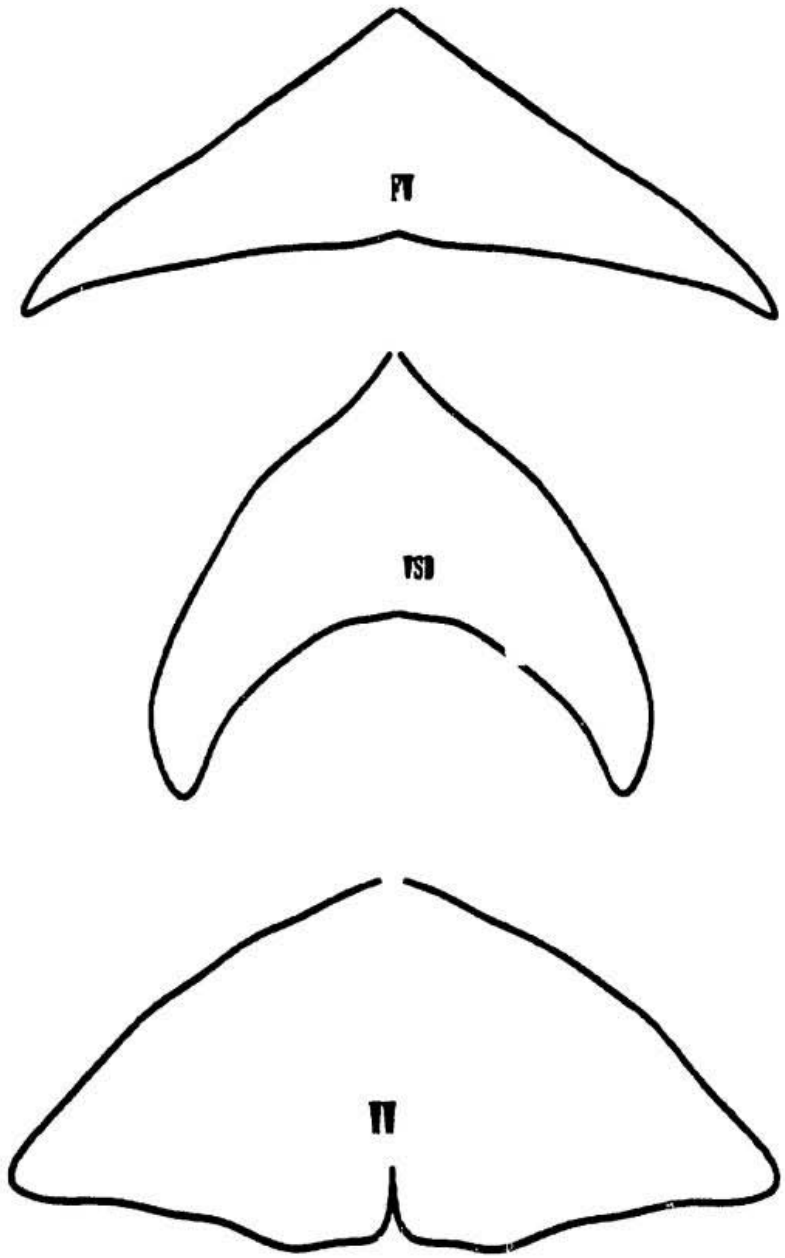

Figure 6.11: Three planforms of the lunate-tails of cetaceans. FW, WSD, and WW stand for fin whale, white-sided dolphin and white whale respectively.

	Span S	Aspect ratio A	Wing area S_w	Root chord C_r	Sweep angle Λ_l
FW	3.0 m	6.10	$1.485m^2$	$0.870m$	31.2
WSD	$0.25m$	2.72	$0.023m^2$	$0.127m$	47.0
WW	$0.758m$	3.25	$0.177m^2$	$0.362m$	28.3

Table 6.1: Main geometric parameters of three cetaceans' flukes. FW, WSD, and WW denote fin whale, white-sided dolphin, and white whale respectively.

these flukes used in calculation are listed in table 6.1.

The propulsive efficiency and thrust coefficient vary with the different heave amplitude h. This makes the comparison of these three planforms difficult. Two ways were considered for choosing h to give a comparable basis: set h as the root chord; or to an averaged chord length.

In the calculation of the predictions in figures 6.9 and 6.10, the amplitude of heave was taken as the root chord C_r (given in table 6.1). All phase angles were $\Phi = \pi/2$, and all angular amplitudes of pitch were $\alpha = 20^0$.

As the aspect ratio of the fin whale's flukes is largest and is about twice that of the white-sided dolphin's and white whale's, the propulsive efficiency and thrust coefficient from this animal's flukes are much higher than those from the others over most of the range of advance ratio, J. The aspect ratio of the white-sided dolphin's flukes is less than that of the white whale's, however, the propulsive efficiency from the flukes of the white-sided dolphin's is noticeable higher. The thrust coefficient of the fin whale's flukes is also much higher than those of others. This is partially due to the choice of the amplitude of heave h (h is chosen as the root chord length C_r); the value of h/B (B is the length of span) of the fin whale's flukes was small, hence

higher thrust coefficient appears (see Eq. (79), Lighthill (1970)).

Further investigations were done on the effects of changes in pitching axis positions and on the phase angle values (pitch leading heave) on the propulsive efficiency and thrust coefficient. In all calculations related to changes in pitching axis, the phase angle was taken as $\Phi_{ph} = \pi/2$; the amplitude of heave, $h = C_r$ (where C_r is the root chord length); reference length $B_r = C_r$; and feathering parameter $\theta = 0.8$ (higher values of feathering parameter lead to higher efficiency). The prediction of propulsive efficiency η, thrust coefficient C_t and leading-edge thrust coefficient C_{tl} against the changes in the pitching axis positions over the range from $-0.5C_r$ to $2.5C_r$, where C_r is the root chord length, for the reduced frequencies, $k = 0.15$ and 0.75 are plotted in figure 6.12 through figure 6.15. These figures show that the maximum propulsive efficiency occurs at the pitching axis position $B_0 = 0.7C_r, 0.8C_r$, and $0.6C_r$ for the flukes of fin whale, white-sided dolphin and white whale respectively. The mean thrust coefficient C_t is minimum at $B_0 \simeq 0.6C_r$ (figures 6.13 and 6.15). Figures 6.12 and 6.14 show that when $k = 0.15$, the variation of the propulsive efficiency η and the total mean thrust coefficient C_t is small: over this range in pitching axis position the variations in efficiency are 0.066, 0.064, 0.115 and in thrust coefficient are 0.0014, 0.0006, 0.0007 for fin whale, white-sided dolphin and white whale respectively.

The results for reduced frequency $k = 0.75$ are shown in figures 6.14 and 6.15. Here the maximum efficiency η occurs at about the same position as in the case of $k = 0.15$. The minimum thrust coefficient C_t occurs at the same position as that of η_{max}. The variation of the efficiency η was larger at this higher value of reduced frequency; over this range of pitching axis position the variations in the propulsive

efficiency η are 0.301, 0.330, and 0.323 for the fin whale's, white-sided dolphin's and white whale's flukes respectively. From $-0.5C_r$ to $2.5C_r$, the changes of the mean total thrust coefficient C_t are also different at this higher value of reduced frequency; the variations are 0.648, 0.320, and 0.298 for the three kinds of flukes. The difference between total mean thrust coefficient C_t and leading edge thrust coefficient C_{tl} over the range of pitching axis locations is almost constant (this result was also found at other reduced frequencies) for the fin whale's flukes and tends to zero at $B_0 = 2.5'$ for the other two sets of flukes (see figure 6.15). For the fin whale's flukes, this means that the increase of total mean thrust coefficient comes mainly from the increase in the leading-edge suction, while the lift contribution to the total thrust is constant throughout the range. For the other two sets of flukes, this means that the lift contribution to the total mean thrust is about zero at $B_0 = 2.5C_r$, i.e. the leading-edge suction is the total thrust when the pitching axis position is at $B_0 = 2.5C_r$.

Figure 6.16 through figure 6.19 show the effects of changing phase angle between heave and pitch on the propulsive efficiency η, mean total thrust coefficient C_t and leading-edge thrust coefficient C_{tl} at the reduced frequencies $k = 0.15$ and $k = 0.75$. The maximum efficiency η occurs at the phase angle in a range of $\Phi_{ph} = 90^0 \sim 110^0$ when both $k = 0.15$ and $k = 0.75$ (see figures 6.16 and 6.18). It is also seen that the positions of maximum efficiency tend to move to higher phase angle values when the reduced frequency k is increased. From figures 6.17 and 6.19, for all these three kinds of the flukes, it is seen that the minimum thrust coefficient C_t occurs at $\Phi_{ph} = 100^0$ for $k = 0.15$ and $\Phi_{ph} = 135^0$ for $k = 0.75$ and the maximum thrust coefficient C_t is at $\Phi_{ph} = 275^0$ for $k = 0.15$ and at $\Phi_{ph} = 280^0$ for $k = 0.75$.

When $60^0 \leq \Phi_{ph} \leq 125^0$ at $k = 0.15$ and $75^0 \leq \Phi_{ph} \leq 130^0$ at $k = 0.75$, the total

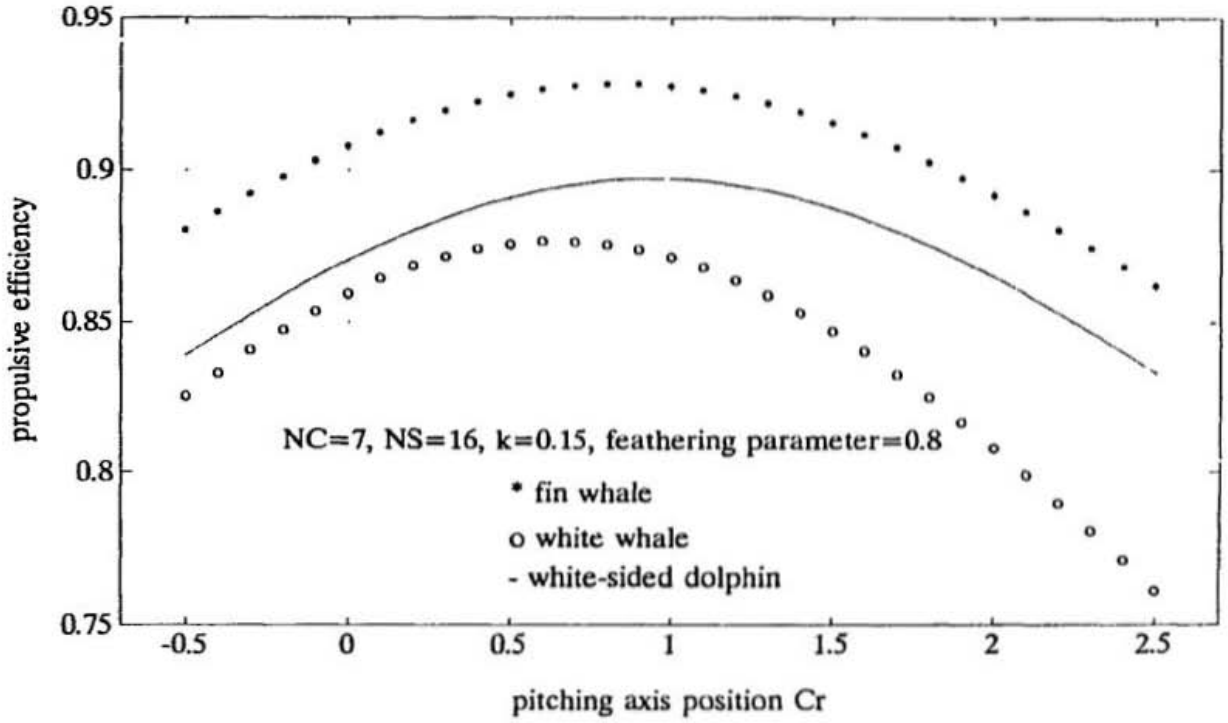

Figure 6.12: Variation of efficiency with change in pitching axis position for three cetaceans' flukes for reduced frequency $k = 0.15$, feathering parameter $\theta = 0.8$.

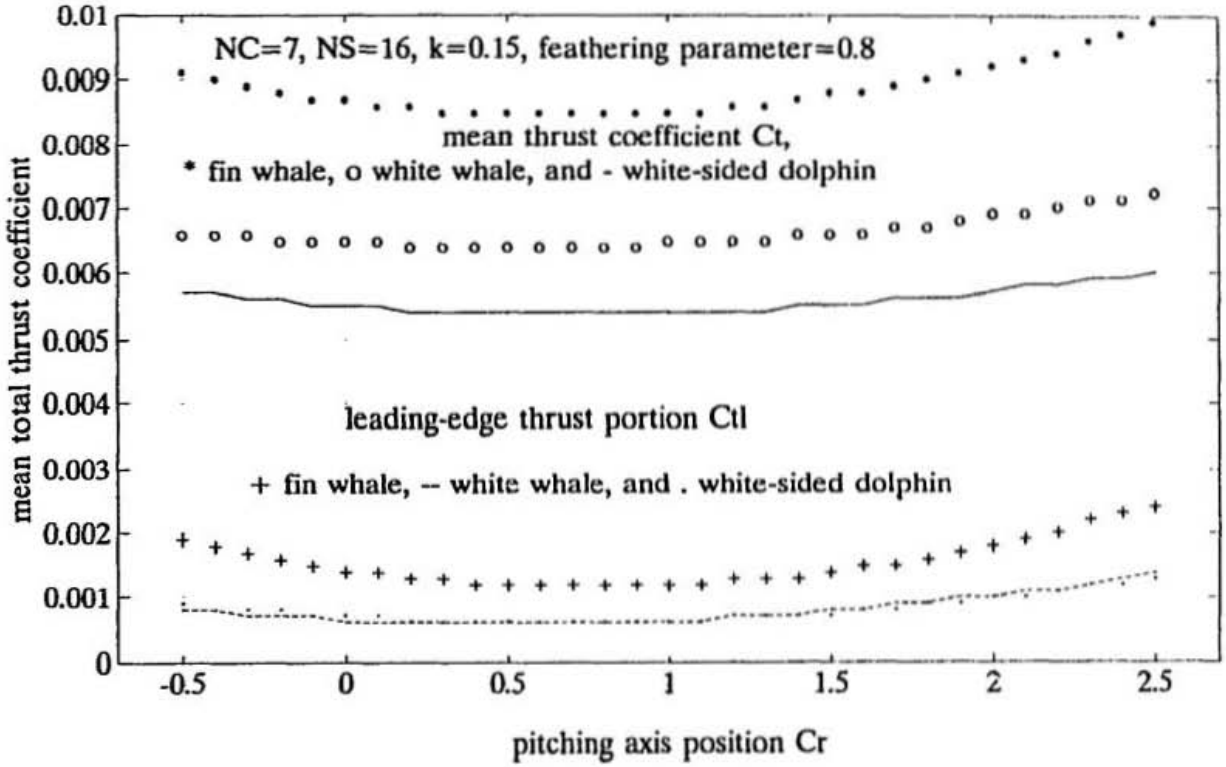

Figure 6.13: Leading-edge thrust and total mean thrust coefficient vs location of pitching axis for the three cetaceans' flukes for reduced frequency $k = 0.15$, feathering parameter $\theta = 0.8$.

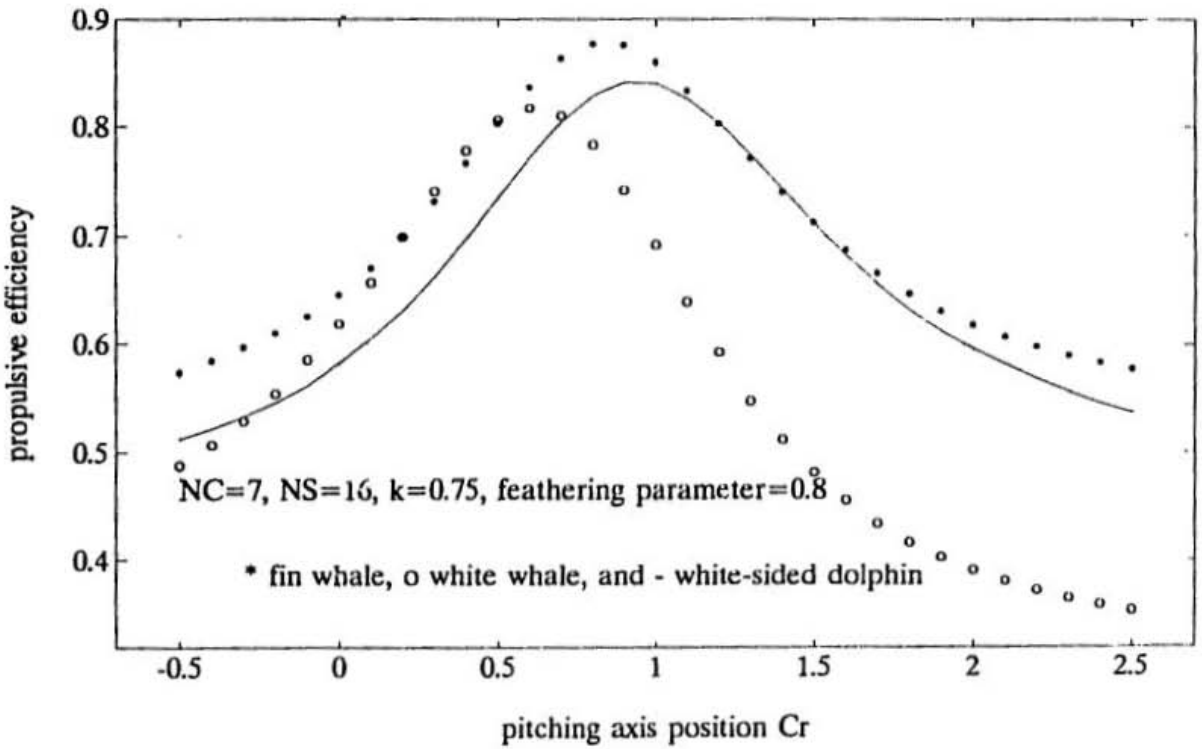

Figure 6.14: Variation of efficiency with change in pitching axis position for three cetaceans' flukes for reduced frequency $k = 0.75$, feathering parameter $\theta = 0.8$.

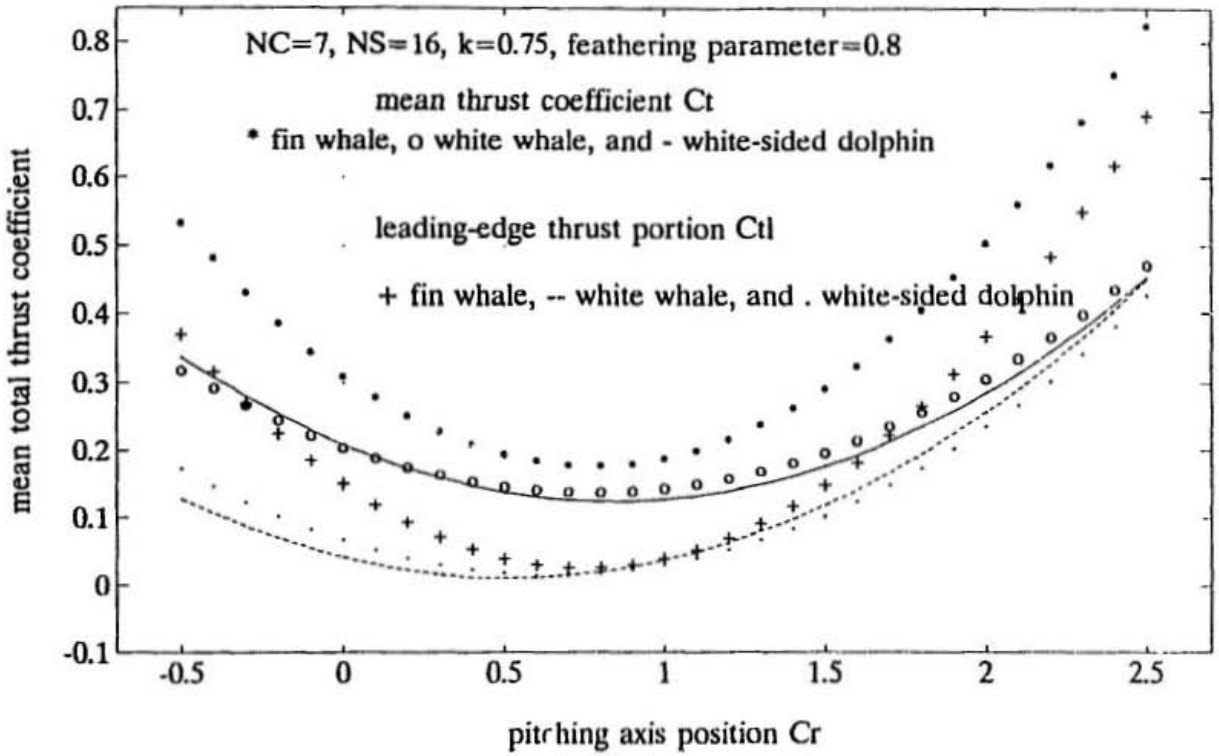

Figure 6.15: Leading-edge thrust and total mean thrust coefficient vs location of pitching axis for three cetaceans' flukes for reduced frequency $k = 0.75$, feathering parameter $\theta = 0.8$.

thrust coefficient is greater than the leading-edge thrust coefficient. This implies that at about $\Phi_{ph} = 100^0$, the lift component $L\alpha$ of the total thrust is a positive contribution, while at $\Phi_{ph} = 270^0$, the lift component $L\alpha$ leads to maximum drag. This is why the maximum efficiency η_{max} occurs at about $\Phi_{ph} = 100^0$ and minimum efficiency η_{min} occurs at about $\Phi_{ph} = 270^0$. Figure 6.16 through 6.19 also reveal that the highest efficiency and the lowest thrust appear at about the same value of phase angle between pitch and heave and vice versa. In addition, the fin whale's flukes can produce positive thrust at any phase angle value. In contrast, when the reduced frequency $k = 0.15$, white whale's flukes produce negative thrust (drag) at $150^0 \leq \Phi_{ph} \leq 330^0$, and when $k = 0.75$, both white whale's and dolphin's flukes produce negative thrust around $\Phi_{ph} = 250^0$, and the range of the phase angle of the production of negative thrust from white whale's flukes is wider. This showed that swept wings with relatively high aspect ratio produce high thrust forces.

6.4 Restrictions on Dimensions of an Oscillating Foil Propeller in Marine Applications

In practical engineering design, questions arise about the size of a real oscillating propeller at the stern of the ship, and its restrictions in terms of pitching and heaving amplitudes. A multiflex cargo ship of length $L = 133.3m$ and displacement $\Delta = 17930\ t$ is given below as an example (Harvald (1983), page 314). The resistance of the ship varies with speed and is listed in table 6.2. Results of performance of the fin whale's flukes are used to obtain dimensions of an oscillating propeller. As the breadth of the ship is $20.5m$, the maximum span of the oscillating foil should not exceed $20.5m$. Assuming that the span of the oscillating propeller is $B_m = 20.5m$,

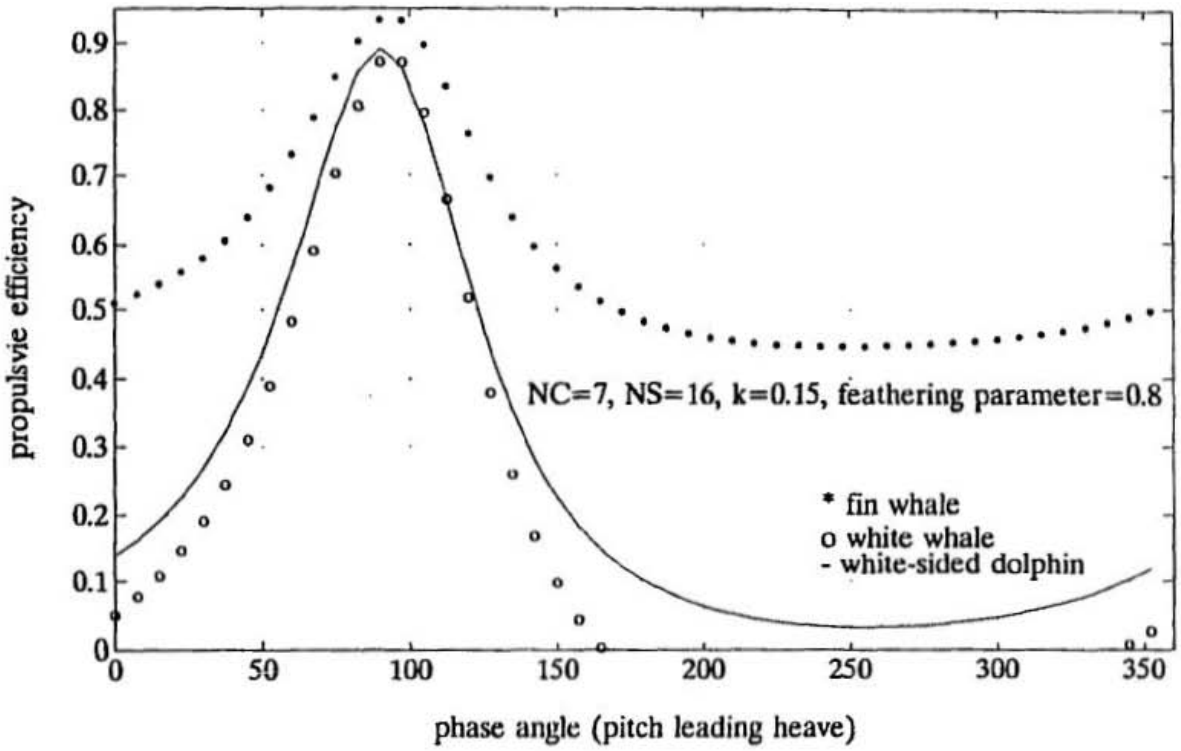

Figure 6.16: Efficiency vs changes in phase angle between heave and pitch motions for three cetaceans' flukes for reduced frequency $k = 0.15$, feathering parameter $\theta = 0.8$.

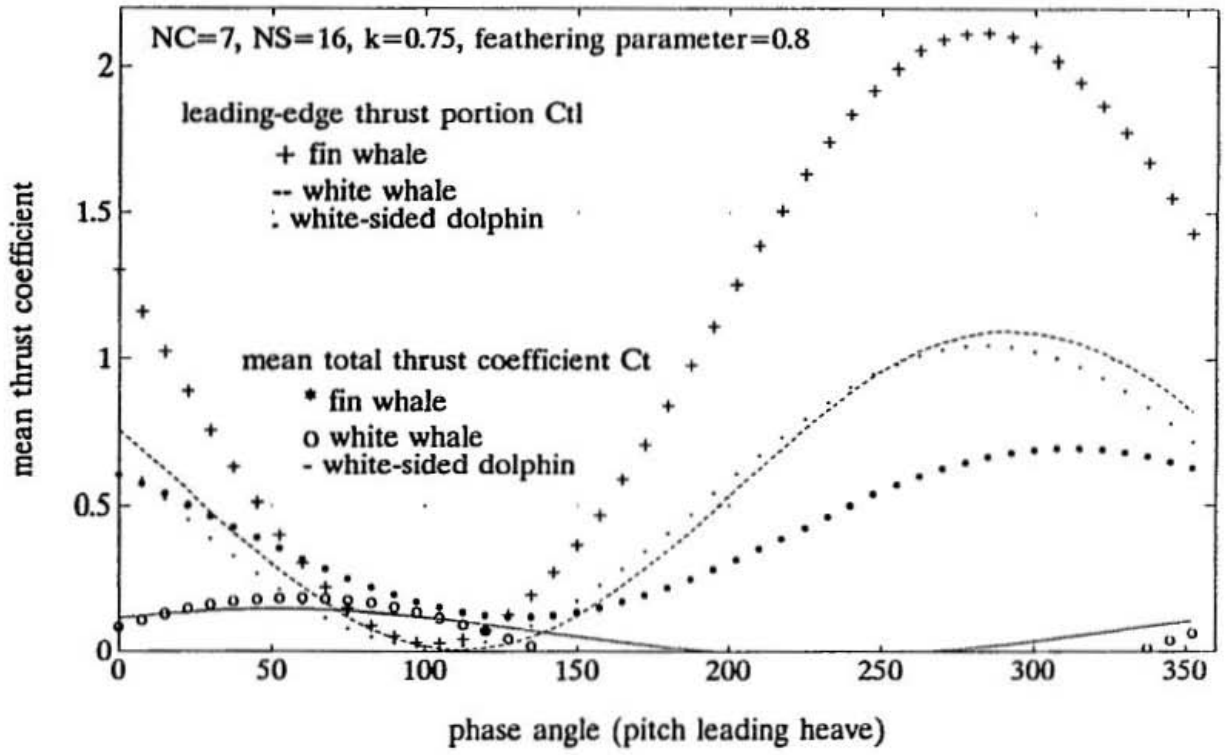

Figure 6.17: Leading-edge thrust and total mean thrust coefficient vs changes in phase angle between heave and pitch motions for three cetaceans' flukes for reduced frequency $k = 0.15$, feathering parameter $\theta = 0.8$.

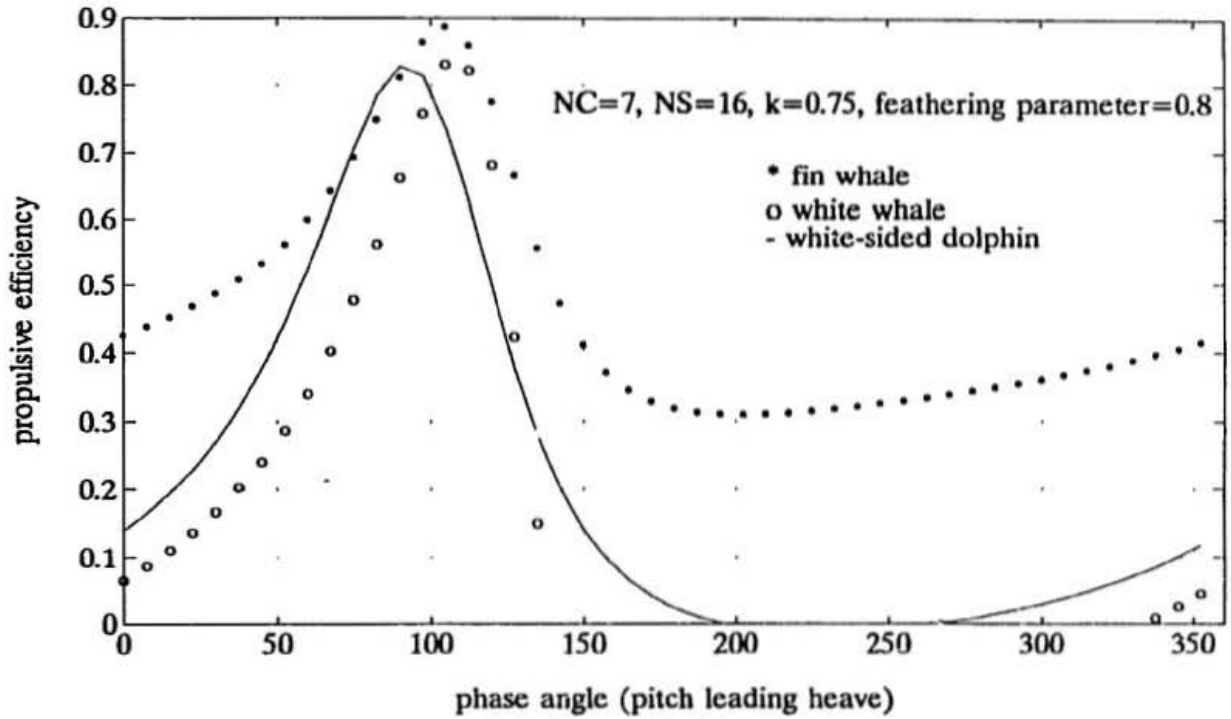

Figure 6.18: Efficiency vs changes in phase angle between heave and pitch motions for the three cetaceans' flukes for reduced frequency $k = 0.75$, feathering parameter $\theta = 0.8$.

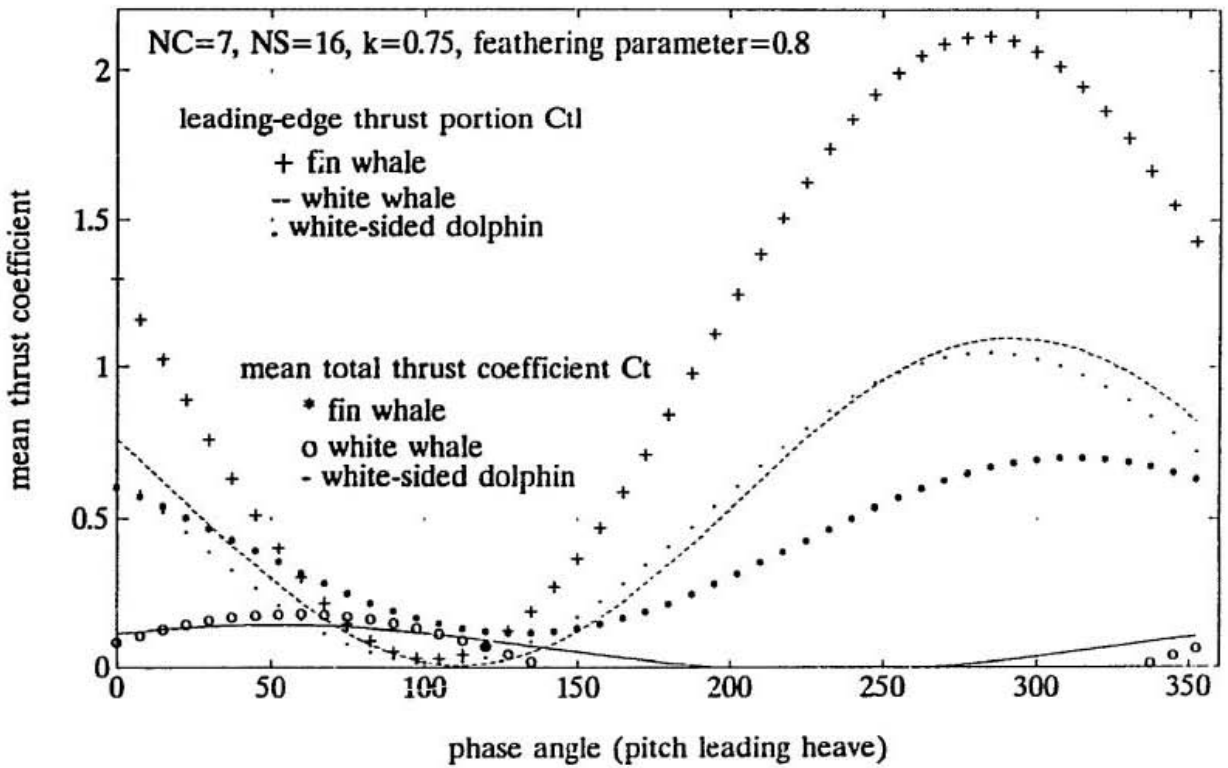

Figure 6.19: Leading-edge thrust and total mean thrust coefficient vs changes in phase angle between heave and pitch motions for the three cetaceans' flukes for reduced frequency $k = 0.75$, feathering parameter $\theta = 0.8$.

- advance ratio $J = 2.95$;
- oscillating frequency $\omega = \pi V_\infty/(Jh) = 2.66 rad/s$;
- propulsive efficiency $\eta = 0.71$;
- reduced frequency $k = 1.064$ (because the reference length is taken as $B_r = h_m = 4.0m$;
- wing area $S = \frac{2R}{\rho V_\infty^2 C_t} = 22.92m^2$;
- the span of the man-made propeller is then $B_m = 11.80m$.

Under the restrictions above on heave amplitude h, the maximum efficiency that can be achieved is 0.71, and the wing's span is $11.80m$. Restrictions on the amplitude of the pitch reduced the propulsive efficiency from 0.82 to 0.71. The propulsive efficiency can be improved by increasing the aspect ratio of the wing while keeping the amplitude of pitch at the maximum possible value.

Table 6.4 shows powering predictions when the example ship is fitted with an oscillating propeller. Variations of the required input power with the changes in speed of the ship are given (drag effects of the propeller are not taken account).

If a higher aspect ratio wing is used, the input power may be reduced. An optimized dimension of an oscillationg foil, and its heaving and pitching amplitudes, should be considered carefully when designing an oscillating propeller. Usually, higher angular pitching amplitude α produces higher thrust coefficient. However, the theory is based on the small amplitude assumption which is not applicable when α is too big.

it can be shown that the wing area is $S = 69.34m^2$; and the root chord length is $5.95m$. By using figures 6.9 and 6.10, and taking the service speed $V_\infty = 10m/sec$, the reference length $B_r = C_r = h$ (where C_r is the root chord length, and h is heave amplitude), the results for the oscillating propeller were obtained and these are listed table 6.3.

For the man-made oscillating propeller, relative parameters were obtained after interpolation: $J = 4.86$, $\eta = 0.82$, $C_t = 0.308$, $\omega \simeq 0.74\ rad/sec$ and $k \simeq 0.45$.

It is noted that the average chord length of the fin whale's flukes is

$$C_a = S_w/B = 1.485/3.0 = 0.495m$$

and the ratio of root chord to average chord is

$$C_r/C_a = 0.87/0.495 = 1.77.$$

Therefore, the average chord of the man-made propeller is

$$C_{am} = B_m/A = 20.5m/6.1 = 3.36m,$$

and the heave amplitude of the propeller is

$$h_m = C_{rm} = 1.77C_{am} = 5.95m.$$

However, the draft of the ship is $T = 9.10m$. As the draft should be $T > 2h_m = 11.90m$, the amplitude h_m is impractical for this ship.

Restrictions on draft lead to a value of heave amplitude of the propeller $h_m \leq (T/2) \simeq 4.0m$. The corresponding heave amplitude h of the fin whale's flukes is then $h = 4.0\frac{C_r}{C_{rm}} = 0.55$. Let $h = 0.5m$, then the thrust coefficient is $C_t = 0.308\frac{0.87^2}{0.50^2} = 0.933$. From C_t, other corresponding values were obtained as:

6.5 Comments on the Planform Configuration of Man-made Oscillating Propellers

It is well known that the higher the aspect ratio of a foil, the higher the propulsive efficiency. That the fin whale's fluke's had maximum propulsive efficiency was mainly due to its flukes aspect ratio. In addition, the thrust coefficient was related to heave amplitude: when the heave amplitude h decreased, the thrust coefficient C_t increased. At fixed phase angle values, the sweep angle of a wing at the leading edge affected the thrust coefficient (figures 6.17 and 6.19); wings with higher sweep angles produced higher thrust coefficient. However, the propulsive efficiency for the swept back wings had a sharp drop at larger reduced frequencies ($k \geq 1$, when the reference length B_r was taken as the root chord length C_r); while at small reduced frequencies ($k \simeq 0.2$), the swept back wings had higher propulsive efficiency than that for a rectangular foil. Over a wide range of reduced frequency k ($0.5 \sim 1.0$), fin whale's flukes were the best planform studied for both maximum propulsive efficiency and thrust coefficient. In engineering applications, the shape of an oscillating foil may be difficult to manufacture in the form of a fin whale's flukes because of the limitations in manufacturing methods. However, a compromise shape between that of a rectangular wing and a fin whale's flukes might be a possible choice.

The propulsive efficiency and thrust coefficient from a flexible, finite span, oscillating foil is relevant to the study of practical oscillating propellers. Generally, oscillating propellers in nature have both spanwise and chordwise flexibility (Bose and Lien, (1989)); this flexibility has been neglected in this work. Further study in aeroelastic propulsion problems is recommended in the investigation of swimming

animals' propulsion phenomena.

V_∞(meter/sec)	10.00	9.00	8.00	7.00	6.00	5.00
V_∞(knots)	19.44	17.50	15.55	13.61	11.66	9.72
R(kN)	1095.9	585.1	385.0	287.8	209.8	144.0
P_e(kW)	11000	5300	3100	2000	1300	700

Table 6.2: Resistance versus speed of an example ship. R is resistance, and P_e is effective power.

k	0.4	0.8	1.2	1.6
$\omega(rad/sec)$	0.67	1.34	2.02	2.69
J	7.86	3.93	2.62	1.96
η	0.90	0.76	0.67	0.60
C_t	0.05	0.587	1.337	2.870
$S(m^2)$	427.60	36.43	16.00	7.45
S/S_w	288	25	11	5
$(S/S_w)^{1/2}$	17.98	4.95	3.28	2.24
B_m(m)	53.94	14.85	9.84	6.72

Table 6.3: Calculation of the dimensions of an oscillating foil propeller. S is required wing area at corresponding speed; B_m is the span of the man-made oscillating propeller; S_w is the area of the fin whale's flukes.

V_∞(meter/sec)	10.00	9.00	8.00	7.00	6.00	5.00
V_∞(knots)	19.44	17.50	15.55	13.61	11.66	9.72
P_e(kW)	11000	5300	3100	2000	1300	700
$I.P$(kW)	1600	7500	4400	2900	1800	1000

Table 6.4: Input power versus speed of an example ship. P_e is effective power, and $I.P.$ is input power.

Chapter 7

Conclusion

Lifting-surface theory for three dimensional, unsteady wings was investigated. A computer program incorporating an unsteady quasi-vortex-lattice method, a numerical method based on the vortex-lattice method, was written. This computer program was checked by comparing its output with the published results from three planforms. From those comparisons, it was seen that the program was reliable. Rapid convergence was found between predicted results and number of vortex lattice elements for rectangular wings; for wings of arbitrary planforms, a larger number of elements were required for similar accuracy. The advantages and disadvantages of the QVLM method were discussed.

In the analysis of fast swimming animal's propulsion, the computer program was used to predict the propulsive performance of the three cetaceans' flukes. The variations of propulsive efficiency and thrust coefficient with changes in pitching axis and phase angle between pitch and heave were analysed. An example of the fin whale as a marine oscillating propeller was given based on a rough calculation. The dimensions of a practical oscillating propeller and its restrictions in operation were discussed. The qualitative analysis of the shape of an oscillating propeller was also

discussed. This shed some light on practical marine oscillating propeller design.

7.1 Verification of the Computer Program

In the verification of the computer program, the predictions for three planforms were checked with previous results. The lift distribution of a circular wing obtained by the present computer program showed accurate predictions compared with analytical results. The predictions of propulsive efficiency and thrust coefficient from a rectangular wing agreed well with the results calculated by Chopra and Kambe (1977). Propulsive efficiency and mean total thrust coefficient of an idealised lunate-shaped wing ($B2$ wing) had reduced values in comparison with a rectangular wing of the same aspect ratio. The results for this lunate-shaped ($B2$) wing had reduced values compared with the results from Chopra and Kambe (1977), especially, at higher reduced frequency. As there were not any experimental or analytical results available for the planform, the reason for these discrepancies is unknown.

7.2 Numerical Model

The unsteady quasi-vortex-lattice method (QVLM) is reliable and accurate in predicting the loading distribution for the circular planform. For a rectangular wing, the predictions of the leading-edge suction, the mean total thrust coefficient and the propulsive efficiency are also reliable. The dependability and reliability of the QVLM in predicting the propulsive performance for sharp tip wings, or wings with high sweep angle, cannot be determined. Experimental data are important in the further development of the method.

The Cauchy singularity problem was only solved in the chordwise direction in

the development of QVLM. A singularity in the spanwise direction exists and this singularity may become important at the sharp variations in the loading function at wing tips.

In the integrations of W_2 and W_3, Lan (1979) followed Albano and Rodden's (1969) approach, employing parabolic functions to approximate the non-singular parts in the integrand of W_2 and W_3. The plots from these non-singular parts have discrepancies compared with the parabolic functions, and the differences vary with the locations of the vortex strips, and the sweep angle of the vortex strips. The accuracy of the results may be improved by using approximating functions with higher orders (the order number should be an even integer). Higher order functions increase the difficulties to integrate the approximated integrand exactly.

Convergence of the computation is rapid for a rectangular wing. Mesh size should be increased when calculating for a wing with higher sweep angle, or sharp tips. An appropriate ratio of chordwise control points to spanwise control points can improve the convergence in terms of program accuracy versus mesh size.

The CPU time of the program is long. Further work on reducing the CPU time, might be accomplished by a rearrangement of the matrix. This rearrangement is only possible when the wing is symmetrical.

7.3 Three Cetaceans' Flukes as an Oscillating Propeller

Among the three planforms studied (fin whale, white whale, and white-sided dolphin), fin whale's flukes produced much higher thrust coefficient and propulsive efficiency. High aspect ratio and an appropriate sweep angle are the main attributes

of a good propulsive performance.

Different planform shapes have a different pitching axis position for the best propulsive efficiency. This position is around the three quarter chord position. The rate of variation in propulsive efficiency with changes in pitching axis is related to the reduced frequency k. When the reduced frequency k is small, the variation is small; when the reduced frequency is large, the variation is large. This indicates that in practical operations, the pitching axis position for the best propulsive efficiency should be placed in accordance with the largest possible operating reduced frequency.

The maximum propulsive efficiency and the smallest thrust coefficient occurred at about the same pitching axis position. This indicates that under low hydrodynamic loading conditions, the foil can achieve a high efficiency. However, if the wing area is limited, some portion of the efficiency has to be sacrificed to create the required thrust to sustain the speed of a marine vehicle.

At the reduced frequency $k = 0.75$, the difference between total mean thrust coefficient C_t and the leading-edge thrust coefficient C_{tl} over the range of pitching axis position is constant for a fin whale's flukes. In another words, with the increase of the pitching axis distance (from the mid-chord towards the trailing edge), the leading-edge thrust portion increases. Especially, for the low aspect ratio planforms studied, when the pitching axis is far behind the mid-chord, the leading-edge thrust increases sharply. Large leading-edge thrust can result in leading-edge separation, reducing the propulsive efficiency in practice. This should be avoided.

For any planform, the phase angle effects on the propulsive efficiency and thrust coefficient were very important. Best phase angle values are around $90^0 \sim 100^0$ (pitch leading heave). In particular, for a low aspect ratio wing , the range of the

best phase angle values is narrow. At certain phase angle values, a low aspect ratio wing with low sweep angle may produce drag rather then thrust. Therefore, in practical operations, the phase angle of the oscillating foil needs to be controlled precisely to achieve the highest possible efficiency.

The maximum propulsive efficiency and the minimum thrust coefficient occurred at about the same phase angle values. The point of low thrust and high efficiency is suitable for an oscillating foil working at high speed, low load operating conditions. Under heavy loading conditions, the propulsive efficiency has to be reduced to obtain high thrust.

7.4 Oscillating Propeller Design

Higher aspect ratio foils can produce higher efficiency and thrust. An oscillating foil with highest possible aspect ratio in a given situation, can achieve the highest possible efficiency. However, the span for an oscillating foil at the stern of a ship cannot be too long. The control of a ship in harbour confines the span of an oscillating foil. Also the draught confines the oscillating foil's heave amplitude; the solution of using higher h to increase η is not possible. These factors reduce the possibility of the highest propulsive efficiency that it is possible to achieve in practice.

The pitching angle amplitude α also affects the efficiency and thrust: the larger the α, the higher the thrust. When the dimension of an oscillating foil is limited, a solution of using higher α to increase thrust is possible. However, when α is too large at a given advance ratio, and especially, when the ratio of ω/V_∞ is also too big, stall and separation will occur. In addition, small amplitude theory is not applicable at large α.

Wings with higher sweep angle produce higher thrust but reduce the propulsive efficiency. A wing of very high sweep back with high aspect ratio adds to the difficulties in manufacture.

If the friction and flexibility of an oscillating propeller are taken into account, the propulsive efficiency will reduce. A precise estimate of this reduction is difficult to obtain. Studies on the frictional drag of a three dimensional oscillating foil and the propulsive performance of a three dimensional flexible fin propeller are necessary for the further development of oscillating propulsion.

Appendices

Appendix A

Integration of Eq. 3.7

The integral part of Eq. 3.7 is the Glauert integral of I_0 (Glauert (1926), *p.*93). When $\theta' \neq \theta$, it can be integrated as follows

$$\begin{aligned}\int \frac{d\theta'}{\cos\theta' - \cos\theta} &= \int \frac{d\theta'}{2\sin[(\theta+\theta')/2]\sin[(\theta-\theta')/2]} \\ &= \int \frac{\frac{1}{2\sin^2[(\theta-\theta')/2]}d\theta'}{\sin[(\theta+\theta')/2]/\sin[(\theta-\theta')/2]}. \qquad \text{(A.1)}\end{aligned}$$

Let

$$\begin{aligned}&\frac{d}{d\theta'}\left\{\frac{\sin[(\theta+\theta')/2]}{\sin[(\theta-\theta')/2]}\right\} \\ &= \frac{\frac{1}{2}\cos[(\theta+\theta')/2]}{\sin[(\theta-\theta')/2]} + \frac{\frac{1}{2}\sin[(\theta+\theta')/2]\cos[(\theta-\theta')/2]}{\sin^2[(\theta-\theta')/2]} \\ &= \frac{\cos[(\theta+\theta')/2]\sin[(\theta-\theta')/2]}{2\sin^2[(\theta-\theta')/2]} + \frac{\sin[(\theta+\theta')/2]\cos[(\theta-\theta')/2]}{2\sin^2[(\theta-\theta')/2]}\end{aligned}$$

$$= \frac{\sin\theta}{2\sin^2[(\theta-\theta')/2]}, \tag{A.2}$$

one has

$$\frac{d\theta'}{2\sin^2[(\theta-\theta')/2]} = \frac{1}{\sin\theta} d\left(\frac{\sin[(\theta+\theta')/2]}{\sin[(\theta-\theta')/2]}\right), \tag{A.3}$$

and hence

$$\int \frac{d\theta'}{\cos\theta'-\cos\theta} = \frac{1}{\sin\theta}\int \frac{(d[\sin[(\theta+\theta')/2]/\sin[(\theta-\theta')/2])}{\sin[(\theta+\theta')/2]/\sin[(\theta-\theta')/2]}$$

$$= \frac{1}{\sin\theta}\ln\left\|\frac{\sin[(\theta+\theta')/2]}{\sin[(\theta-\theta')/2]}\right\|. \tag{A.4}$$

As there is a singularity when $\theta' = \theta$, a limit integral is used as

$$\int_0^\pi \frac{d\theta'}{\cos\theta'-\cos\theta} = \lim_{\epsilon\to 0}\left[\int_0^{\theta-\epsilon} \frac{d\theta'}{\cos\theta'-\cos\theta} + \int_{\theta+\epsilon}^{\pi} \frac{d\theta'}{\cos\theta'-\cos\theta}\right]$$

$$= \lim_{\epsilon\to 0}\frac{1}{\sin\theta}\left\{\ln\left\|\frac{\sin[(\theta+\theta-\epsilon)/2]}{\sin[(\theta-\theta+\epsilon)/2]}\right\|\right.$$
$$-\ln\left\|\frac{\sin[(\theta+0)/2]}{\sin[(\theta-0)/2]}\right\|$$
$$+\ln\left\|\frac{\sin[(\theta+\pi)/2]}{\sin[(\theta-\pi)/2]}\right\|$$
$$\left.-\ln\left\|\frac{\sin[(\theta+\theta+\epsilon)/2]}{\sin[(\theta-\theta-\epsilon)/2]}\right\|\right\}$$

$$= \lim_{\epsilon\to 0}\frac{1}{\sin\theta}\ln\left\|\frac{\sin[\theta-\epsilon/2]}{\sin[\theta+\epsilon/2]}\right\| = 0. \tag{A.5}$$

Appendix B

Use of the Midpoint Trapezoidal Rule in the Integration of Eq. 3.7

Referring to Burden (1984), let $f \in C^2[a,b]$, with $h = (b-a)/(2m+2)$ and $x_j = a + (j+1)h$ for each $j = -1, 0, \cdots, 2m+1$, the **composite midpoint rule** for $m+1$ intervals is

$$\int_a^b f(x)dx = 2h\sum_{j=1}^{m} f(x_{2j}) + \frac{(b-a)h^2}{6}f''(u), \tag{B.1}$$

for some $u \in (a,b)$.

From Eq. 3.7, let

$$I = \int_0^{\pi} \frac{g(\theta') - g(\theta)}{\cos\theta - \cos\theta'}d\theta', \tag{B.2}$$

$a = 0$, $b = \pi$, $h = \pi/(2m+2)$, $x_j = a + (j+1)h = 0 + (j+1)\pi/(2m+2)$, $x_{2j} = (2j+1)\pi/(2m+2)$. Therefore,

$$I = \int_0^{\pi} \frac{g(\theta') - g(\theta)}{\cos\theta - \cos\theta'}d\theta'$$

$$= 2h\sum_{j=0}^{m} \frac{g(\theta_{2j}) - g(\theta)}{\cos\theta - \cos\theta_{2j}} + \frac{\pi h^2}{6}[\frac{g(u) - g(\theta)}{\cos\theta - \cos(u)}]''$$

$$\simeq 2h \sum_{j=0}^{m} \frac{g(\theta_{2j}) - \theta)}{\cos\theta - \cos\theta_{2j}}$$

$$= \frac{2\pi}{(2m+2)} \sum_{j=0}^{m} \frac{g((2j+1)\pi/(2m+2)) - g(\theta)}{\cos\theta - \cos((2j+1)\pi/(2m+2))}$$

$$= \frac{\pi}{(m+1)} \sum_{j=0}^{m} \frac{g((2j+1)\pi/(2(m+1))) - g(\theta)}{\cos\theta - \cos((2j+1)\pi/(2(m+1)))}$$

$$= \frac{\pi}{(m+1)} \sum_{j=1}^{m+1} \frac{g((2j-1)\pi/(2(m+1))) - g(\theta)}{\cos\theta - \cos((2j-1)\pi/(2(m+1)))}$$

$$= \frac{\pi}{N} \sum_{j=1}^{N} \frac{g((2j-1)\pi/(2N)) - g(\theta)}{\cos\theta - \cos((2j-1)\pi/(2N))} \qquad \text{(B.3)}$$

which is in Eq. 3.8.

This numerical integration has an error

$$E = \frac{\pi h^2}{6} [\frac{g(u) - g(\theta)}{\cos\theta - \cos(u)}]'' . \qquad \text{(B.4)}$$

Appendix C

Application of Chebychev Polynomials to Eq. 3.8

Consider Chebychev polynomials of the first kind,

$$T_n(\lambda) = \begin{cases} (\cos(n)\arccos\lambda), & |\lambda| \leq 1 \\ \coth(n\coth^{-1}(\lambda)), & |\lambda| > 1 \end{cases} \tag{C.1}$$

where $\lambda = \cos\theta$, and $|\lambda| \leq 1$ in this case. Then Eq. C.1 when $|\lambda| \leq 1$ can be written as

$$\begin{aligned} T_n(\lambda) &= \cos n\theta = \frac{1}{2}(e^{in\theta} + e^{-in\theta}) \\ &= \frac{1}{2}[(\cos\theta + i\sin\theta)^n + (\cos\theta - i\sin\theta)^n] \\ &= \frac{1}{2}[(\lambda + i\sqrt{1-\lambda^2})^n + (\lambda + i\sqrt{1-\lambda^2})^n] \\ &= \frac{1}{2}[(\lambda + \sqrt{\lambda^2-1})^n + (\lambda - i\sqrt{\lambda^2-1})^n] \end{aligned} \tag{C.2}$$

where n is positive integer. Expanding the first part of Eq. C.2, one has

$$\begin{aligned} A &= \lambda^n + n\lambda^{n-1}\sqrt{\lambda^2-1} + \frac{n(n-1)}{2!}\lambda^{n-2}(\sqrt{\lambda^2-1})^2 \\ &+ \frac{n(n-1)(n-2)}{3!}\lambda^{n-3}(\sqrt{\lambda^2-1})^3 + \cdots \\ &+ \frac{n(n-1)\cdots(n-k+1)}{K!}\lambda^{n-K}(\sqrt{\lambda^2-1})^K + \cdots, \end{aligned} \tag{C.3}$$

and the second part after expansion will be

$$\begin{aligned} B &= \lambda^n - n\lambda^{n-1}\sqrt{\lambda^2-1} + \frac{n(n-1)}{2!}\lambda^{n-2}(\sqrt{\lambda^2-1})^2 \\ &\quad -\frac{n(n-1)(n-2)}{3!}\lambda^{n-3}(\sqrt{\lambda^2-1})^3 + \cdots \\ &\quad +(-1)^n\frac{n(n-1)\cdots(n-k+1)}{K!}\lambda^{n-K}(\sqrt{\lambda^2-1})^K + \cdots. \end{aligned} \tag{C.4}$$

Therefore,

$$\begin{aligned} T_n(\lambda) &= \frac{1}{2}(A+B) \\ &= \lambda^n + \frac{n(n-1)}{2!}\lambda^{n-2}(\lambda^2-1) \\ &\quad +\frac{n(n-1)(n-2)(n-4)}{4!}\lambda^{n-4}(\lambda^2-1)^2 + \cdots \\ &\quad +\frac{n(n-1)\cdots(n-k+1)}{K!}\lambda^{n-K}(\lambda^2-1)^K + \cdots, \end{aligned} \tag{C.5}$$

where K is an even integer. Further, $T_n(\lambda)$ can be written as

$$T_n(\lambda) = C_n^0\lambda^n + C_n^2\lambda^{n-2} + C_n^4\lambda^{n-4} + \cdots \tag{C.6}$$

From Eq. C.6 one has

$$\begin{array}{ll} T_0(\lambda) = 1 & T_0(\cos\theta) = 1 \\ T_1(\lambda) = \lambda & T_1(\cos\theta) = \cos\theta \\ T_2(\lambda) = 2\lambda^2 - 1 & T_2(\cos\theta) = \cos 2\theta \\ T_3(\lambda) = 4\lambda^3 - 3\lambda & T_3(\cos\theta) = \cos 3\theta \\ T_4(\lambda) = 8\lambda^4 - 8\lambda^2 + 1 & T_4(\cos\theta) = \cos 4\theta \\ T_5(\lambda) = 16\lambda^5 - 20\lambda^3 + 5\lambda & T_5(\cos\theta) = \cos 5\theta \\ T_6(\lambda) = 32\lambda^6 - 48\lambda^4 + 18\lambda^2 - 1 & T_6(\cos\theta) = \cos 6\theta \\ \cdots & \cdots \\ \cdots & \cdots \end{array} \tag{C.7}$$

Eq. C.6 only has n-number roots. For $T_n(\lambda) = 0$, therefore, there must be n-numbers of $\lambda's$, i.e. $\lambda_1, \lambda_2, \lambda_3, \lambda_4, \cdots \lambda_n$. Therefore,

$$T_n(\lambda) = 0 = K(\lambda-\lambda_1)(\lambda-\lambda_2)(\lambda-\lambda_3)\cdots(\lambda-\lambda_n) \tag{C.8}$$

$$\begin{aligned} T_n'(\lambda) &= K[(\lambda - \lambda_2)(\lambda - \lambda_3)\cdots(\lambda - \lambda_n) \\ &+ (\lambda - \lambda_1)(\lambda - \lambda_3)\cdots(\lambda - \lambda_n) \\ &+ \cdots(\lambda - \lambda_1)(\lambda - \lambda_2)(\lambda - \lambda_2)\cdots(\lambda - \lambda_{n-1})]. \end{aligned} \tag{C.9}$$

Hence

$$\frac{T_n'(\lambda)}{T_n(\lambda)} = \frac{1}{\lambda - \lambda_1} + \frac{1}{\lambda - \lambda_2} + \cdots \frac{1}{\lambda - \lambda_n} = \sum_{k=1}^{N} \frac{1}{\lambda - \lambda_k}. \tag{C.10}$$

Since $\lambda = \cos\theta$ and $T_n(\cos\theta) = \cos(n\theta)$, and for $T_n(\cos\theta) = 0$, $\cos(n\theta) = 0$,

$$n\theta = \frac{\pi}{2} = (2k-1)\pi/2, k = 1, 2, \cdots N.$$

Substituting $\lambda = \cos\theta$, $\theta_k = (2k-1)\pi/(2N)$ into Eq. C.10, it follows that

$$\frac{T_n'(\lambda)}{T_n(\lambda)} = \sum_{k=1}^{N} \frac{1}{\cos\theta - \cos((2k-1)\pi/(2N))}, \tag{C.11}$$

which is the same as Eq. 11.a in Lan (1979).

Since it is hoped that

$$\begin{aligned} T_n'(\lambda) &= \frac{dT_n(\lambda)}{d\theta}\frac{d\theta}{d\lambda} = \frac{d\cos(n\theta)}{d\theta}\frac{d\theta}{d\cos\theta} \\ &= \frac{n(-\sin(n\theta))}{-\sin\theta} = \frac{n\sin(n\theta)}{\sin\theta} = 0, \end{aligned} \tag{C.12}$$

$\sin(n\theta)$ must be zero. It follows that $n\theta_i$ must be $i\pi$, i.e.

$$\lambda = \cos\theta_i = \cos(i\pi/N), i = 1, 2, 3, \cdots N-1. \tag{C.13}$$

Therefore,

$$T_n'(\lambda_i) = n\frac{\sin(n\theta_i)}{\sin\theta_i}, \theta_i = i\pi/N. \tag{C.14}$$

Since

$$\begin{aligned}\sin(n\theta) &= n\cos^{n-1}\theta\sin\theta - C_n^3\cos^{n-3}\theta\sin\theta^3 \\ &+ C_n^5\cos^{n-5}\theta\sin\theta^5 - \cdots,\end{aligned} \tag{C.15}$$

one has

$$\begin{aligned}\frac{n\sin(n\theta)}{\sin\theta} &= n^2\cos^{n-1}\theta\sin^0\theta - nC_n^3\cos^{n-3}\theta\sin^2\theta \\ &+ nC_n^5\cos^{n-5}\theta\sin^4\theta - \cdots \\ &= n^2\cos^{n-1}\theta\sin^0\theta - n^2C_{n-1}^2\cos^{n-3}\theta\sin^2\theta \\ &+ n^2C_{n-1}^4\cos^{n-5}\theta\sin^4\theta - \cdots,\end{aligned} \tag{C.16}$$

where $n-3=(n-1)-2, n-5=(n-1)-4$. Assuming $n-1=m$, it follows that

$$\begin{aligned}\frac{n\sin(n\theta)}{\sin\theta} &= n^2\cos^m\theta - n^2C_m^2\cos^{m-2}\theta\sin^2\theta \\ &+ n^2C_m^4\cos^{m-4}\theta\sin^4\theta - \cdots.\end{aligned} \tag{C.17}$$

Since

$$\begin{aligned}\cos(m\theta_i) &= \cos^m\theta_i - C_m^2\cos^{m-2}\theta_i\sin^2\theta_i \\ &+C_m^4\cos^{m-4}\theta_i\sin^4\theta_i - \cdots,\end{aligned} \tag{C.18}$$

one has

$$\begin{aligned}\frac{n\sin(n\theta_i)}{\sin\theta_i} &= n^2\cos^m\theta_i = n^2\cos[(n-1)\theta_i] \\ &= n^2\cos[(n-1)i\pi/n].\end{aligned} \tag{C.19}$$

For $i=N$,

$$T_N'(\lambda_i) = N^2\cos((N-1)\pi) = -N^2\cos(N\pi). \tag{C.20}$$

Therefore,

$$\frac{T'_N(\lambda_i)}{T_N(\lambda_i)} = \frac{-N^2 \cos(N\pi)}{\cos(N\pi)} = -N^2. \tag{C.21}$$

Appendix D

Mathematical Formulation of a Vorticity Field

A vorticity field of a vortex line parallel to V_∞ with strength Γ is given by Ward (1955, *pp.*42 – 43) as

$$\vec{V}(R) = \frac{\beta^2\Gamma}{4\pi}\int_l \frac{(\vec{R}_1 - \vec{R}) \times d\vec{l}}{R_\beta^3}. \tag{D.1}$$

Let

$$\begin{aligned}
\vec{a} &= (x_1 - x)\vec{i} + (y_1 - y)\vec{j} + (z_1 - z)\vec{k};\\
\vec{a'} &= (x_1 - x)\vec{i} + \beta(y_1 - y)\vec{j} + \beta(z_1 - z)\vec{k};\\
\vec{b} &= (x_2 - x)\vec{i} + (y_2 - y)\vec{j} + (z_2 - z)\vec{k};\\
\vec{b'} &= (x_2 - x)\vec{i} + \beta(y_2 - y)\vec{j} + \beta(z_2 - z)\vec{k},
\end{aligned}$$

then

$$\vec{R}_1 - \vec{R} = \vec{a} + \tau\vec{l}, \tag{D.2}$$

where $0 \leq \tau \leq 1$. The modulus of $\vec{R}_1 - \vec{R}$ will be

$$|\vec{R}_1 - \vec{R}| = |\vec{a} + \tau\vec{l}|$$

$$
\begin{aligned}
&= |a_i + \tau l_i, a_j + \tau l_j, a_k + \tau l_k| \\
&= [(a_i^2 + 2\tau a_i l_i + \tau^2 l_i^2) + (a_j^2 + 2\tau a_j l_j + \tau^2 l_j^2) \\
&+ (a_k^2 + 2\tau a_k l_k + \tau^2 l_k^2)]^2 \\
&= \sqrt{(\vec{a} + \tau\vec{l})^2} = \sqrt{\vec{a}^2 + 2\tau\vec{a}\cdot\vec{l} + \tau^2\vec{l}^2}. \qquad \text{(D.3)}
\end{aligned}
$$

Considering the factor τ, it follows that

$$
\begin{aligned}
(\vec{R}_1 - \vec{R} \times d\vec{l}) &= (\vec{a} + \tau\vec{l}) \times d(\tau\vec{l}) \\
&= \vec{a} \times d(\tau\vec{l}) + \tau\vec{l} \times d(\tau\vec{l}) \\
&= \vec{a} \times d(\tau\vec{l}) = \vec{a} \times \vec{l} d\tau. \qquad \text{(D.4)}
\end{aligned}
$$

On the other hand,

$$
\vec{R}_\beta = \vec{a'} + \tau\vec{l'}, \qquad \text{(D.5)}
$$

and

$$
|\vec{R}_\beta| = |\vec{a'} + \tau\vec{l'}| = \sqrt{\vec{a'}^2 + 2\tau\vec{a'}\cdot\vec{l'} + \tau^2\vec{l'}^2}. \qquad \text{(D.6)}
$$

Let $\bar{A} = \vec{l'}^2$, $\bar{B} = 2\vec{a'}\cdot\vec{l'}$, and $\bar{C} = \vec{a'}^2$, Eq. D.1 can be written as

$$
\vec{V}(R) = \frac{\beta^2\Gamma}{4\pi}(\vec{a} \times \vec{l}) \int_l \frac{d\tau}{[\bar{A}\tau^2 + \bar{B}\tau + \bar{C}]^{\frac{3}{2}}}. \qquad \text{(D.7)}
$$

When integrating Eq. C.7, the value of $\bar{B}^2 - 4\bar{A}\bar{C}$ should be identified. Expanding $\bar{B}^2 - 4\bar{A}\bar{C}$ it follows that

$$
\begin{aligned}
\bar{B}^2 - 4\bar{A}\bar{C} &= 4(\vec{a'}\cdot\vec{l'})^2 - 4(\vec{l'}^2(\vec{a}^2)) \\
&= 4[(a_i l_i + a_j l_j + a_k l_k)^2 - (l_i^2 + l_j^2 + l_k^2)(a_i^2 + a_j^2 + a_k^2)] \\
&= -4[(a_i l_i)^2 + (a_i l_k)^2 + (a_j l_i)^2 + (a_j l_k)^2 + (a_k l_i)^2 + (a_k l_j)^2 \\
&- 2a_i a_j l_i l_j - 2a_i a_k l_i l_k - 2a_j a_k l_j l_k] \\
&= -4|\vec{a'} \times \vec{l'}|^2 \neq 0. \qquad \text{(D.8)}
\end{aligned}
$$

Therefore, Eq. D.8 has a unique solution and can be obtained as

$$\vec{V}(R) = \frac{\beta^2\Gamma}{4\pi}(\vec{a}\times\vec{l})[\frac{2\bar{B}}{(\bar{B}^2-4\bar{A}\bar{B})\bar{C}^{1/2}} - \frac{2(2\bar{A}+\bar{B})}{(\bar{B}^2-4\bar{A}\bar{C})(\bar{A}+\bar{B}+\bar{C})^{1/2}}] \qquad (D.9)$$

which is Eq. (A3) of Lan (1974).

Transforming

$$2\bar{A}+\bar{B} = 2(\vec{l'}\cdot\vec{l'}) + 2(\vec{a'}\cdot\vec{l'}) = 2(\vec{a'}+\vec{l'})\cdot\vec{l'} = 2(\vec{b'}\cdot\vec{l'}) \qquad (D.10)$$

and

$$\bar{A}+\bar{B}+\bar{C} = (\vec{l'}\cdot\vec{l'}) + 2(\vec{a'}\cdot\vec{l'}) + \vec{a'}\cdot\vec{a'} = |(\vec{a'}+\vec{l'})^2| = |\vec{b'}|^2, \qquad (D.11)$$

and substituting Eq. D.10 and D.9, into Eq. 3.16, for a variable vortex distribution Γ along the span, Eq. D.9 can be written as

$$\vec{V}(R) = \frac{\beta^2}{4\pi}\int_{x_l}^{x_t}\gamma(x')dx'\frac{\vec{a}\times\vec{l}}{|\vec{a'}\times\vec{l'}|^2}[\frac{\vec{b'}}{|\vec{b'}|} - \frac{\vec{a'}}{|\vec{a'}|}]\cdot\vec{l'}. \qquad (D.12)$$

which is Eq.(29) of Lan (1974).

By using Eq. 3.16 and Eq. D.12, and noticing

$$\begin{aligned}
\vec{a'}\times\vec{l'} &= \beta\vec{k}\{(x_1-x)(y_2-y_1) - (x_2-x_1)(y_1-y)\} \\
\vec{b'}\times\vec{l'} &= (x_2-x_1)(x_2-x) + \beta^2(y_2-y_1)(y_2-y) \\
\vec{a'}\times\vec{l'} &= (x_2-x_1)(x_1-x) + \beta^2(y_2-y_1)(y_1-y), \qquad (D.13)
\end{aligned}$$

where $\beta = (1-M_\infty^2)^{1/2}$, the portion of the downwash by bound vortices can be written as

$$\begin{aligned}
W_b &= q_b\cdot\vec{k} \\
&= \frac{1}{4\pi}\int_{x_l}^{x_t}\frac{\gamma(x')}{(x_1-x)(y_2-y_1)-(x_2-x_1)(y_1-y)}.
\end{aligned}$$

$$\left\{ \frac{(x_2 - x_1)(x_2 - x) + \beta^2(y_2 - y_1)(y_2 - y)}{[(x_2 - x)^2 + \beta^2(y_2 - y)^2]^{1/2}} \right.$$
$$\left. - \frac{(x_2 - x_1)(x_1 - x) + \beta^2(y_2 - y_1)(y_1 - y)}{[(x_1 - x)^2 + \beta^2(y_1 - y)^2]^{1/2}} \right\} dx'; \qquad \text{(D.14)}$$

the portion of the downwash by the trailing vortex starting from the point (x_1, y_1) as

$$W_1 = \frac{1}{4\pi} \int_{x_l}^{x_t} \frac{\gamma(x')}{y_1 - y} \left[1 - \frac{x_1 - x}{[(x_1 - x)^2 + \beta^2(y_1 - y)^2]^{1/2}} \right] dx'; \qquad \text{(D.15)}$$

and the portion of the downwash by the trailing vortex starting from the point (x_2, y_2) as

$$W_1 = -\frac{1}{4\pi} \int_{x_l}^{x_t} \frac{\gamma(x')}{y_2 - y} \left[1 - \frac{x_2 - x}{[(x_2 - x)^2 + \beta^2(y_2 - y)^2]^{1/2}} \right] dx'. \qquad \text{(D.16)}$$

Total downwash due to a whole horseshoe vortex is

$$W_s = W_b + W_1 + W_2. \qquad \text{(D.17)}$$

Appendix E

Boundary Condition for an Oscillating Wing and Integration of the Steady and Unsteady Doublet Velocity Potentials

(A) Boundary Condition When the wing is in harmonic motion, the following relations are assumed:

$$\begin{aligned} \bar{w}(x,y) &= Re(we^{i\omega t}), \\ \bar{\alpha}(x,y) &= Re(\alpha e^{i\omega t}), \\ \bar{h}(x,y) &= Re(he^{i\omega t}). \end{aligned} \tag{E.1}$$

Therefore,

$$\begin{aligned} \dot{\bar{h}} &= h\omega \sin(\omega t), \\ \dot{\bar{\alpha}} &= \alpha\omega \sin(\omega t), \\ \bar{\alpha} &= \alpha \cos(\omega t). \end{aligned} \tag{E.2}$$

Hence

$$\begin{aligned}\bar{w}(x,y) &= -\frac{\omega}{V_\infty}h\sin(\omega t) - \alpha\cos(\omega t) - \frac{\omega}{V_\infty}\alpha\sin(\omega t)(x - x_a) \\ &= A\cos(\omega t) + B\sin(\omega t), \end{aligned} \tag{E.3}$$

where

$$\begin{aligned} A &= -\alpha, \\ B &= -\frac{\omega}{V_\infty}h - \frac{\omega}{V_\infty}\alpha\omega(x - x_a). \end{aligned} \tag{E.4}$$

Let $w = A' + iB'$, it follows that

$$\begin{aligned}\bar{w}(x,y) &= Re(we^{i\omega t}) = Re((A' + iB')e^{i\omega t}) \\ &= Re[(A' + iB')(\cos(\omega t) + i\sin(\omega t))] \\ &= Re[(A'\cos(\omega t) - B'\sin(\omega t)) + i(A'\sin(\omega t) + B'\cos(\omega t))] \\ &= A'\cos(\omega t) - B'\sin(\omega t). \end{aligned} \tag{E.5}$$

Therefore,

$$\begin{aligned} A' &= A = -\alpha, \\ -B' &= B = \frac{\omega}{V_\infty}h + \frac{\omega}{V_\infty}\alpha(x - x_a) \\ w &= A' + iB' = -\alpha - \frac{\omega}{V_\infty}h - \frac{\omega}{V_\infty}\alpha(x - x_a). \end{aligned} \tag{E.6}$$

(B) Integration of Eq. 4.9

The integrand of Eq. 4.9 contains two parts. The first part of the equation is

$$\Phi_{11} = \int_L \frac{z_0}{r^2}d\eta, \tag{E.7}$$

and the second part is

$$\Phi_{12} = \int_L \frac{x_0 z_0}{Rr^2}d\eta. \tag{E.8}$$

To integrate Eq. E.7, the integration variable needs to be changed. Referring to Lan (1979), τ can be written as

$$\tau = \frac{\eta - y_1}{y_2 - y_1}, d\tau = \frac{d\eta}{y_2 - y_1}. \tag{E.9}$$

hence

$$\Phi_{11} = \frac{(y_2 - y_1)z_0}{8\pi} \int_L \frac{d\tau}{[(y - y_1) - \tau(y_2 - y_1)]^2 + z_0^2}. \tag{E.10}$$

After a simple mathematical manipulation and looking up integration tables (Wang, et al. (1977), $p.262$) the first part of the Eq. 4.9 can be written as

$$\Phi_{11} = \frac{1}{8\pi} \arctan(\frac{2a\tau + b}{2(y_2 - y_1)z}), \tag{E.11}$$

where $a = (y_2 - y_1)^2$, and $b = 2(y_2 - y_1)(y - y_1)$.

To integrate Eq. E.8, assume

$$v = (y_2 - y_1)\tau - (y - y_1) = \eta - y, \quad d\eta = dv, \tag{E.12}$$

and

$$\begin{aligned} Q &= (x_2 - x_1)(y - y_1) - (x - x_1)(y_2 - y_1), \\ A &= (x_2 - x_1)^2 + (y_2 - y_1)^2, \\ B &= -2[(x - x_1)(x_2 - x_1) + (y - y_1)(y_2 - y_1)], \\ C &= (x - x_1)^2 + (y - y_1)^2 + z^2, \end{aligned} \tag{E.13}$$

which is Eq. 2.17 in Lan (1979). Substituting Eq. E.13 into Eq. E.8, we have

$$\Phi_{12} = \frac{1}{8\pi} \int_L \frac{x - x_1 - (\eta - y_1)(x_2 - x_1)/(y_2 - y_1)}{(v^2 + z^2)R} z_0 dv, \tag{E.14}$$

where

$$R = [A(\frac{\eta - y}{y_2 - y_1})^2 + B(\frac{\eta - y}{y_2 - y_1}) + C]^{1/2}. \tag{E.15}$$

To change η to v, it follows that

$$\begin{aligned} R &= \{A(\frac{1}{(y_2-y_1)^2})v^2 + (2A\frac{y-y_1}{(y_2-y_1)^2} + B\frac{1}{y_2-y_1})v \\ &+ [(\frac{y-y_1}{y_2-y_1})^2 + B\frac{y-y_1}{y_2-y_1}) + C]\}^{1/2}. \end{aligned} \tag{E.16}$$

where

$$\begin{aligned} A' &= A, \\ 2B' &= [2A(y-y_1)(y_2-y_1) + B(y_2-y_1)], \\ C' &= (y-y_1)^2 + B(y-y_1)(y_2-y_1) + C(y_2-y_1)^2. \end{aligned} \tag{E.17}$$

Substituting Eq. E.16 and E.17 into Eq. E.14, the integration can be written as

$$\Phi_{12} = \frac{z_0}{8\pi}\int_L \frac{[-Q-(x_2-x_1)v]dv}{(v^2+z_0^2)[A'v^2+2B'v+C']^{1/2}}. \tag{E.18}$$

Finally, Eq. E.18 can be written as the form suggested by Lan (1989),

$$\begin{aligned} \Phi_{12} &= \frac{Qz_0}{8\pi}\int_L \frac{dv}{(v^2+z_0^2)[A'v^2+2B'v+C']^{1/2}} \\ &- \frac{Qz_0(x_2-x_1)}{8\pi}\int_L \frac{vdv}{(v^2+z_0^2)[A'v^2+2B'v+C']^{1/2}}. \end{aligned} \tag{E.19}$$

Eq. E.19 can be solved by reference to Woodward, et al. (1967), and be written as

$$\Phi_{12} = -\frac{1}{8\pi}\arctan\left(\frac{Qv-(x_2-x_1)z_0^2}{z_0(y_2-y_1)(A\tau^2+B\tau+C)^{1/2}}\right). \tag{E.20}$$

(C) Integration of the Unsteady Doublet Velocity Potential

In order to obtain the second term of Eq. 4.8, which is

$$\Phi_2 = \frac{-1}{8\pi}\int\int \Delta C_p \left\{\frac{i\omega}{V_\infty}\frac{z_0}{r_1}e^{-i\omega x_0/V_\infty}\int_{u_1}^{\infty}[1-\frac{\lambda}{(1+\lambda^2)^{1/2}}]e^{-i\omega r_1\lambda/V_\infty}d\lambda\right\}d\xi d\eta, \tag{E.21}$$

integrate the second term of Eq. 4.8 in the η direction first, it follows that

$$\begin{aligned}
\Phi_2 &= \frac{-i\omega}{8V_\infty\pi}\int\int \Delta C_p \left\{\frac{z_0}{r_1^2}e^{-i\omega x_0/V_\infty} r_1 \int_{u_1}^{\infty}[1-\frac{\lambda}{(1+\lambda^2)^{1/2}}]e^{-i\omega r_1\lambda/V_\infty}d\lambda\right\} d\xi d\eta \\
&= \frac{-i\omega}{8V_\infty\pi}\int \Delta C_p \left\{\int \frac{z_0}{r_1^2}[r_1 e^{-i\omega x_0/V_\infty}\int_{u_1}^{\infty}[1-\frac{\lambda}{(1+\lambda^2)^{1/2}}]e^{-i\omega r_1\lambda/V_\infty}d\lambda]d\eta\right\} d\xi \\
&= \frac{-i\omega}{8V_\infty\pi}\int \Delta C_p \left\{[\int_L \frac{z_0}{r_1^2}d\eta] r_1 e^{-i\omega x_0/V_\infty}\int_{u_1}^{\infty}[1-\frac{\lambda}{(1+\lambda^2)^{1/2}}]e^{-i\omega r_1\lambda/V_\infty}d\lambda\right. \\
&\quad \left. -\int_L[\frac{z_0}{r_1^2}d\eta]\frac{\partial}{\partial\eta}[r_1 e^{-i\omega x_0/V_\infty}\int_{u_1}^{\infty}[1-\frac{\lambda}{(1+\lambda^2)^{1/2}}]e^{-i\omega r_1\lambda/V_\infty}d\lambda]\right\} d\xi \\
&= \frac{-i\omega}{8V_\infty\pi}\int \Delta C_p \left\{\arctan[\frac{2a\tau+b}{2(y_2-y_1)z}]I|_L - \int_L \arctan[\frac{2a\tau+b}{2(y_2-y_1)z}]\frac{\partial I}{\partial\eta}d\eta\right\} d\xi,
\end{aligned} \tag{E.22}$$

where

$$I = r_1 e^{-i\omega x_0/V_\infty}\int_{u_1}^{\infty}[1-\frac{\lambda}{(1+\lambda^2)^{1/2}}]e^{-i\omega r_1\lambda/V_\infty}d\lambda. \tag{E.23}$$

Appendix F

Differentiation of the Steady and Unsteady Doublet Velocity Potentials

Differentiating the steady term Φ_1 in Eq. 4.10, which is the summation of Eq. E.11 and Eq. E.20, it follows that

$$\begin{aligned}\frac{\partial \Phi_1}{\partial z} &= \frac{\partial \Phi_{11} + \partial \Phi_{12}}{\partial z} \\ &= \frac{1}{8\pi}\left\{-\frac{\eta - y}{(\eta - y)^2 + z^2} + \frac{1}{[(x-\xi)^2 + (\eta - y)^2 + z^2]^{1/2}} \cdot \right. \\ &\quad \left. \left[\frac{(\eta - y)(\xi - x)}{(\eta - y)^2 + z^2} + Q\frac{(\xi - x)(x_2 - x_1) + (y_2 - y_1)(\eta - y)}{Q^2 + z^2[(x_2 - x_1)^2 + (y_2 - y_1)^2]}\right]_{(x_1, y_1)}^{(x_2, y_2)}\right\},\end{aligned} \tag{F.1}$$

where $Q = (x_2 - x_1(y - y_1) - (x - x_1)(y_2 - y_1)$. Differentiating the unsteady term Φ_2 in Eq. 4.10, it follows that

$$\begin{aligned}\frac{\partial \Phi_2}{\partial z} &= \frac{-i\omega}{8V_\infty \pi}\int \Delta C_p \frac{\partial}{\partial z}\left\{(\varrho) I|_L - \frac{\partial}{\partial z}\int_L (\varrho)\frac{\partial I}{\partial \eta} d\eta\right\} d\xi \\ &= \frac{-i\omega}{8V_\infty \pi}\int \Delta C_p \left\{[\frac{\partial}{\partial z}[\varrho] I\|_L - \frac{\partial}{\partial z}\int_L (\varrho)\frac{\partial I}{\partial \eta} d\eta\right\} d\xi\end{aligned}$$

$$= \frac{-i\omega}{8V_\infty \pi} \int \Delta C_p \left\{ [I\frac{\partial}{\partial z}(\varrho) + (\varrho)\frac{\partial I}{\partial z}]_L \right.$$
$$\left. - \int_L [\frac{\partial I}{\partial \eta}\frac{\partial}{\partial z}(\varrho) + (\varrho)\frac{\partial^2 I}{\partial \eta \partial z}]d\eta \right\} d\xi, \qquad \text{(F.2)}$$

where $\varrho = \arctan \frac{2a\tau + b}{2(y_2 - y_1)z}$. Let

$$\begin{aligned} \tau &= \frac{\eta - y}{y_2 - y_1} \\ a &= (y_2 - y_1)^2 \\ b &= -2(y - y_1)(y_2 - y_1) \\ 2a\tau + b &= 2(y_2 - y_1)(\eta - y_1) - 2(y_2 - y_1)(y - y_1), \end{aligned} \qquad \text{(F.3)}$$

one has

$$\frac{2a\tau + b}{2(y_2 - y_1)z} = \frac{\eta - y}{z}. \qquad \text{(F.4)}$$

Further, let

$$a^* = \left[I\frac{\partial}{\partial z} \arctan[\frac{2a\tau + b}{2(y_2 - y_1)z}] \right]_L = \left(I\frac{\partial}{\partial z} \arctan[\frac{\eta - y}{z}] \right)_L = \frac{I(\eta - y)}{z^2 + (\eta - y)^2},$$

$$b^* = \left(\arctan[\frac{\eta - y}{z}]\frac{\partial I}{\partial z} \right)_L,$$

$$c^* = -\int_L \frac{\partial I}{\partial \eta}\frac{\partial}{\partial z} \arctan[\frac{\eta - y}{z}]d\eta,$$

$$d^* = -\int_L \arctan[\frac{\eta - y}{z}]\frac{\partial^2 I}{\partial \eta \partial z}d\eta, \qquad \text{(F.5)}$$

The unsteady downwash can be written as

$$\frac{\partial \Phi_2}{\partial z} = \frac{-i\omega}{8V_\infty \pi} \int \Delta C_p \{a^* + b^* + c^* + d^*\} d\xi. \qquad \text{(F.6)}$$

It is noted that $d\eta = (y_2 - y_1)d\tau$, where $0 \leq \tau \leq$. Further, c^* and d^* can be written as

$$c^* = -\int_0^1 \frac{\partial I}{\partial \eta} \left\{ \frac{\partial}{\partial z} \arctan[\frac{\eta - y}{z}] \right\} (y_2 - y_1)d\tau, \tag{F.7}$$

and

$$d^* = -\int_0^1 \frac{\partial^2 I}{\partial \eta \partial z} \arctan[\frac{\eta - y}{z}](y_2 - y_1)d\tau, \tag{F.8}$$

which are W_2 and W_3 in Eq. 4.11.

Appendix G

Formulation of the Non-singular Term in the Integration of W_2 and W_3

In evaluating $\partial I/\partial \eta$, Eq. 4.14 is used, which is

$$I = T_1 = \int_{u_1 r_1}^{\infty} \left[1 - \frac{\tau_1}{(\tau_1^2 + r_1^2)^{1/2}}\right] e^{-i\omega(\tau_1 + x_0)/V_\infty} d\tau_1. \tag{G.1}$$

Differentiating I with respect to r_1 and noting that

$$u_1 r_1 = -x_0 = -(x - \xi)$$

, which is not a function of r_1, one gets

$$\begin{aligned} \frac{\partial I}{\partial r_1} &= \int_{u_1 r_1}^{\infty} e^{-i\omega(\tau_1 + x_0)/V_\infty} \frac{\partial}{\partial r_1} \left[1 - \frac{\tau_1}{(\tau_1^2 + r_1^2)^{1/2}}\right] d\tau_1 \\ &= r_1 \int_{u_1 r_1}^{\infty} \left[1 - \frac{\tau_1}{(\tau_1^2 + r_1^2)^{3/2}}\right] e^{-i\omega(\tau_1 + x_0)/V_\infty} d\tau_1; \end{aligned} \tag{G.2}$$

and by differentiating r_1 with respect to η, the differentiation of I with respect to x_0 is

$$\frac{\partial r_1}{\partial \eta} = \frac{\partial}{\partial \eta} \sqrt{(y - \eta)^2 + z_0^2}$$

$$= \frac{1}{2}[(y-\eta)^2 + z_0^2]^{-1/2}(2)(y-\eta)\cdot(-1)$$
$$= -\frac{y-\eta}{r_1}. \qquad \text{(G.3)}$$

Therefore,

$$\frac{\partial I}{\partial r_1}\frac{\partial r_1}{\partial \eta} = -(y-\eta)\int_{u_1 r_1}^{\infty}\left[1 - \frac{\tau_1}{(\tau_1^2 + r_1^2)^{3/2}}\right] e^{-i\omega(\tau_1+x_0)/V_\infty} d\tau_1. \qquad \text{(G.4)}$$

When obtaining $\frac{\partial I}{\partial x_0}$, it is noted that $x_0 = -u_1 r_1$ and let $u_1 r_1 = b(x_0)$, then $u_1 r_1$ is a function of x_0. From the mathematical definition:

$$\frac{d}{dt}\int_a^{b(t)} f(x,t)dx = \int_a^b f_t'(x,t)dx + f[b(t),t]\frac{db(t)}{dt}, \qquad \text{(G.5)}$$

one has

$$\frac{\partial I}{\partial x_0} = \frac{d}{dx_0}\int_{-x_0}^{b(t)} f(\tau_1, x_0)d\tau_1$$

$$= \int_{-x0}^{\infty}\frac{d}{dx_0}\left\{[1 - \frac{\tau_1}{(\tau_1^2 + r_1^2)^{1/2}}]e^{-i\omega(\tau_1+x_0)/V_\infty}\right\}d\tau_1$$
$$-[1 - \frac{-x_0}{[(-x_0)^2 + r_1^2]^{1/2}}]e^{-i\omega(-x_0+x_0)/V_\infty}\frac{d}{dx_0}(-x_0)$$

$$= -i\frac{\omega}{V_\infty}\int_{u_1 r_1}^{\infty}\left[1 - \frac{\tau_1}{(\tau_1^2 + r_1^2)^{1/2}}\right] e^{-i\omega(\tau_1+x_0)/V_\infty} d\tau_1$$
$$+[1 - \frac{u_1 r_1}{[(u_1 r_1)^2 + r_1^2]^{1/2}}]. \qquad \text{(G.6)}$$

Since

$$x_0 = x - x_1 - \tau(x_2 - x_1)$$
$$y - \eta = y - y_1 - \tau(y_2 - y_1)$$
$$\eta - y = \tau(y_2 - y_1), \qquad \text{(G.7)}$$

one has

$$x_0 = x - x_1 - \frac{\eta - y_1}{y_2 - y_1}(x_2 - x_1), \tag{G.8}$$

and

$$\frac{\partial x_0}{\partial \eta} = -\frac{x_2 - x_1}{y_2 - y_1}. \tag{G.9}$$

Hence,

$$\begin{aligned}
\frac{\partial I}{\partial x_0}\frac{\partial x_0}{\partial \eta} &= i\frac{\omega}{V_\infty}\left[\int_{u_1 r_1}^{\infty}\left[1 - \frac{\tau_1}{(\tau_1^2 + r_1^2)^{1/2}}\right]e^{-i\omega(\tau_1 + x_0)/V_\infty}d\tau_1\right]\frac{x_2 - x_1}{y_2 - y_1} \\
&\quad - \left[1 - \frac{u_1}{(1 + u_1^2)^{1/2}}\right]\frac{x_2 - x_1}{y_2 - y_1} \\
&= i\frac{\omega}{V_\infty}I\frac{x_2 - x_1}{y_2 - y_1} - \left[1 - \frac{u_1}{(1 + u_1^2)^{1/2}}\right]\frac{x_2 - x_1}{y_2 - y_1}.
\end{aligned} \tag{G.10}$$

Finally, the non-singular terms of W_2 become

$$\begin{aligned}
\frac{\partial I}{\partial \eta} &= \frac{\partial I}{\partial r_1}\frac{\partial r_1}{\partial \eta} + \frac{\partial I}{\partial x_0}\frac{\partial x_0}{\partial \eta} \\
&= -(y - \eta)\int_{u_1 r_1}^{\infty}\frac{\tau_1}{(\tau_1^2 + r_1^2)^{3/2}}e^{-i\omega(\tau_1 + x_0)/V_\infty}d\tau_1 \\
&\quad + i\frac{\omega}{V_\infty}I\frac{x_2 - x_1}{y_2 - y_1} - \left[1 - \frac{u_1}{(1 + u_1^2)^{1/2}}\right]\frac{x_2 - x_1}{y_2 - y_1}.
\end{aligned} \tag{G.11}$$

which is Eq. 4.14.

differentiating $\frac{\partial I}{\partial \eta}$ with respect to z and noting that $\frac{\partial r_1}{\partial z} = \frac{z}{r_1}$, $\frac{partial^2 I}{\partial z \partial \eta}$ can be written as

$$\begin{aligned}
\frac{partial^2 I}{\partial z \partial \eta} &= \left(\frac{\partial}{\partial r_1}\frac{\partial I}{\partial \eta}\right)\frac{\partial r_1}{\partial z} \\
&= \frac{\partial}{\partial r_1}\left\{-(y - \eta)\int_{u_1 r_1}^{\infty}\frac{\tau_1}{(\tau_1^2 + r_1^2)^{3/2}}e^{-i\omega(\tau_1 + x_0)/V_\infty}d\tau_1\right.
\end{aligned}$$

$$+i\frac{\omega}{V_\infty}I\frac{x_2-x_1}{y_2-y_1}-\left[1-\frac{u_1}{(1+u_1^2)^{1/2}}\right]\frac{x_2-x_1}{y_2-y_1}\Bigg\}\frac{z}{r_1}$$

$$= \frac{3(y-\eta)z}{r_1^2}T_2+i\frac{\omega}{V_\infty}\frac{z}{r_1}\frac{\partial I}{\partial r_1}\frac{x_2-x_1}{y_2-y_1}$$
$$+\frac{1}{(1+u_1^2)^{3/2}}\frac{x_2-x_1}{y_2-y_1}\left(\frac{x_0 z}{r_1^3}\right). \qquad \text{(G.12)}$$

where

$$T_2 = r_1^2\int_{u_1 r_1}^{\infty}\frac{\tau_1}{(\tau_1^2+r_1^2)^{5/2}}e^{-i\omega(\tau_1+x_0)/V_\infty}d\tau_1 \qquad \text{(G.13)}$$

Appendix H

Numerical Approximations in the Integration of W_2 and W_3

A. Integration of W_2 In the numerical approximation of W_2, a parabolic function

$$A\tau^2 + B\tau + C$$

is used to substitute for Eq. 4.16. Consider Eq. 4.16,

$$\begin{aligned}\frac{\partial I}{\partial \eta} &= \frac{\partial I}{\partial r_1}\frac{\partial r_1}{\partial \eta} + \frac{\partial I}{\partial x_0}\frac{\partial x_0}{\partial \eta} \\ &= -(y-\eta)T_3 \\ &\quad + i\frac{\omega}{V_\infty} I \frac{x_2 - x_1}{y_2 - y_1} - [1 - \frac{u_1}{(1+u_1^2)}]\frac{x_2 - x_1}{y_2 - y_1}, \end{aligned} \tag{H.1}$$

where

$$T_3 = \int_{u_1 r_1}^{\infty} \frac{\tau_1 e^{-i\omega(\tau_1 + x_0)/V_\infty} d\tau_1}{(\tau_1^2 + r_1^2)^{3/2}}. \tag{H.2}$$

Let

$$\frac{\partial I}{\partial \eta} \simeq A\tau^2 + B\tau + C, \tag{H.3}$$

Eq. 4.15 can be written as

$$W_2 \simeq y_{21} \int_0^1 \left[A\tau^2 + B\tau + C\right] \frac{y_{21}\tau + y_{1i}}{[y_{21}\tau + y_{1i}]^2 + z^2} d\tau, \tag{II.4}$$

where $y_{21} = y_2 - y_1$, $y_{1i} = y_i - y$. The coefficient A, B, and C for each element of the induced downwash matrices can be obtained from

$$\begin{aligned} A &= 2.0\left[\frac{\partial I}{\partial \eta}(1) - 2\frac{\partial I}{\partial \eta}(1/2) + \frac{\partial I}{\partial \eta}(0)\right], \\ B &= 4\frac{\partial I}{\partial \eta}(1/2) - \frac{\partial I}{\partial \eta}(1) - 3\frac{\partial I}{\partial \eta}(0), \\ C &= \frac{\partial I}{\partial \eta}(0). \end{aligned} \tag{II.5}$$

To change the variable of the integral, let $\beta = y_{21}\tau - y_{1i}$, hence $\tau = \frac{\beta - y_{1i}}{y_{21}}$, $d\tau = \frac{d\beta}{y_{21}}$, the upper and lower limits of the integral then are $\beta_2 = y_{1i}$ and $\beta_1 = y_{2i}$ respectively, where $y_{2i} = y_2 - y$. Therefore, the approximation terms are written as

$$\begin{aligned} A\tau^2 + B\tau + C &= \frac{A}{y_{21}^2}\beta^2 + \left(\frac{B}{y_{21}} - \frac{2Ay_{1i}}{y_{21}^2}\right)\beta \\ &+ \left(\frac{Ay_{1i}^2}{y_{21}^2} + C - \frac{By_{1i}}{y_{21}}\right). \end{aligned} \tag{II.6}$$

Let

$$\begin{aligned} R &= \frac{A}{y_{21}} \\ S &= \frac{B}{y_{21}} - \frac{2Ay_{1i}}{y_{21}^2} \\ T &= \frac{Ay_{1i}^2}{y_{21}^2} + C - \frac{By_{1i}}{y_{21}}, \end{aligned} \tag{II.7}$$

W_2 can be written as

$$W_2 \simeq \int_{\beta_1}^{\beta_2} \frac{\beta}{\beta^2 + z^2}[R\beta^2 + S\beta + T]d\beta. \tag{H.8}$$

The result of this integration is then

$$\begin{aligned} W_2 \;=\; & A\left[\frac{1}{2} - \frac{y_{1i}}{y_{21}}\right] + B \\ & + \left[\frac{Ay_{1i}^2}{y_{21}^2} - B\frac{y_{1i}}{y_{21}} + C - \frac{Az^2}{y_{21}^2}\right] \\ & \cdot\frac{1}{2}\ln\left(\frac{z^2 + y_{2i}^2}{z^2 + y_{1i}^2}\right) - z\left(\frac{B}{y_{21}} - \frac{2Ay_{1i}}{y_{21}^2}\right) \\ & \cdot\left[\arctan\frac{y_{2i}}{z} - \arctan\frac{y_{1i}}{z}\right]. \end{aligned} \tag{H.9}$$

A. Integration of W_3

From the results of Appendix G,

$$\begin{aligned} \frac{\partial^2 I}{\partial z \partial \eta} \;=\; & \left(\frac{\partial}{\partial r_1}\frac{\partial I}{\partial \eta}\right)\frac{\partial r_1}{\partial z} \\ = \; & \left\{-(y-\eta)\int_{u_1 r_1}^{\infty} \frac{\tau_1}{(\tau_1^2 + r_1^2)^{3/2}} e^{-i\omega(\tau_1 + x_0)/V_\infty} d\tau_1 \right. \\ & \left. + i\frac{\omega}{V_\infty} I\frac{x_2 - x_1}{y_2 - y_1} - \left[1 - \frac{u_1}{(1+u_1^2)^{1/2}}\right]\frac{x_2 - x_1}{y_2 - y_1}\right\}\frac{z}{r_1} \\ = \; & \frac{3(y-\eta)z}{r_1^2} T_2 + i\frac{\omega}{v_\infty}\frac{z}{r_1}\frac{\partial I}{\partial r_1}\frac{x_2 - x_1}{y_2 - y_1} \\ & + \frac{1}{(1+u_1^2)^{3/2}}\frac{x_2 - x_1}{y_2 - y_1}\left(\frac{x_0 z}{r_1^3}\right). \end{aligned} \tag{H.10}$$

where

$$T_2 = r_1^2 \int_{u_1 r_1}^{\infty} \frac{\tau_1}{(\tau_1^2 + r_1^2)^{5/2}} e^{-i\omega(\tau_1 + x_0)/V_\infty} d\tau_1. \tag{II.11}$$

Let

$$G_2 = 3T_2 \tag{II.12}$$

$$G_1 = \left[i\frac{\omega}{V_\infty} T_3 + \frac{1}{(1+u_1^2)^{3/2}} \frac{x_0}{r_1^3} \right] \frac{x_2 - x_1}{y_2 - y_1}, \tag{II.13}$$

The non-singular part of the integrand W_3 becomes

$$\frac{\partial^2 I}{\partial z \partial \eta} = \frac{y - \eta}{r_1^2} z G_2 + z G_1. \tag{II.14}$$

W_3 can then be written as

$$W_3 \simeq -y_{21} z \int_0^1 \arctan\left(\frac{y_{21}\tau + y_{1i}}{z}\right) \left(G_1 - \frac{y_{21}\tau + y_{1i}}{r_1^2} G_2 \right) d\tau. \tag{II.15}$$

Let

$$\begin{aligned} G_1 &= A_1\tau^2 + B_1\tau + C_1, \\ G_2 &= A_2\tau^2 + B_2\tau + C_2, \end{aligned} \tag{II.16}$$

The parabolic approximation of the integration of W_3 is formed as

$$\begin{aligned} W_3 = & -y_{21} z \int_0^1 \arctan\left(\frac{y_{21}\tau + y_{1i}}{z}\right) \\ & \cdot \left[A_1\tau^2 + B_1\tau + C_1 - \frac{y_{21}\tau + y_{1i}}{r_1^2} \left(A_2\tau^2 + B_2\tau + C_2 \right) \right] d\tau. \end{aligned} \tag{II.17}$$

After separated the variables in the integrand and changing the limits of the integral, the result of the approximation is

$$W_3 = \frac{A_1 z}{6 y_{21}^2} \left\{ -2y_{2i}^3 \arctan\left(\frac{y_{2i}}{z}\right) - 2y_{1i}^3 \arctan\left(\frac{y_{1i}}{z}\right) \right.$$

where $ATOX$ is an approximate integration of

$$\int_{\beta_1}^{\beta_2} \frac{\arctan(\beta)}{\beta} d\beta. \tag{II.19}$$

The integrand of this equation can expanded as an infinite series (see page 81, Abramowitz, et. al. (1964))

$$\frac{\arctan(\beta)}{\beta} = \frac{1}{1+\beta^2}\left\{1 + \frac{2}{3}\frac{\beta^2}{1+\beta^2} + \frac{2\cdot 4}{3\cdot 5}\left(\frac{\beta^2}{1+\beta^2}\right)^2 + \frac{2\cdot 4\cdot 6}{3\cdot 5\cdot 7}\left(\frac{\beta^2}{1+\beta^2}\right)^3 + \cdots\right\}, \tag{H.20}$$

where $\beta \neq -1$. Taking the first ten terms of this infinite series, the integral is then solved analytically.

$$+z\left(y_{21}^3+2y_{21}y_{1i}\right)-z^3\ln\frac{z^2+y_{2i}^2}{z^2+y_{1i}^2}\Bigg\}$$

$$+\frac{z}{2}\left(\frac{B_1}{y_{21}}-\frac{2A_1y_{1i}}{y_{21}^2}\right)\left\{-y_{2i}^2\arctan\left(\frac{y_{2i}}{z}\right)+y_{1i}^2\arctan\left(\frac{y_{1i}}{z}\right)\right.$$

$$\left.+zy_{21}-z^2[\arctan\left(\frac{y_{2i}}{z}\right)-\arctan\left(\frac{y_{1i}}{z}\right)]\right\}$$

$$+z\left(\frac{A_1y_{1i}^2}{y_{21}^2}+C_1-\frac{B_1y_{1i}}{y_{21}}\right)\left\{-y_{2i}\arctan\left(\frac{y_{2i}}{z}\right)+y_{1i}\arctan\left(\frac{y_{1i}}{z}\right)\right.$$

$$\left.+\frac{z}{2}\ln\left[\frac{z^2+y_{2i}^2}{z^2+y_{2i}^2}\right]\right\}$$

$$+\frac{A_2z}{2y_{21}^2}\left\{-y_{2i}^2\arctan\left(\frac{y_{2i}}{z}\right)+y_{1i}^2\arctan\left(\frac{y_{1i}}{z}\right)\right.$$

$$\left.+zy_{21}-z^2\left[\arctan\left(\frac{y_{2i}}{z}\right)-\arctan\left(\frac{y_{1i}}{z}\right)\right]\right\}$$

$$z\left(\frac{A_2y_{1i}^2}{y_{21}^2}+C_2-\frac{B_2y_{1i}}{y_{21}}\right)\left[ATOX\left(\frac{y_{1i}}{z}\right)-ATOX\left(\frac{y_{2i}}{z}\right)\right]$$

$$+z\left(\frac{B_2}{y_{21}}-\frac{2A_2y_{1i}}{y_{21}^2}\right)\left\{-y_{2i}\arctan\left(\frac{y_{2i}}{z}\right)+y_{1i}\arctan\left(\frac{y_{1i}}{z}\right)\right.$$

$$\left.\frac{z}{2}\ln\frac{z^2+y_{21}^2}{z^2+y_{1i}^2}\right\}, \qquad \text{(H.18)}$$

Appendix I

Numerical Results of the Integrals in the Unsteady Downwash Equation

There are three kinds of integrals in Eq. 4.8, which cannot be integrated exactly. These integrals are: Eq. 4.14,

$$\begin{aligned} T_1 &= \int_{u_1 r_1}^{\infty} \left[1 - \frac{\tau_1}{(\tau_1^2 + r_1^2)^{1/2}}\right] e^{-i\omega(\tau_1 + x_0)/V_\infty} d\tau_1 \\ &= r_1 e^{-i\omega x_0/V_\infty} \int_{u_1}^{\infty} \left[1 - \frac{\lambda}{(1+\lambda^2)^{1/2}}\right] e^{-i\omega r_1 \lambda/V_\infty} d\lambda; \end{aligned} \tag{I.1}$$

Eq. H.11,

$$\begin{aligned} T_2 &= r_1^2 \int_{u_1 r_1}^{\infty} \frac{\tau_1}{(\tau_1^2 + r_1^2)^{5/2}} e^{-i\omega(\tau_1 + x_0)/V_\infty} d\tau_1 \\ &= \frac{e^{-i\omega x_0/V_\infty}}{r_1} \int_{u_1}^{\infty} \frac{\lambda}{(1+\lambda)^{5/2}} e^{-i\omega\lambda r_1/V_\infty} d\lambda \end{aligned} \tag{I.2}$$

and Eq. H.12,

$$T_3 = \int_{u_1 r_1}^{\infty} \frac{\tau_1}{(\tau_1^2 + r_1^2)^{1/2}} e^{-i\omega(\tau_1 + x_0)/V_\infty} d\tau_1$$

$$= \frac{e^{-i\omega x_0/V_\infty}}{r_1}\int_{u_1}^{\infty}\frac{\lambda e^{-i\omega r_1\lambda/V_\infty}}{(1+\lambda^2)^{1/2}}d\lambda. \tag{I.3}$$

In the case of $u_1 \geq 0.0$, these equations are integrated by parts first, and then Jordan's (1976) approximation is applied to Eq. 4.17. The approximate solutions for these integrals are as follows:

$$T_1 = T_{1r} + iT_{1i}, \tag{I.4}$$

where

$$T_{1r} = r_1\sum_{n=1}^{10}\left(a_n c_n e^{-c_n u_1}\right)/\left(c_n^2+(\omega/V_\infty)^2 r_1^2\right), \tag{I.5}$$

$$T_{1i} = -r_1^2\frac{\omega}{V_\infty}\sum_{n=1}^{10}\frac{a_n e^{-c_n u_1}}{(c_n^2+(\omega/V_\infty)^2 r_1^2}; \tag{I.6}$$

$$T_2 = T_{2r} + iT_{2i}, \tag{I.7}$$

where

$$T_{2r} = \frac{1}{3r_1(1+u_1^2)^{3/2}} - \frac{1}{3r_1}(\frac{\omega r_1}{V_\infty})^2\sum_{n=1}^{10}\frac{a_n c_n e^{-c_n u_1}}{c_n^2+(\omega/V_\infty)^2 r_1^2}, \tag{I.8}$$

$$\begin{aligned} T_{2i} &= -\frac{\omega}{3V_\infty}\left(1-\frac{u_1}{(1+u_1^2)^{1/2}}\right), \\ &\quad +\frac{1}{3r_1}(\frac{\omega r_1}{V_\infty})^3\sum_{n=1}^{10}\frac{a_n e^{-c_n u_1}}{c_n^2+(\omega/V_\infty)^2 r_1^2}; \end{aligned} \tag{I.9}$$

$$T_3 = T_{3r} + iT_{3i}, \tag{I.10}$$

where

$$\begin{aligned} T_{3r} &= \frac{u_1}{r_1}\left(1 - \frac{u_1}{(1+u_1^2)^{1/2}}\right) + \frac{1}{r_1}\sum_{n=1}^{10}\frac{a_n c_n e^{-c_n u_1}}{c_n^2 + (\omega/V_\infty)^2 r_1^2} \\ &\quad + \frac{1}{r_1}\sum_{n=1}^{10}\frac{a_n e^{-c_n u_1}}{c_n^2 + (\omega/V_\infty)^2 r_1^2}\left\{(\frac{\omega r_1}{V_\infty})^2 u_1 (c_n^2 - (\frac{\omega r_1}{V_\infty})^2)\right. \\ &\quad \left. -2c_n(\frac{\omega r_1}{V_\infty})^2(c_n u_1 + 1)\right\}, \end{aligned} \tag{I.11}$$

$$\begin{aligned} T_{3i} &= -\frac{1}{r_1}\left\{\frac{\omega r_1}{V_\infty}\sum_{n=1}^{10}\frac{a_n e^{-c_n u_1}}{c_n^2 + (\omega/V_\infty)^2 r_1^2} + \sum_{n=1}^{10}\frac{a_n e^{-c_n u_1}}{c_n^2 + (\omega/V_\infty)^2 r_1^2}\right. \\ &\quad \left. \cdot\left[2c_n(\frac{\omega r_1}{V_\infty})^3 u_1 + (\frac{\omega r_1}{V_\infty})(c_n u_1 + 1)(c_n^2 - (\frac{\omega r_1}{V_\infty})^2)\right]\right\}; \end{aligned} \tag{I.12}$$

When $u_1 < 0.0$, the power of the exponential in Jordan's (1976) approximation becomes positive, hence the integrations involved in T_1, T_2, T_3 will diverge. Therefore, further treatment of the formulation of these integrals is necessary. This treatment is to change the limits of the integrals (see Lan (1979)). Numerical results of these integrals in the case of $u_1 < 0.0$ are listed as follows:

$$T_1 = T_{1r} + iT_{1i}, \tag{I.13}$$

where

$$T_{1r} = r_1\left\{\cos(\omega r_1/V_\infty u_1)\cdot T_{1ri} - \sin(\omega r_1/V_\infty u_1)\cdot T_{1ii}\right\}, \tag{I.14}$$

$$T_{1i} = r_1\left\{\sin(\omega r_1/V_\infty u_1)\cdot T_{1ri} + \cos(\omega r_1/V_\infty u_1)\cdot T_{1ii}\right\}, \tag{I.15}$$

$$\begin{aligned} T_{1ri} &= \cos(\omega r_1/V_\infty|u_1|)\sum_{n=1}^{10}\frac{a_n c_n e^{-c_n|u_1|}}{c_n^2 + (\omega r_1/V_\infty)^2} + 2\sin(\omega r_1/V_\infty|u_1|)/(\omega r_1/V_\infty) \\ &\quad -(\omega r_1/V_\infty)\sin(\omega r_1/V_\infty|u_1|)\sum_{n=1}^{10}\frac{a_n e^{-c_n|u_1|}}{c_n^2 + (\omega r_1/V_\infty)^2}, \end{aligned} \tag{I.16}$$

$$T_{1ii} = -2(\omega r_1/V_\infty)\sum_{n=1}^{10}\frac{a_n}{c_n^2+(\omega r_1/V_\infty)^2}+2\left(1-\cos\left(\omega r_1/V_\infty|u_1|\right)\right)$$
$$+(\omega r_1/V_\infty)\cos\left(\omega r_1/V_\infty|u_1|\right)\sum_{n=1}^{10}\frac{a_n e^{-c_n|u_1|}}{c_n^2+(\omega r_1/V_\infty)^2}$$
$$+\sin\left(\omega r_1/V_\infty|u_1|\right)\sum_{n=1}^{10}\frac{a_n c_n e^{-c_n|u_1|}}{c_n^2+(\omega r_1/V_\infty)^2}; \tag{I.17}$$

$$T_2 = T_{2r}+iT_{2i}, \tag{I.18}$$

where

$$T_{2r} = \frac{1}{3r_1}\left\{\cos\left(\omega r_1/V_\infty u_1\right)\cdot T_{2a}-\sin\left(\omega r_1/V_\infty u_1\right)\cdot T_{2b}\right\}, \tag{I.19}$$

$$T_{2i} = \frac{1}{3r_1}\left\{\cos\left(\omega r_1/V_\infty u_1\right)\cdot T_{2b}+\sin\left(\omega r_1/V_\infty u_1\right)\cdot T_{2a}\right\}, \tag{I.20}$$

$$T_{2a} = \cos\left(\omega r_1/V_\infty|u_1|\right)\left[\frac{1}{(1+u_1^2)^{3/2}}-(\omega r_1/V_\infty)^2\sum_{n=1}^{10}\frac{a_n c_n e^{-c_n|u_1|}}{c_n^2+(\omega r_1/V_\infty)^2}\right]$$
$$+\sin\left(\omega r_1/V_\infty|u_1|\right)\left[(\omega r_1/V_\infty)^3\sum_{n=1}^{10}\frac{a_n e^{-c_n|u_1|}}{c_n^2+(\omega r_1/V_\infty)^2}\right.$$
$$\left.-(\omega r_1/V_\infty)\left(1+\frac{u_1}{(1+u_1^2)^{1/2}}\right)\right] \tag{I.21}$$

$$T_{2b} = 2(\omega r_1/V_\infty)\left[(\omega r_1/V_\infty)^2\sum_{n=1}^{10}\frac{a_n}{c_n^2+(\omega r_1/V_\infty)^2}-1\right]$$
$$-\cos\left(\omega r_1/V_\infty|u_1|\right)\left[(\omega r_1/V_\infty)^3\sum_{n=1}^{10}\frac{a_n e^{-c_n|u_1|}}{c_n^2+(\omega r_1/V_\infty)^2}\right.$$
$$\left.-(\omega r_1/V_\infty)\left(1+\frac{u_1}{(1+u_1^2)^{1/2}}\right)\right]$$
$$+\sin\left(\omega r_1/V_\infty|u_1|\right)\left[\frac{1}{(1+u_1^2)^{3/2}}-(\omega r_1/V_\infty)^2\sum_{n=1}^{10}\frac{a_n c_n e^{-c_n|u_1|}}{c_n^2+(\omega r_./V_\infty)^2}\right]. \tag{I.22}$$

$$T_3 = T_{3r} + iT_{3i}, \tag{I.23}$$

where

$$T_{3r} = \frac{1}{r_1}\left\{\cos(\omega r_1/V_\infty u_1)\cdot T_{3a} - \sin(\omega r_1/V_\infty u_1)\left(T_{3b} - 2\frac{\omega}{V_\infty}B_k\right)\right\}, \tag{I.24}$$

$$T_{3i} = \frac{1}{r_1}\left\{\sin(\omega r_1/V_\infty u_1)\cdot T_{3a} + \cos(\omega r_1/V_\infty v_1)\left(T_{3b} - 2\frac{\omega}{V_\infty}B_k\right)\right\}, \tag{I.25}$$

$$\begin{aligned} T_{3a} = {} & \cos(\omega r_1/V_\infty|u_1|)\left\{|u_1|\left(1-\frac{u_1}{(1+u_1^2)^{1/2}}\right)+\sum_{n=1}^{10}\frac{a_n c_n e^{-c_n|u_1|}}{c_n^2+(\omega r_1/V_\infty)^2}\right. \\ & +u_1(\omega r_1/V_\infty)^2\sum_{n=1}^{10}\frac{a_n e^{-c_n|u_1|}}{c_n^2+(\omega r_1/V_\infty)^2} \\ & \left.-2(\omega r_1/V_\infty)^2\sum_{n=1}^{10}\frac{a_n c_n e^{-c_n|u_1|}}{(c_n^2+(\omega r_1/V_\infty)^2)^2}\right\} - (\omega r_1/V_\infty)\sin(\omega r_1/V_\infty|u_1|) \\ & \left\{\left[\sum_{n=1}^{10}\frac{a_n e^{-c_n|u_1|}}{c_n^2+(\omega r_1/V_\infty)^2}\right](1+|u_1|c_n)\right. \\ & \left.+\sum_{n=1}^{10}\frac{a_n\left(c_n^2-(\omega r_1/V_\infty)^2\right)e^{-c_n|u_1|}}{(c_n^2+(\omega r_1/V_\infty)^2)^2}\right\} \end{aligned} \tag{I.26}$$

$$\begin{aligned} T_{3b} = {} & \sin(\omega r_1/V_\infty|u_1|)\left\{|u_1|\left(1-\frac{u_1}{(1+u_1^2)^{1/2}}\right)+\sum_{n=1}^{10}\frac{a_n c_n e^{-c_n|u_1|}}{c_n^2+(\omega r_1/V_\infty)^2}\right. \\ & -u_1(\omega r_1/V_\infty)^2\sum_{n=1}^{10}\frac{a_n e^{-c_n|u_1|}}{c_n^2+(\omega r_1/V_\infty)^2} \\ & \left.-2(\omega r_1/V_\infty)^2\sum_{n=1}^{10}\frac{a_n c_n e^{-c_n|u_1|}}{(c_n^2+(\omega r_1/V_\infty)^2)^2}\right\}, \\ & +(\omega r_1/V_\infty)\cos(\omega r_1/V_\infty|u_1|)\left\{(1+|u_1|c_n)\sum_{n=1}^{10}\frac{a_n e^{-c_n|u_1|}}{c_n^2+(\omega r_1/V_\infty)^2}\right. \\ & \left.+\sum_{n=1}^{10}\frac{a_n\left(c_n^2-(\omega r_1/V_\infty)^2\right)e^{-c_n|u_1|}}{(c_n^2+(\omega r_1/V_\infty)^2)^2}\right\}, \end{aligned} \tag{I.27}$$

$$B_k = K_0(\omega r_1/V_\infty), \tag{I.28}$$

the modified Bessel function of zero order (see Lan(1979). By reference to Abramowitz et al. (1970,*pp.*378 – 379), the result of this function can be obtained by the use of polynomial approximations.

Appendix J

Mathematical Formulation of the Leading-edge Suction Force, Mean Total Thrust Coefficient and Propulsive Efficiency

A: Equations for calculating leading-edge suction force

Similar to the equations in the two dimensional case, Lan (1979) defined a leading-edge singularity parameter C_s as

$$C_s = \lim_{x \to x_l} 2u(x)[(x - x_l)/c]^{1/2}, \tag{J.1}$$

where x_l is the location of leading-edge vortex strip, $u(x)$ is the velocity on the wing in x-direction. The singularity term in the downwash formula is W_b in Appendix D because W_b has a Cauchy singularity when $\theta = \theta'$. Let

$$W_b = \frac{1}{4\pi} \int_{x_l}^{x_t} \frac{\gamma(x) D(\theta)}{(x_1 - x)(y_2 - y1) - (x_2 - x_1)(y_1 - y)}, \tag{J.2}$$

and note

$$\begin{aligned} (x_{l2} - x_l)/(y_2 - y_l) &= (x_{l2} - x_{l1})/(y_2 - y_1) = \tan \Lambda_l \\ (x_l - x_{l1})/(y_l - y_1) &= (x_{l2} - x_{l1})/(y_2 - y_1) = \tan \Lambda_l \end{aligned}$$

where the subscript l denotes the values at leading edge, Λ_l is the leading edge sweep angle, the value of $D(\theta)/(y_2 - y_1)$ when θ tends to zero is

$$\lim_{\theta \to 0} D(\theta)/(y_2 - y_1) = 2[\tan^2 \Lambda_l + 1]^{1/2}. \tag{J.3}$$

It follows that the leading-edge suction parameter C_s can be obtained by solving the following equation:

$$N_c C_s [\tan^2 \Lambda_l + 1]^{1/2} = \sum\sum \Delta C_p \left[\frac{\partial \Phi_1}{\partial z} + \frac{\partial \Phi_2}{\partial z}\right]_{(x_l, y_l)} - W(x_l, y_l). \tag{J.4}$$

Since the wing is in harmonic motion, the mean sectional suction parameter C_{sm} should be the real part of $C_s e^{i\omega t}$ after the time average as

$$C_{sm} = \frac{1}{2}(C_{sr}^2 + C_{si}^2), \tag{J.5}$$

where C_{sr} and C_{si} are the real and imaginary parts of C_s respectively. The mean sectional leading-edge thrust coefficient therefore is $C_t = \pi C_{sm}(2\cos \Lambda_l)$. Once C_t is known, the total mean leading-edge thrust coefficient $\bar{C}_{tl}$ is known (see Lan (1974)).

B: Mean total thrust coefficient calculation and propulsive efficiency formulation

The thrust coefficient is contributed by two parts: the mean leading-edge thrust coefficient $\bar{C}_{tl}$ and the lift vector, $L\bar{\alpha}$ (Lan (1979)). The sectional lift vector component can be calculated by following Lan (1979) as

$$- qcR_e[C_{l(\ )} e^{i\omega t}] R_e[\alpha(y) e^{i(\Phi_{ph} - \pi)} e^{i\omega t}] dy, \tag{J.6}$$

where q is dynamic pressure, c is local chord length, Re is the real part, C_l is sectional complex lifting coefficient. Applying Eq. 2.7, the mean value of Eq. J.6 over one cycle can be written as

$$-qc\frac{1}{2}\left\{C_{lr}(y)R_e[\alpha(y)e^{i(\Phi_{ph}-\pi)}]\right.$$
$$\left.C_{li}(y)I_m[\alpha(y)e^{i(\Phi_{ph}-\pi)}]\right\}dy, \tag{J.7}$$

where $C_{lr}(y)$ and $C_{li}(y)$ are the real part and imaginary part of the complex sectional lifting coefficient. Therefore, the mean total thrust is

$$\begin{aligned}\bar{T} &= C_l q S_w \\ &= S_w q\left\{\bar{C}_{tl} - \frac{1}{2S}\int_{-b/2}^{b/2}\left[C_{lr}(y)R_e[\alpha(y)e^{i(\Phi_{ph}-\pi)}]\right.\right. \\ &\quad \left.\left. + C_{li}(y)I_m[\alpha(y)e^{i(\Phi_{ph}-\pi)}]\right]c(y)dy\right\}.\end{aligned} \tag{J.8}$$

Similarly, the input power consisting of $-L\dot{\bar{h}}$ (h is positive downward), the lift production, and $M\dot{\bar{\alpha}}$, the moment production, can be written as

$$\begin{aligned}IP &= L\dot{\bar{h}} - M\dot{\bar{\alpha}} \\ &= q\int_{-b/2}^{b/2} R_e[C_l(y)e^{i\omega t}]R_e[i\omega h(y)e^{i\omega t}]c(y)dy \\ &\quad -q\int_{-b/2}^{b/2} R_e[C_m(y)e^{i\omega t}]R_e[i\omega\alpha(y)e^{i\omega t}e^{i(\Phi_{ph}-\pi)}]c^2(y)dy.\end{aligned} \tag{J.9}$$

Applying Fourier synthesis in Eq. 2.7, the mean value of Eq. J.9 can be determined as

$$\begin{aligned}\bar{IP} &= \frac{q}{2}\omega\int_{-b/2}^{b/2} h(y)C_{li}c(y)dy \\ &\quad -\frac{q}{2}\omega\int_{-b/2}^{b/2}\left[C_{mi}(y)R_e[\alpha(y)e^{i(\Phi_{ph}-\pi)}] - C_{mr}(y)I_m[\alpha(y)e^{i(\Phi_{ph}-\pi)}]\right]c^2(y)dy,\end{aligned} \tag{J.10}$$

which is Eq. 2.31 of Lan (1979).

The propulsive efficiency is determined by

$$\eta = \bar{T} \cdot V_\infty / \bar{IP}. \tag{J.11}$$

Appendix K

The Program Listing

The program for a rectangular wing of aspect ratio eight in unsteady motion is listed as follows. It is quite easy to use this program: choose the oscillating parameters as indicated in Chapter 5; set appropriate N_c and N_s; determine N_i, which is from the wing's offsets record. For symmetrical wing, only $(N_i/2+1)$ points of each curve (on the leading edge and the trailing edge) need to be input. The input geometrical values in the following program are of a rectangular wing. If the curves of the wing cannot be expressed by one or two simple functions, but it is symetrical, delete the 'doloop' 255 and input the values of the two curves at $(N_i/2+1)$ points; if the wing is asymmetrical,delete both doloops 255 and 256, and input the values at all points on the curves; if the wing is non-planar, delete the doloop 257, and input the z value at each control point. When running the program at larger N_c and N_s, long CPU times are expected.

```
C**********************************************************************
C* NC          NUMBER OF CHORDWISE CONTROL POINT
C* M2 NUMBER OF SPANWISE VORTEX STRIPS
C* ASR          ASPECT RATIO
C* ALPHA          ANGLE OF ATTACK
C* CCOTR(M2) THE CHORD LENGTH AT CONTROL POINTS
C* CSTRIP(M2) THE CHORD LENGTH AT VORTEX STRIPS
C* CA              AVERAGE CHORD
C* B THE LENGTH OF THE SPAN
C* SW WING AREA
C* XLCOTR(M2) THE DISTANCE FROM Y-AXIS TO THE LEADING EDGE
C*                        AT CONTROL POINTS
C* XLSTRIP(M2) THE DISTANCE FROM Y-AXIS TO THE LEADING EDGE
C*                        AT STRIPS
C* DELTP(NC,M2) NONDIMENSIONAL VORTEX DENSITY REFERRED TO LOCAL
C* CHORD AND FREESTREAM VELOCITY
C* CLL(M2)  SECTIONAL LIFTING COEFFICIENT
C* CL(M2M1) TOTAL LIFTING COEFFICIENT
C* CML(M2)  SECTIONAL PITCHING MOMENT COEFFICIENT
C* CM(M2M1) TOTAL PITCHING MOMENT COEFFICIENT
C* CTL(M2)  SECTIONAL LEADING-EDGE THRUST COEFFICIENT
C* CT(M2)   TOTAL LEADING-EDGE THRUST COEFFICIENT
C* THETKN(NC)       CHORDWISE LOCATION OF THE VORTICES
C* THETKI(NC)       CHORDWISE (X-COORDINATE) LOCATION OF CONTROL POINT
C* THETMJ(M2)       SPANWISE (Y-COORDINATE) LOCATIONS OF VORTEX STRIPS
```

```
* THETMI(M2)       SPANWISE (Y-COORDINATE) LOCATIONS OF CONTROL POINTS
* ALPHAD           ANGLE OF ATTACK IN DEGREES
* ALPHAR           ANGLE OF ATTACK IN RADIUS
*       ALPHAS(M2)       SECTIONAL SWEEP ANGLE
* CLS(M2)   SECTIONAL LEADING EDGE SUCTION PARAMETER
* CTS(M2)          SECTIONAL LEADING EDGE SUCTION THRUST COEFFICIENT
* NI NUMBER OF GIVEN GEOMETRY INTERPOLATION
*                  SECTIONS
* NIP1 NUMBER OF GIVEN GEOMETRY INTERPOLATION
*                  POINTS
*================================================================
*----------------------------------------------------------------
*  A1RECTAN.FOR PROGRAM FOR 3D THIN FOIL AERODYNAMIC CHARACTERISTICS
*           COMPUTATION BY QVLM REFERRED TO LAN'S PAPER IN 1979
*----------------------------------------------------------------
* MAIN PROGRAM
*----------------------------------------------------------------
IMPLICIT REAL*8(A-H,O-Z)
PARAMETER (NC=3,MI=5,MII=5,M2=MI+MII,NI=40)
        PARAMETER (M2M1=M2-1,NIP1=NI+1,NID2=NI/2,NID2P1=NID2+1)
        PARAMETER (N=NC*M2M1,NP1=N+1,NCP1=NC+1)
        PARAMETER (NID2P2=NID2+2)
DIMENSION CCOTR(M2),CSTRIP(M2),XLCOTR(M2),XLSTP(M2),
     #             THETKN(NC),THETKI(NC),XIK(NC),XI(NCP1,M2),PHI(M2)
DIMENSION X1K(NC,M2),X2K(NC,M2),YJ(M2),YI(M2),DSINKN(NC),
     #             DSINMI(M2),ALPHAS(M2)
DIMENSION THETMJ(M2),THETMI(M2),C2S(M2),CTSA(M2),CTA(M2)
DIMENSION YII(M2),AI(M2M1),BI(M2M1,3),ZZ(NC,M2),
     #            YA(M2M1),ALPHSE(NC,M2)
DIMENSION YY(NIP1),XX1(NIP1),XX2(NIP1),
     #             S2(NIP1),H(NIP1),DY(NIP1),E(NIP1)
DIMENSION Y(NIP1),T(M2),F(M2),F1(M2),
     #            F2(M2),XI1(M2),XI2(M2),XJ1(M2),XJ2(M2),S(NIP1)
COMPLEX*8 T1E,T2,T3E,PW2,G1,G2,W2,W3,T11,T12,T31,EPS,
     #          T32,DPHI2,DPHI,WXY(NCP1,M2),DELTP(NC,M2),VAR,
     #          AA(NC,M2,NC,M2),A(N,NP1),SUMI(M2,NC,M2),CLS(M2),
     #             CLL(M2,NC),CML(M2,NC),EIPH,
     #             CDI(M2),CDII,CDCL,CDCD,
     #             CTS(M2),CT(M2),CL(M2),CM(M2)
EXTERNAL T1E,T2,T3E,PW2,G1,G2,W2,W3,T11,T12,T31,
     #           T32,ATOX,DPHI2,DPHI1,DPHI
OPEN(UNIT=7,FILE='UNQV.OUT',STATUS='UNKNOWN')
*----------------------------------------------------------------
* INPUT DATA: THE VALUES OF WING SHAPE CURVES
*----------------------------------------------------------------
B=6.0
        BR=0.750
B0=0.75*0.75
        HEAV=0.750
PI=3.141592654
BD2=B/2.0
DELTY=B/DFLOAT(NI)
DO 49 IMM=1,NIP1
YY(IMM)=(IMM-1)*DELTY-BD2
 49 CONTINUE
DO 255 LHS=1,NID2P1
XX1(LHS)=-0.5625
XX2(LHS)=0.1875
 255 CONTINUE
```

```
      DO 256 KIJ=NID2P2,NIP1
      KIK=2*NID2P1-KIJ
      XX1(KIJ)=XX1(KIK)
      XX2(KIJ)=XX2(KIK)
       256 CONTINUE
      DO 257 I=1,NC
      DO 257 J=1,M2
      ZZ(I,J)=0.0
       257 CONTINUE
      CR=DABS(XX1(NID2P1)-XX2(NID2P1))
      *-----------------------------------------------------------------
      CALL GEOR(NC,MI,MII,M2,M2M1,PI,NI,NIP1,YY,XX1,XX2,
           #       CSTRIP,XLCOTR,XLSTP,YJ,YI,NID2,NID2P1,B,CCOTR,
           #    ALPHAS,S2,H,DY,E,THETMJ,THETMI,SPLINE,F,F1,Y,T,
           #    F2,XI1,XI2,XJ1,XJ2,S,SW1,SW2)
      *-----------------------------------------------------------------
      SW=SW2-SW1
      CA=SW/B
      BD2=B/2.0
      ASR=SW/(CA*CA)
      *-----------------------------------------------------------------
      *CALCULATION OF CHORDWISE ANGLER CONTROL POINTS AND VORTEX LOCATIONS
      *-----------------------------------------------------------------
      DO 20 K=1,NC
      THETKN(K)=(2.0*DFLOAT(K)-1.0)*PI/(2.0*DFLOAT(NC))
      XIK(K)=(1.0-DCOS(THETKN(K)))/2.0
      THETKI(K)=DFLOAT(K)*PI/DFLOAT(NC)
       20     CONTINUE
      *-----------------------------------------------------------------
      * CHORDWISE CONTROL POINTS XI(NC,M2),VORTEX LOCATIONS
      * X1K(NC,M2),X2K(NC,M2)
      *-----------------------------------------------------------------
             DO 1130 I=1,NC
      DO 1130 J=1,M2M1
      *
      XI(I,J)=XLCOTR(J)+CCOTR(J)*(1.0-DCOS(THETKI(I)))/2.0
      *
      X1K(I,J)=XLSTP(J)+CSTRIP(J)*XIK(I)
      *
      X2K(I,J)=XLSTP(J+1)+CSTRIP(J+1)*XIK(I)
      *
      DXDYE=(X2K(I,J)-X1K(I,J))/(YJ(I+1)-YJ(I))
      *
      ALPHSE(I,J)=DATAN(DXDYE)
      *
       1130     CONTINUE
      DO 3210 I=1,M2M1
      XI(NCP1,I)=XLCOTR(I)
       3210 CONTINUE
      PHIPH=PI/2.0
      *=================================================================
      WRITE(7,290) NC,M2M1,B,ASR,SW,CA,BR,BO,CR,HEAV,PHIPH
       290    FORMAT(5X,'NUMBER OF CHORDWISE CONTROL POINT NC=',I4,//,
           #     5X,'NUMBER OF SPANWISE CONTROL POINT NS=',I4,//,
           #     5X,'THE LENGTH OF THE SPAN B=',F9.5,//,
           #     5X,'ASPECT RATIO ASR=',F9.5,//,
           #     5X,'WING AREA SW=',F9.5,//,
           #     5X,'AVERAGE CHORD LENGTH CA=',F9.5,//,
           #     5X,'REFERENCE LENGTH BR=',F9.5,//,
           #     5X,'PITCHING AXIS POSITION BO=',F9.5,//,
```

```
     #     5X,'ROOT CHORD LENGTH CR=',F9.5,//,
     #     5X,'AMPLITUDE OF WING HEAV=',F9.5,//,
     #     5X,'PHASE ANGLE (PITCH LEADS HEAVE) PHIPH=',F9.5,//)
WRITE(7,5820)
 5820 FORMAT(X,'RED-FRE k',x,'PR-EF eta',x,'PR-THR Ct',
     #         X,'LE-TH Ctl',X,
     #         'ABC-CL|Cl|',X,'FEAT-P theta')
*=====================================================================
DO 1 LFE=1,2
              FEATHP=(DFLOAT(LFE)-1.0)*0.4
DO 2 LRFK=1,10
              RFK=DFLOAT(LRFK)*0.2
OMOV=RFK/BR
ALPHAR=HEAV*OMOV*FEATHP
*---------------------------------------------------------------------
*  MATRIX CALCULATION: II,JJ, DELTP(II,JJ)'S LOCATIONS IN X AND Y
*  DIRECTIONS.KI,KJ THE VORTEX STRIP LOCATIONS IN X AND Y DIRECTIONS
*---------------------------------------------------------------------
ANGL=PHIPH-PI
VAR=(DCOS(ANGL)+(0.0,1.0)*DSIN(ANGL))
VAR=ALPHAR*VAR
DO 541 II=1,NCP1
DO 541 JJ=1,M2M1
WXY(II,JJ)=-(0.0,1.0)*OMOV*HEAV-VAR-(0.0,1.0)*VAR
     #              *OMOV*(XI(II,JJ))
 541 CONTINUE
*
DO 80 KJ=1,M2M1
DO 80 II=1,NC
DO 80 JJ=1,M2M1
DO 80 KI=1,NC
*
X2X1=X2K(KI,KJ)-X1K(KI,KJ)
*
X2XI=X2K(KI,KJ)-XI(II,JJ)
*
X1XI=X1K(KI,KJ)-XI(II,JJ)
*
Y2Y1=YJ(KJ+1)-YJ(KJ)
*
Y2YI=YJ(KJ+1)-YI(JJ)
*
Y1YI=YJ(KJ)-YI(JJ)
*
Z=ZZ(II,JJ)
*
IF(OMOV.LE.1.0E-10)THEN
AA(II,JJ,KI,KJ)=DPHI1(Z,X2X1,X2XI,X1XI,Y2Y1,Y2YI,Y1YI,PI)
     # *CCOTR(KJ)*DSIN(THETKN(KI))/(16.0*DFLOAT(NC))
ELSE
        AA(II,JJ,KI,KJ)=DPHI(Z,X2X1,X1XI,X2XI,Y2Y1,Y2YI,Y1YI,OMOV,PI,
     #          T1E,T2,T3E,PW2,W2,W3,G1,G2,T11,T12,T31,
     #          T32,ATOX,DPHI1,DPHI2)
     # *CCOTR(KJ)*DSIN(THETKN(KI))/(16.0*DFLOAT(NC))
END IF
 80     CONTINUE
*---------------------------------------------------------------------
DO 901 II=1,NC
DO 901 JJ=1,M2M1
DO 901 KI=1,NC
```

```
      DO 901 KJ=1,M2M1
             IC=II+(JJ-1)*NC
      ID=KI+(KJ-1)*NC
      A(IC,ID)=AA(II,JJ,KI,KJ)
       901    CONTINUE
      *-----------------------------------------------------------------
      DO 542 I=1,NC
      DO 542 J=1,M2M1
      KIJ=I+(J-1)*NC
      * KIJ=J+(I-1)*M2M1
      A(KIJ,NP1)=WXY(I,J)
       542 CONTINUE
      *-----------------------------------------------------------------
      CALL GAUSS(N,NP1,A,EPS)
      *-----------------------------------------------------------------
      DO 33 I=1,NC
      DO 33 J=1,M2M1
      KM=I+(J-1)*NC
      DELTP(I,J)=A(KM,NP1)
       33 CONTINUE
      *-----------------------------------------------------------------
      *SECTIONAL LEADING EDGE THRUST COEFFICIENT  (CTS) COMPUTATION
      *-----------------------------------------------------------------

      DO 85 KJ=1,M2M1
      DO 85 JJ=1,M2M1
      DO 85 KI=1,NC
      *
      X2X1=X2K(KI,KJ)-X1K(KI,KJ)
      *
      X2XI=X2K(KI,KJ)-XLCOTR(JJ)
      *
      X1XI=X1K(KI,KJ)-XLCOTR(JJ)
      *
      Y2Y1=YJ(KJ+1)-YJ(KJ)
      *
      Y2YI=YJ(KJ+1)-YI(JJ)
      *
      Y1YI=YJ(KJ)-YI(JJ)
      *
      Z=ZZ(1,JJ)
      *
              SUMI(JJ,KI,KJ)=DELTP(KI,KJ)*
           #                 DPHI(Z,X2X1,X1XI,X2XI,Y2Y1,Y2YI,Y1YI,OMOV,PI,
           #           T1E,T2,T3E,PW2,W2,W3,G1,G2,T11,T12,T31,
           #           T32,ATOX,DPHI1,DPHI2)
           #                 *CCOTR(KJ)*DSIN(THETKN(KI))/(16.0*DFLOAT(NC))
       85     CONTINUE
      *
      DO 86 JJ=1,M2M1
      DO 87 KJ=1,M2M1
      DO 87 KI=2,NC
      *
      SUMI(JJ,KI,KJ)=SUMI(JJ,KI-1,KJ)+SUMI(JJ,KI,KJ)
       87     CONTINUE
      *
      DO 88 KJ=2,M2M1
      *
      SUMI(JJ,NC,KJ)=SUMI(JJ,NC,KJ-1)+SUMI(JJ,NC,KJ)
       88     CONTINUE
      *
```

```
 86     CONTINUE
*
DO 190 JJ=1,M2M1
CLS(JJ)=(SUMI(JJ,NC,M2M1)-WXY(NCP1,JJ))/
     #          (DFLOAT(NC)*((DTAN(ALPHAS(JJ)))**2.0+1.0)**0.5)
 190 CONTINUE
*-----------COMPLEX TRANSFORM AND AVERAGE-------------------------
DO 590 JJ=1,M2M1
CLSRE=REAL(CLS(JJ))
CLSIM=AIMAG(CLS(JJ))
C2S(JJ)=(CLSRE*CLSRE+CLSIM*CLSIM)/2.0
 590 CONTINUE
*-----------------------------------------------------------------
DO 91 JJ=1,M2M1
CTSA(JJ)=PI*C2S(JJ)/(2.0*DCOS(ALPHAS(JJ)))
 91     CONTINUE
DO 391 JJ=1,M2M1
CTS(JJ)=PI*(CLS(JJ)*CLS(JJ))/(2.0*DCOS(ALPHAS(JJ)))
 391    CONTINUE
*-----------------------------------------------------------------
*SECTIONAL PITCHING MOMENT  AND LIFT COEFFICIENTS COMPUTATION
*-----------------------------------------------------------------
DO 41 I=1,M2M1
DSINKN(1)=DSIN(THETKN(1))
CLL(I,1)=DELTP(1,I)*DSINKN(1)*PI/(DFLOAT(NC)*2.0)
CML(I,1)=-DELTP(1,I)*DSIN(THETKN(1))*(XLCOTR(I)
     #          +CCOTR(I)*XIK(1))*PI/(DFLOAT(NC)*CA*2.0)
DO 75 K=2,NC
DSINKN(K)=DSIN(THETKN(K))
CLL(I,K)=CLL(I,K-1)+DELTP(K,I)*DSINKN(K)*PI/(DFLOAT(NC)*2.0)
CML(I,K)=-DELTP(K,I)*DSIN(THETKN(K))*(XLCOTR(I)
     #           +CCOTR(I)*XIK(K))*PI/(DFLOAT(NC)*CA*2.0)+CML(I,K-1)
*
 75     CONTINUE
 41     CONTINUE
*=================================================================
*TOTAL PITCHING MOMENT (CM), LEADING EDGE THRUST (CT) AND LIFT (CL)
*COEFFICIENTS COMPUTATION
*=================================================================
DO 78 KK=1,M2
DO 78 JJ=1,NC

CM(KK)=0.0
CT(KK)=0.0
CL(KK)=0.0
 78     CONTINUE
*
DSINMI(1)=DSIN(THETMI(1))
CL(1)=(PI*B*CLL(1,NC)*CCOTR(1)*DSINMI(1))/(2.0*SW*DFLOAT(M2))
CT(1)=(PI*B*CTS(1)*CCOTR(1)*DSINMI(1))/(2.0*SW*DFLOAT(M2))
CTA(1)=(PI*B*CTSA(1)*CCOTR(1)*DSINMI(1))/(2.0*SW*DFLOAT(M2))
CM(1)=(PI*B*CML(1,NC)*CCOTR(1)*DSINMI(1))/
     #         (2.0*SW*DFLOAT(M2))
*
DO 185 I=2,M2M1
DSINMI(I)=DSIN(THETMI(I))
CL(I)=((PI*B*CLL(I,NC)*CCOTR(I)*DSINMI(I))/(2.0*SW*DFLOAT(M2)))
     #         +CL(I-1)
*
CT(I)=(PI*B*CTS(I)*CCOTR(I)*DSINMI(I))/(2.0*SW*DFLOAT(M2))
```

```
     #         +CT(I-1)
CTA(I)=(PI*B*CTSA(I)*CCOTR(I)*DSINMI(I))/(2.0*SW*DFLOAT(M2))
     #         +CTA(I-1)
*
CM(I)=CM(I-1)+(PI*B*CML(I,NC)*CCOTR(I)*DSINMI(I))/
     #         (2.0*SW*DFLOAT(M2))
*
 185     CONTINUE
*
CDII=CL(M2M1)-CT(M2M1)
*-----------------------------------------------------------------------
CDCL=CDII/(CL(M2M1)*CL(M2M1))
*-----------------------------------------------------------------------
*--------------------THRUST COEFFICIENT COMPUTATION---------------------
PT=0.0
PP=0.0
EIPH=DCOS(ANGL)+(0.0,1.0)*DSIN(ANGL)
EIPHRE=REAL(EIPH)
EIPHIM=AIMAG(EIPH)
DO 739 I=1,M2M1
CLLRE=REAL(CLL(I,NC))
CLLIM=AIMAG(CLL(I,NC))
CMLRE=REAL(CML(I,NC))
CMLIM=AIMAG(CML(I,NC))
PT=PT+(ALPHAR*PI*B/(4.0*DFLOAT(M2)))*CCOTR(I)*DSIN(THETMI(I))
     #         *(CLLRE*EIPHRE+CLLIM*EIPHIM)
PP=PP+OMOV*((B*PI/(4.0*DFLOAT(M2)))
     #      *HEAV*CLLIM*CCOTR(I)*DSIN(THETMI(I))
     #        -(B*PI/(4.0*DFLOAT(M2)))*ALPHAR*CCOTR(I)*CCOTR(I)
     #        *(CMLIM*EIPHRE-CMLRE*EIPHIM)*DSIN(THETMI(I)))
 739 CONTINUE
TOQ=SW*CTA(M2M1)-PT
CCTT=TOQ/SW
PQV=PP
PROE=TOQ/PQV
*=====================================================================
***-------------------------------------------------------------------
* WRITE(6,160) CL(M2M1),CM(M2M1),CTA(M2M1),CT(M2M1)
* 160    FORMAT(///,2X,'CL(TOTAL)=',2F14.9,'i',/
*     #          ,2X,'CM(TOTAL)=',2F14.9,'i',/
*     #         ,2X,'CTA(TOTAL)=',F14.9,/,
*     #         /,2X,'CT(TOTAL)=',2F14.9,'i',//))
*---------------------------------------------------------------------
* WRITE(6,771) PT,PP,TOQ,PQV,PROE,CCTT
* 771 FORMAT (4X, 'THE LIFT VECTOR COMPONENT PT(LA)=',F14.9,/,
*     #                '   INPUT POWER OVER OMOV  PP=',F14.7,/,
*     #                '   PROPULSIVE THRUST TOQ=',F14.9,/,
*     #                '   INPUT POWER  PQV=',F14.9,/,
*     #                '   PROPULSIVE EFFICIENCY PROE(ZETA)=',F14.9,
*     #                '   CCTT =',F14.9)
*---------------------------------------------------------------------
CTOK2=CCTT/(RFK*RFK)
CLABS=CABS(CL(M2M1))
CTL=CTA(M2M1)
CTLK2=CTL/(RFK*RFK)
XA=BSTAR*CO
WRITE(7,582) RFK,PROE,CCTT,CTL,CLABS,FEATHP
```

```
 582 FORMAT(x,F9.5,x,F9.5,x,F9.5,X,F9.5,X,
     #         F9.5,X,F9.5)
 2 CONTINUE
 1 CONTINUE
CLOSE (UNIT=7)
STOP
END

*-----------------------------------------------------------------------
*SUBROUTINE GAUSS IS LINEAR SYSTEM SOLVER
*-----------------------------------------------------------------------
SUBROUTINE GAUSS(N,N1,A,EPS)
IMPLICIT REAL*8(A-H,O-Z)
COMPLEX*8 A(N,N1),T
*
DO 50 K=1,N
BMAX=0.0
DO 20 I=K,N
IF(BMAX-CABS(A(I,K))) 10, 20, 20
  10  BMAX=CABS(A(I,K))
L=I
  20    CONTINUE
IF (BMAX.LT.EPS) STOP 7777
IF (L.EQ.K) GO TO 30
DO 25 J=K,N1
T=A(L,J)
A(L,J)=A(K,J)
  25  A(K,J)=T
  30    T=1.0/A(K,K)
K1=K+1
DO 40 J=K1,N1
A(K,J)=A(K,J)*T
DO 40 I=K1,N
  40    A(I,J)=A(I,J)-A(I,K)*A(K,J)
  50 CONTINUE
DO 60 IK=2,N
I=N1-IK
I1=I+1
DO 60 J=I1,N
  60 A(I,N1)=A(I,N1)-A(I,J)*A(J,N1)
RETURN
END
*-----------------------------------------------------------------------
*SUBROUTINE LAQ IS USED FOR THE 3-POINT PARABOLIC INTERPOLATION
*-----------------------------------------------------------------------
SUBROUTINE LAQ(N,L,X,A,B,YA)
*
IMPLICIT REAL*8(A-H,O-Z)
*
DIMENSION A(N),B(N,L),YA(L)
*
N1=N-2
DO 10 I=1,N1
IF(X.LE.A(I+1)) GO TO 20
 10 CONTINUE
I=N1
 20 IF(I.EQ.1) GO TO 30
IF(X-A(I).GE.A(I+1)-X) GO TO 30
I=I-1
 30 A1=A(I)
```

```
A2=A(I+1)
A3=A(I+2)
U=(X-A2)*(X-A3)/((A1-A2)*(A1-A3))
V=(X-A1)*(X-A3)/((A2-A1)*(A2-A3))
W=(X-A1)*(X-A2)/((A3-A1)*(A3-A2))
DO 40 J=1,L
 40 YA(J)=U*B(I,J)+V*B(I+1,J)+W*B(I+2,J)
RETURN
END
***=========================================================================
* SUBROUTINE GEOR IS FOR GEOMETRY INTERPOLATION
*-------------------------------------------------------------------------
SUBROUTINE GEOR(NC,MI,MII,M2,M2M1,PI,NI,NIP1,YY,XX1,XX2,
     #       CSTRIP,XLCOTR,XLSTP,YJ,YI,NID2,NID2P1,B,CCOTR,
     #    ALPHAS,S2,H,DY,E,THETMJ,THETMI,SPLINE,F,F1,Y,T,
     #    F2,XI1,XI2,XJ1,XJ2,S,SW1,SW2)
IMPLICIT REAL*8(A-H,O-Z)
DIMENSION CCOTR(M2),CSTRIP(M2),XLCOTR(M2),XLSTP(M2)
DIMENSION YJ(M2),YI(M2),YY(NIP1),XX1(NIP1),XX2(NIP1),
     #          ALPHAS(M2),S2(NIP1),H(NIP1),DY(NIP1),E(NIP1)
DIMENSION THETMJ(M2),THETMI(M2),Y(NIP1),T(M2),F(M2),F1(M2),
     #          F2(M2),XI1(M2),XI2(M2),XJ1(M2),XJ2(M2),S(NIP1)
* GEOMETRY PARAMETERS
BD2=B/2.0
* SPANWISE VORTEX STRIP LOCATION THETMJ(M2) AND YJ(M2),
*       CONTROL PoINTS THETMI(M2),YI(M2)
DO 40 J=1,MI
THETMI(J)=DFLOAT(J)*PI/DFLOAT(MI)
THETMJ(J)=(2.0*DFLOAT(J)-1.0)*PI/(2.0*DFLOAT(MI))
YI(J)=(BD2)*(1.0-DCOS(THETMI(J)))/2.0-BD2
YJ(J)=(BD2)*(1.0-DCOS(THETMJ(J)))/2.0-BD2
 40     CONTINUE
DO 50 JJ=1,MII
J=JJ+MI
THETMI(J)=DFLOAT(JJ)*PI/DFLOAT(MII)
THETMJ(J)=(2.0*DFLOAT(JJ)-1.0)*PI/(2.0*DFLOAT(MII))
YI(J)=(BD2)*(1.0-DCOS(THETMI(J)))/2.0
YJ(J)=(BD2)*(1.0-DCOS(THETMJ(J)))/2.0
 50     CONTINUE
*-------------------------------------------------------------------------
DO 59 I=1,M2
T(I)=YI(I)
 59 CONTINUE
DO 51 I=1,NIP1
Y(I)=XX1(I)
 51 CONTINUE
CALL SPLN(NIP1,M2,0,YY,Y,T,F,F1,F2,SUM,S2,H,DY,E,S)
DO 52 I=1,M2
XI1(I)=F(I)
 52 CONTINUE
SW1=SUM
*-------------------------------------------------------------------------
DO 53 I=1,NIP1
Y(I)=XX2(I)
 53 CONTINUE
CALL SPLN(NIP1,M2,0,YY,Y,T,F,F1,F2,SUM,S2,H,DY,E,S)
DO 54 I=1,M2
XI2(I)=F(I)
```

```
 54 CONTINUE
SW2=SUM
*-----------------------------------------------------------------------
DO 55 I=1,M2
T(I)=YJ(I)
 55 CONTINUE
*
DO 56 I=1,NIP1
Y(I)=XX1(I)
 56 CONTINUE
CALL SPLN(NIP1,M2,0,YY,Y,T,F,F1,F2,SUM,S2,H,DY,E,S)
*
DO 521 I=1,M2
*
XJ1(I)=F(I)
 521 CONTINUE
SW1=SUM
*-----------------------------------------------------------------------
DO 57 I=1,NIP1
*
Y(I)=XX2(I)
 57 CONTINUE
*
CALL SPLN(NIP1,M2,0,YY,Y,T,F,F1,F2,SUM,S2,H,DY,E,S)
*
DO 58 I=1,M2
*
XJ2(I)=F(I)
 58 CONTINUE
SW2=SUM
*-----------------------------------------------------------------------
DO 60 I=1,M2
*
XLCOTR(I)=XI1(I)
*
XLSTP(I)=XJ1(I)
*
CCOTR(I)=XI2(I)-XI1(I)
*
CSTRIP(I)=XJ2(I)-XJ1(I)
 60 CONTINUE
*
DO 411 I=1,M2M1
*
DXDYL=(XJ1(I+1)-XJ1(I))/(YJ(I+1)-YJ(I))
ALPHAS(I)=DATAN(DXDYL)
*
 411 CONTINUE
RETURN
END
*************************************************************************
SUBROUTINE SPLN(N,M,KN,X,Y,T,F,F1,F2,SUM,S2,H,DY,E,S)
IMPLICIT REAL*8(A-H,O-Z)
DIMENSION X(N),Y(N),S2(N),H(N),DY(N),E(N),S(N),
*
     #            T(M),F(M),F1(M),F2(M)
*
N1=N-1
N2=N-2
DO 10 I=1,N1
H(I)=X(I+1)-X(I)
 10 DY(I)=(Y(I+1)-Y(I))/H(I)
S2(1)=0.
S2(N)=0.
```

```
      DO 20 I=2,N1
       20 S2(I)=6.0*(DY(I)-DY(I-1))
      Z=0.5/(H(1)+H(2))
      S(1)=-H(2)*Z
      E(1)=S2(2)*Z
      DO 30 I=2,N2
      Z=1.0/(2.0*(H(I)+H(I+1))+H(I)*S(I-1))
            S(I)=-H(I+1)*Z
       30 E(I)=(S2(I+1)-H(I)*E(I-1))*Z
      S2(N1)=E(N2)
      DO 40 I1=2,N2
      I=N2+2-I1
       40 S2(I)=S(I-1)*S2(I+1)+E(I-1)
      DO 50 I=1,N1
       50 S(I)=(S2(I+1)-S2(I))/H(I)
      I=2
      K=1
      DO 60 J=1,M
       55 IF (T(J).LE.X(I)) GOTO 58
      K=I
      I=I+1
      GOTO 55
       58 H1=T(J)-X(K)
            H2=T(J)-X(I)
      H3=H1*H2
      H4=S2(K)+H1*S(K)
      Z=(S2(I)+S2(K)+H4)/6.0
      F(J)=Y(K)+H1*DY(K)+H3*Z
      IF (KN.EQ.1.OR.KN.EQ.3) GOTO 60
      F1(J)=DY(K)+Z*(H1+H2)+H3*S(K)/6.0
      F2(J)=H4
       60 CONTINUE
      IF(KN.EQ.1.OR.KN.EQ.2) GOTO 80
            SUM=0.0
      DO 70 I=1,N1
       70 SUM=SUM+0.5*(H(I)*(Y(I)+Y(I+1)))
     #      -H(I)**3*(S2(I)+S2(I+1))/24.0
     *
       80 RETURN
            END

     ***********************************************************************
      FUNCTION DPHI(Z,X2X1,X1XI,X2XI,Y2Y1,Y2YI,Y1YI,OMOV,PI,
     #           T1E,T2,T3E,PW2,W2,W3,G1,G2,T11,T12,T31,
     #           T32,ATOX,DPHI1,DPHI2)
      IMPLICIT REAL*8(A-H,O-Z)
      EXTERNAL T1E,T2,T3E,PW2,G1,G2,W2,W3,T11,T12,
     #           T31,T32,DPHI2,DPHI1
      COMPLEX*8 T1E,T2,T3E,PW2,G1,G2,W2,W3,T11,T12,
     #           T31,T32,DPHI,DPHI2
      IF(OMOV.LE.1.0E-3)THEN
      DPHI=DPHI1(Z,X2X1,X2XI,X1XI,Y2Y1,Y2YI,Y1YI,PI)
      ELSE
      DPHI=DPHI1(Z,X2X1,X2XI,X1XI,Y2Y1,Y2YI,Y1YI,PI)
     #        +DPHI2(Z,X2X1,X1XI,X2XI,Y2Y1,Y2YI,Y1YI,OMOV,PI,
     #           T1E,T2,T3E,PW2,W2,W3,G1,G2,T11,T12,T31,T32,ATOX)
      END IF
      RETURN
```

```
END
***=================================================================
FUNCTION DPHI2(Z,X2X1,X1XI,X2XI,Y2Y1,Y2YI,Y1YI,OMOV,PI,
     #          T1E,T2,T3E,PW2,W2,W3,G1,G2,T11,T12,T31,T32,ATOX)
IMPLICIT REAL*8(A-H,O-Z)
COMPLEX*8 T1E,T2,T3E,PW2,G1,G2,W2,W3,T11,T12,T31,T32,DPHI2,
     #          P00,P05,P10,G100,G105,G110,G200,G205,G210,
     # AP,BP,CP,AG1,BG1,CG1,AG2,BG2,CG2
EXTERNAL T1E,T2,T3E,PW2,G1,G2,W2,W3,T11,T12,T31,T32
XY=X2X1/Y2Y1
X000=-X1XI
X005=-X1XI-X2X1/2.0
X010=-X1XI-X2X1
YETA00=-Y1YI
YETA05=-Y1YI-Y2Y1/2.0
IF(DABS(YETA05).LE.1.0E-08)THEN
YETA05=1.0E-08
ELSE
YETA05=YETA05
END IF
YETA10=-Y1YI-Y2Y1
R100=DABS(YETA00)
R105=DABS(YETA05)
R110=DABS(YETA10)
U100=-X000/R100
U105=-X005/R105
U110=-X010/R110
P00=PW2(R100,U100,OMOV,YETA00,XY,T1E,T3E)
G100=G1(R100,U100,OMOV,YETA00,XY,T3E,X000)
G200=G2(R100,U100,OMOV,YETA00,XY,T2)
P05=PW2(R105,U105,OMOV,YETA05,XY,T1E,T3E)
G105=G1(R105,U105,OMOV,YETA05,XY,T3E,X005)
G205=G2(R105,U105,OMOV,YETA05,XY,T2)
P10=PW2(R110,U110,OMOV,YETA10,XY,T1E,T3E)
G110=G1(R110,U110,OMOV,YETA10,XY,T3E,X010)
G210=G2(R110,U110,OMOV,YETA10,XY,T2)
*
AP=2.0*(P10-2.0*P05+P00)
BP=4.0*P05-P10-3.0*P00
CP=P00
AG1=2.0*(G110-2.0*G105+G100)
BG1=4.0*G105-G110-3.0*G100
CG1=G100
AG2=2.0*(G210-2.0*G205+G200)
BG2=4.0*G205-G210-3.0*G200
CG2=G200
IF(DABS(Z).LE.1.0E-10)THEN
DPHI2=-(0.0,1.0)*OMOV*(-(Y2Y1+Y1YI)*
     #         T12(X2XI,Y2YI,OMOV,T1E)/((Y2Y1+Y1YI)**2.0)
     #         +Y1YI*T11(X1XI,Y1YI,OMOV,T1E)/(Y1YI*Y1YI)
     #        +W2(Z,Y2Y1,Y2YI,Y1YI,AP,BP,CP))
        ELSE
DPHI2=-(0.0,1.0)*OMOV*(-(Y2Y1+Y1YI)*
     #         T12(X2XI,Y2YI,OMOV,T1E)/((Y2Y1+Y1YI)**2.0+Z*Z)
     #         +Y1YI*T11(X1XI,Y1YI,OMOV,T1E)/(Y1YI*Y1YI+Z*Z)
     #         +DATAN((Y2Y1+Y1YI)/Z)*Z*T32(X2XI,Y2YI,OMOV,T3E)
     #         -DATAN(Y1YI/Z)*Z*T31(X1XI,Y1YI,OMOV,T3E)
```

```
     #       +W2(Z,Y2Y1,Y2YI,Y1YI,AP,BP,CP)
     #       +W3(Z,Y2Y1,Y1YI,Y2YI,AG1,BG1,CG1,AG2,BG2,CG2,ATOX))
END IF
RETURN
END
*****************************************************************
FUNCTION W2(Z,Y2Y1,Y2YI,Y1YI,AP,BP,CP)
IMPLICIT REAL*8(A-H,O-Z)
COMPLEX*8 W2,AP,BP,CP
IF(Z.LE.1.0E-10)THEN
W2=AP*(0.5-Y1YI/Y2Y1)+BP+(AP*Y1YI*Y1YI/(Y2Y1*Y2Y1)
     #      -BP*Y1YI/Y2Y1+CP)*0.5*
     #      DLOG((Y2YI*Y2YI)/(Y1YI*Y1YI))
ELSE
W2=AP*(0.5-Y1YI/Y2Y1)+BP+(AP*Y1YI*Y1YI/(Y2Y1*Y2Y1)
     #      -BP*Y1YI/Y2Y1+CP-AP*Z*Z/(Y2Y1*Y2Y1))*0.5*
     #      DLOG((Z*Z+Y2YI*Y2YI)/(Z*Z+Y1YI*Y1YI))
     #      -Z*(BP/Y2Y1-2.0*AP*Y1YI/(Y2Y1*Y2Y1))*
     #     (DATAN(Y2YI/Z)-DATAN(Y1YI/Z))
END IF
RETURN
END
*****************************************************************
FUNCTION W3(Z,Y2Y1,Y1YI.Y2YI,AG1,BG1,CG1,AG2,BG2,CG2,ATOX)
IMPLICIT REAL*8(A-H,O-Z)
COMPLEX*8 W3,AG1,BG1,CG1,AG2,BG2,CG2
EXTERNAL ATOX
IF(Z.LE.1.0E-10)THEN
W3=0.0
ELSE
Z2=Z*Z
Z3=Z2*Z
Y2Y12=Y2Y1*Y2Y1
Y1YI2=Y1YI*Y1YI
Y1YI3=Y1YI2*Y1YI
B1=Y1YI/Z
B2=(Y2YI)/Z
YY=Y2YI
YY2=YY*YY
YY3=YY2*YY
AB1=DATAN(B1)
AB2=DATAN(B2)
RLOG=DLOG((Z2+YY2)/(Z2+Y1YI2))
W3=(AG1*Z/(6.0*Y2Y12))*(-2.0*YY3*AB2+2.0*Y1YI3*AB1
     #                  +Z*(Y2Y12+2.0*Y2Y1*Y1YI)-Z3*RLOG)
     #      +(Z/2.0)*(BG1/Y2Y1-2.0*AG1*Y1YI/Y2Y12)
     #           *(-YY2*AB2+Y1YI2*AB1+Z*Y2Y1-Z2*(AB2-AB1))
     #      +Z*(AG1*Y1YI2/Y2Y12+CG1-BG1*Y1YI/Y2Y1)
     #           *(-YY*AB2+Y1YI*AB1+(Z/2.0)*RLOG)
     #      +(AG2*Z/(2.0*Y2Y12))*(-YY2*AB2+Y1YI2*AB1+Z*Y2Y1
     #                                    -Z2*(AB2-AB1))
     #      +Z*(BG2/Y2Y1-2.0*AG2*Y1YI/Y2Y12)
     #           *(-YY*AB2+Y1YI*AB1+(Z/2.0)*RLOG)
     #      +Z*(AG2*Y1YI2/Y2Y12+CG2-BG2*Y1YI/Y2Y1)
     #           *(ATOX(B1)-ATOX(B2))
END IF
RETURN
END
*****************************************************************
```

```
      FUNCTION T11(X1XI,Y1YI,OMOV,T1E)
      IMPLICIT REAL*8(A-H,O-Z)
      COMPLEX*8 T11,T1E
      EXTERNAL T1E
      XO1=-X1XI
      R11=DABS(Y1YI)
      U11=-XO1/R11
      T11=T1E(R11,U11,OMOV)
      RETURN
      END
***********************************************************************
      FUNCTION T12(X2XI,Y2YI,OMOV,T1E)
      IMPLICIT REAL*8(A-H,O-Z)
      COMPLEX*8 T12,T1E
      EXTERNAL T1E
      XO2=-X2XI
      R12=DABS(Y2YI)
      U12=-XO2/R12
      T12=T1E(R12,U12,OMOV)
      RETURN
      END
***********************************************************************
      FUNCTION T31(X1XI,Y1YI,OMOV,T3E)
      IMPLICIT REAL*8(A-H,O-Z)
      COMPLEX*8 T31,T3E
      EXTERNAL T3E
      XO1=-X1XI
      R11=DABS(Y1YI)
      U11=-XO1/R11
      T31=T3E(R11,U11,OMOV)
      RETURN
      END
***********************************************************************
      FUNCTION T32(X2XI,Y2YI,OMOV,T3E)
      IMPLICIT REAL*8(A-H,O-Z)
      COMPLEX*8 T32,T3E
      EXTERNAL T3E
      XO2=-X2XI
      R12=DABS(Y2YI)
      U12=-XO2/R12
      T32=T3E(R12,U12,OMOV)
      RETURN
      END
***********************************************************************
      FUNCTION PW2(R1,U1,OMOV,YETA,XY,T1E,T3E)
      IMPLICIT REAL*8(A-H,O-Z)
      COMPLEX*8 T1E,T3E,PW2
      EXTERNAL T1E,T3E
      PW2=-YETA*T3E(R1,U1,OMOV)+(0.0,1.0)*OMOV*XY*T1E(R1,U1,OMOV)
     #          -(1.0-U1/(1.0+U1*U1)**0.5)*XY
      RETURN
      END
***********************************************************************
      FUNCTION G1(R1,U1,OMOV,YETA,XY,T3E,XO)
      IMPLICIT REAL*8(A-H,O-Z)
      COMPLEX*8 T3E,G1
      EXTERNAL T3E
      A=XO*XY/(R1*R1*R1*(1.0+U1*U1)**1.5)
      G1=A+(0.0,1.0)*OMOV*XY*T3E(R1,U1,OMOV)
```

```
RETURN
END
*****************************************************************
FUNCTION G2(R1,U1,OMOV,YETA,XY,T2)
IMPLICIT REAL*8(A-H,O-Z)
COMPLEX*8 T2,G2
EXTERNAL T2
G2=3.0*T2(R1,U1,OMOV)
RETURN
END
*****************************************************************
FUNCTION T1E(R1,U1,OMOV)
IMPLICIT REAL*8(A-H,O-Z)
DIMENSION A(10),C(10),C2(10)
COMPLEX*8 T1E,CPC
DATA A/0.002907843,0.002591528,0.02667074,
     #                        0.070971,0.347837,0.5556069,0.7048426,
     #                        -0.7769790,0.07004561,-0.004557519/
DATA C/0.0625,0.125,0.25,0.5,
     #                        1.0,2.0,3.0,4.0,8.0,16.0/
DATA C2/0.00390625,0.015625,0.0625,0.25,1.0,4.0,
     #     9.0,16.0,64.0,256.0/
CPC=(0.0,1.0)
OVR=OMOV*R1
OVR2=OVR*OVR
OVR3=OVR2*OVR
OMOV2=OMOV*OMOV
OMOV3=OMOV2*OMOV
IF(U1.LT.0.0) GO TO 555
ACE=0.0
AE=0.0
DO 10 I=1,10
CU1=C(I)*U1
IF(CU1.GE.40.0)THEN
ECU1=0.0
ELSE IF(CU1.GE.0.0.AND.CU1.LT.1.0E-20)THEN
ECU1=1.0
ELSE
ECU1=DEXP(-CU1)
END IF
CWR=C2(I)+OVR2
ACE=ACE+A(I)*C(I)*ECU1/CWR
AE=AE+A(I)*ECU1/CWR
 10 CONTINUE
T1R=R1*ACE
T1I=-OVR*R1*AE
GO TO 1000
 555 CONTINUE
AU1=DABS(U1)
OVRU=OVR*AU1
COU=DCOS(OVRU)
SOU=DSIN(OVRU)
ACE=0.0
AE=0.0
AS=0.0
DO 20 I=1,10
CU1=C(I)*AU1
IF(CU1.GE.40.0)THEN
ECU1=0.0
ELSE IF(CU1.GE.0.0.AND.CU1.LT.1.0E-20)THEN
```

```
ECU1=1.0
ELSE
ECU1=DEXP(-CU1)
END IF
CWR=C2(I)+OVR2
ACE=ACE+A(I)*C(I)*ECU1/CWR
AE=AE+A(I)*ECU1/CWR
AS=AS+A(I)/CWR
 20 CONTINUE
T1RI=COU*ACE-OVR*SOU*AE+2.0*SOU/OVR
T1II=-2.0*OVR*AS+2.0*(1.0-COU)/OVR+OVR*COU*AE+SOU*ACE
OVRU1=OVR*U1
COU1=DCOS(OVRU1)
SOU1=DSIN(OVRU1)
T1R=R1*(COU1*T1RI-SOU1*T1II)
T1I=R1*(SOU1*T1RI+COU1*T1II)
 1000 CONTINUE
T1E=T1R+CPC*T1I
RETURN
END
***=================================================================
FUNCTION T2(R1,U1,OMOV)
IMPLICIT REAL*8(A-H,O-Z)
DIMENSION A(10),C(10),C2(10)
COMPLEX*8 T2,CPC
DATA A/0.002907843,0.002591528,0.02667074,
     #                      0.070971,0.347837,0.5556069,0.7048426,
     #                      -0.7769790,0.07004561,-0.004557519/
DATA C/0.0625,0.125,0.25,0.5,
     #                      1.0,2.0,3.0,4.0,8.0,16.0/
DATA C2/0.00390625,0.015625,0.0625,0.25,1.0,4.0,
     #     9.0,16.0,64.0,256.0/
CPC=(0.0,1.0)
OVR=OMOV*R1
OVR2=OVR*OVR
OVR3=OVR2*OVR
OMOV2=OMOV*OMOV
OMOV3=OMOV2*OMOV
IF(U1.LT.0.0) GO TO 555
ACE=0.0
AE=0.0
DO 10 I=1,10
CU1=C(I)*U1
IF(CU1.GE.40.0)THEN
ECU1=0.0
ELSE IF(CU1.GE.0.0.AND.CU1.LT.1.0E-20)THEN
ECU1=1.0
ELSE
ECU1=DEXP(-CU1)
END IF
CWR=C2(I)+OVR2
ACE=ACE+A(I)*C(I)*ECU1/CWR
AE=AE+A(I)*ECU1/CWR
 10 CONTINUE
T2R=1.0/(3.0*R1*(1.0+U1*U1)**1.5)-OVR2*ACE/(3.0*R1)
T2I=(U1/(1.0+U1*U1)**0.5-1.0)*OMOV/3.0+OVR3*AE/(3.0*R1)
GO TO 1000
 555 CONTINUE
AU1=DABS(U1)
```

```
IF(CU1.GE.40.0)THEN
ECU1=0.0
ELSE IF(CU1.GE.0.0.AND.CU1.LT.1.0E-20)THEN
ECU1=1.0
ELSE
ECU1=DEXP(-CU1)
END IF
CWR=C2(I)+OVR2
CWR2=CWR*CWR
ACE=ACE+A(I)*C(I)*ECU1/(CWR*R1)
AE=AE+A(I)*ECU1/CWR
AE1=AE1+(OMOV2*R1*U1*(C2(I)-OVR2)-2.0*C(I)
     #    *OMOV2*R1*(C(I)*U1+1.0))*A(I)*ECU1/CWR2
AE2=AE2+(2.0*C(I)*OVR2*U1+(C(I)*U1+1.0)*(C2(I)-OVR2))
     #  *A(I)*ECU1/CWR2
 10 CONTINUE
IF(U1.GE.1.0E08)THEN
U1H=0.5/U1
ELSE
U1H=U1*(1.0-U1/(1.0+U1*U1)**0.5)
END IF
T3R=U1H/R1+ACE+AE1
T3I=-OMOV*(AE+AE2)
GO TO 1000
 555 CONTINUE
* USING BESSEL FUNCTION
AU1=DABS(U1)
OVRU=OVR*AU1
COU=DCOS(OVRU)
SOU=DSIN(OVRU)
ACE=0.0
ACE2=0.0
AE=0.0
ACWE=0.0
DO 20 I=1,10
CU1=C(I)*AU1
IF(CU1.GE.40.0)THEN
ECU1=0.0
ELSE IF(CU1.GE.0.0.AND.CU1.LT.1.0E-20)THEN
ECU1=1.0
ELSE
ECU1=DEXP(-CU1)
END IF
CWR=C2(I)+OVR2
CWR2=CWR*CWR
ACE=ACE+A(I)*C(I)*ECU1/(CWR*R1)
ACE2=ACE2+A(I)*C(I)*ECU1/CWR2
AE=AE+A(I)*ECU1/CWR
ACWE=ACWE+A(I)*(C2(I)-OVR2)*ECU1/(CWR2)
 20 CONTINUE
IF(AU1.GE.1.0E08)THEN
U1H=0.5/AU1
ELSE
U1H=AU1*(1.0-AU1/(1.0+AU1*AU1)**0.5)
END IF
OVRU1=OVR*U1
COU1=DCOS(OVRU1)
SOU1=DSIN(OVRU1)
IF(OVR.LE.3.75) THEN
TT=OVR/3.75
```

```
OVRU=OVR*AU1
COU=DCOS(OVRU)
SOU=DSIN(OVRU)
ACE=0.0
AE=0.0
AS=0.0
DO 20 I=1,10
CU1=C(I)*AU1
IF(CU1.GE.40.0)THEN
ECU1=0.0
ELSE IF(CU1.GE.0.0.AND.CU1.LT.1.0E-20)THEN
ECU1=1.0
ELSE
ECU1=DEXP(-CU1)
END IF
CWR=C2(I)+OVR2
ACE=ACE+A(I)*C(I)*ECU1/CWR
AE=AE+A(I)*ECU1/CWR
AS=AS+A(I)/CWR
 20 CONTINUE
U23=1.0/(1.0+AU1*AU1)**1.5
U1H=1.0-AU1/(1.0+AU1*AU1)**0.5
T2A=COU*(U23-OVR2*ACE)+SOU*(OVR3*AE-OVR*U1H)
T2B=2.0*OVR*(OVR2*AS-1.0)-COU*(OVR3*AE-OVR*U1H)
     #       +SOU*(U23-OVR2*ACE)
OVRU1=OVR*U1
COU1=DCOS(OVRU1)
SOU1=DSIN(OVRU1)
T2R=(COU1*T2A-SOU1*T2B)/(3.0*R1)
T2I=(COU1*T2B-SOU1*T2A)/(3.0*R1)
 1000 CONTINUE
T2=T2R+CPC*T2I
RETURN
END
*=====================================================================
FUNCTION T3E(R1,U1,OMOV)
IMPLICIT REAL*8(A-H,O-Z)
DIMENSION A(10),C(10),C2(10)
COMPLEX*8 T3E,CPC
DATA A/0.002907843,0.002591528,0.02667074,
     #                         0.070971,0.347837,0.5556069,0.7048426,
     #                         -0.7769790,0.07004561,-0.004557519/
DATA C/0.0625,0.125,0.25,0.5,
     #                         1.0,2.0,3.0,4.0,8.0,16.0/
DATA C2/0.00390625,0.015625,0.0625,0.25,1.0,4.0,
     #     9.0,16.0,64.0,256.0/
CPC=(0.0,1.0)
OVR=OMOV*R1
OVR2=OVR*OVR
OVR3=OVR2*OVR
OMOV2=OMOV*OMOV
OMOV3=OMOV2*OMOV
IF(U1.LT.0.0) GO TO 555
ACE=0.0
AE=0.0
AE2=0.0
AE1=0.0
DO 10 I=1,10
CU1=C(I)*U1
```

```
BIX=1.0+3.5156229*TT**2.0+3.0899424*TT**4.0
     #      +1.2067492*TT**6.0+0.2659732*TT**8.0
     #            +0.03060768*TT**10.0+0.0045813*TT**12.0
ELSE
TT=OVR/3.75
BIX=(0.39894228+0.01328592*TT**(-1.0)+0.00225319*TT**(-2.0)
     #       -0.00157565*TT**(-3.0)+0.00916281*TT**(-4.0)
     #       -0.02057706*TT**(-5.0)+0.02635537*TT**(-6.0)
     #       -0.01647633*TT**(-7.0)+0.00392377*TT**(-8.0))
     #       /(OVR**0.5*DEXP(-OVR))
END IF
IF(OVR.LE.2.0) THEN
BK=-DLOG(OVR/2.0)*BIX-0.57721566+0.42278420*(OVR/2.0)**2.0
     #      +0.23069756*(OVR/2.0)**4.0+0.03488590*(OVR/2.0)**6.0
     #      +0.00262698*(OVR/2.0)**8.0+0.00010750*(OVR/2.0)**10.0
     #      +0.00000740*(OVR/2.0)**12
ELSE
BK=(1.25311414-0.07832358*(2.0/OVR)
     #      +0.02189568*(2.0/OVR)**2.0-0.01062446*(2.0/OVR)**3.0
     #      +0.00587872*(2.0/OVR)**4.0-0.00251540*(2.0/OVR)**5.0
     #      +0.00053208*(2.0/OVR)**6.0)
     #      /(OVR**0.5*DEXP(OVR))
END IF
T3B=COU*(U1H/R1+ACE-AU1*OMOV2*R1*AE-2.0*OMOV2*R1*ACE2)-OMOV
     #       *SOU*(AE+AU1*ACE*R1+ACWE)
T3C=SOU*(U1H/R1+ACE-AU1*OMOV2*R1*AE-2.0*OMOV2*R1*ACE2)+OMOV
     #       *COU*(AE+AU1*ACE*R1+ACWE)
T3R=(COU1*T3B-SOU1*(T3C-2.0*OMOV*BK))
T3I=(SOU1*T3B+COU1*(T3C-2.0*OMOV*BK))
 1000 CONTINUE
T3E=T3R+CPC*T3I
RETURN
END

*********************************************************************
FUNCTION DPHI1(Z,X2X1,X2XI,X1XI,Y2Y1,Y2YI,Y1YI,PI)
IMPLICIT REAL*8(A-H,O-Z)
Q=-X2X1*Y1YI+X1XI*Y2Y1
Q2=Q*Q
Y2YI2=Y2YI*Y2YI
Y1YI2=Y1YI*Y1YI
Y2Y12=Y2Y1*Y2Y1
X2XI2=X2XI*X2XI
O2O+2=O2O+*O2O+
X1XI2=X1XI*X1XI
Z2=Z*Z
W12=-Y2YI/(Y2YI2+Z2)+(1.0/DSQRT(X2XI2+Y2YI2+Z2))
     #       *(Y2YI*X2XI/(Y2YI2+Z2)+Q*(X2XI*X2X1+Y2Y1*Y2YI)/
     #        (Q2+Z2*(X2X12+Y2Y12)))
W11=-Y1YI/(Y1YI2+Z2)+(1.0/DSQRT(X1XI2+Y1YI2+Z2))
     #       *(Y1YI*X1XI/(Y1YI2+Z2)+Q*(X1XI*X2X1+Y2Y1*Y1YI)/
     #        (Q2+Z2*(X2X12+Y2Y12)))
DPHI1=(W12-W11)
RETURN
END
*********************************************************************
FUNCTION ATOX(X)
IMPLICIT REAL*4(A-H,O-Z)
A=78157368240./36108704126880.
```

```
  B=859731050640./36108704126880.
C=4298655253200./36108704126880.
D=12895965759600./36108704126880.
E=25791931519200./36108704126880.
F=36108704126880./36108704126880.
G=104704455135./36108704126880.
H=866818214990./36108704126880.
O=3400985546707./36108704126880.
P=8133919447592./36108704126880.
Q=12998047815470./36108704126880.
R=14422975535380./36108704126880.
S=11217953946350./36108704126880.
T=6026219223592./36108704126880.
U=2136707615987./36108704126880.
V=451074322510./36108704126880.
W=43020241215./36108704126880.
A1=35137127025./36108704126880.
B1=386508397275./36108704126880.
C1=1932541986375./36108704126880.
D1=5797625959125./36108704126880.
E1=11595251918250./36108704126880.
F1=16233352685550./36108704126880.
XABS=ABS(X)
IF(XABS.LT.2.0)THEN
X2=X*X
X3=X2*X
X4=X3*X
X5=X4*X
X6=X5*X
X7=X6*X
X8=X7*X
X9=X8*X
X10=X9*X
X11=X10*X
X12=X11*X
X13=X12*X
X14=X13*X
X15=X14*X
X16=X15*X
X17=X16*X
X18=X17*X
X19=X18*X
X20=X19*X
X21=X20*X
X22=X21*X
ATOX=((A*X22+B*X20+C*X18+D*X16+E*X14+F*X12+F*X10+E*X8+D*X6
     #          +C*X4+B*X2+A)*ATAN(X)-G*X21-H*X19-O*X17-P*X15-Q*X13
     #          -R*X11-S*X9-T*X7-U*X5-V*X3-W*X)/
     #        (A1*X22+B1*X20+C1*X18+D1*X16+E1*X14+F1*X12+F1*X10+E1*X8
     #        +D1*X6+C1*X4+B1*X2+A1)
ELSE IF(XABS.GE.30000.AND.X.LT.0.0)THEN
ATOX=-3.4938319221
ELSE IF(XABS.GE.30000.AND.X.GT.0.0)THEN
ATOX=3.4938319221
ELSE
X=1.0/X
X2=X*X
X3=X2*X
X4=X3*X
X5=X4*X
X6=X5*X
```

```
X7=X6*X
X8=X7*X
X9=X8*X
X10=X9*X
X11=X10*X
X12=X11*X
X13=X12*X
X14=X13*X
X15=X14*X
X16=X15*X
X17=X16*X
X18=X17*X
X19=X18*X
X20=X19*X
X21=X20*X
X22=X21*X
ATOX=((A+B*X2+C*X4+D*X6+E*X8+F*X10+F*X12+E*X14+D*X16
     #       +C*X18+B*X20+A*X22)*ATAN(1.0/X)-G*X-H*X3-O*X5-P*X7-Q*X9
     #         -R*X11-S*X13-T*X15-U*X17-V*X19-W*X21)/
     #       (A1*X22+B1*X20+C1*X18+D1*X16+E1*X14+F1*X12+F1*X10+E1*X8
     #       +D1*X6+C1*X4+B1*X2+A1)
END IF
RETURN
END
```

An output called "*UNQV.OUT*" is listed below. Several input data were given in the output: the number of chordwise control points N_c, the number of spanwise control points N_s (i.e. $MI + MII - 1$), The root chord length C_r, the pitching axis position B_0, phase angle $\Phi = 90^0$, the amplitude of heave h. The output data listed in columns are: the reduced frequency k, the propulsive efficiency η, the mean total thrust coefficient C_t, the leading-edge suction coefficient C_{tl}, The modulus of the lift coefficient $|C_l|$, and the feathering parameter θ. The range of the calculation was $k = 0.2 \sim 2.0$, in a steps of 0.2, $\theta = 0.0$ and $\theta = 0.4$.

```
NUMBER OF CHORDWISE CONTROL POINT NC=   3
NUMBER OF SPANWISE CONTROL POINT NS=   9
THE LENGTH OF THE SPAN B=  6.000000
ASPECT RATIO ASR=  8.000000
WING AREA SW=  4.500000
AVERAGE CHORD LENGTH CA=  0.750000
REFERENCE LENGTH BR=  0.750000
PITCHING AXIS POSITION B0=  0.562500
ROOT CHORD LENGTH CR=  0.750000
AMPLITUDE OF WING HEAV=  0.750000
PHASE ANGLE (PITCH LEADS HEAVE) PHIPH=  1.570796

 RED-FRE k PR-EF eta PR-THR Ct LE-TH Ctl ABC-CL|Cl| FEAT-P theta
  0.200000  0.777841  0.066911  0.066911  0.860589  0.000000
  0.400000  0.735500  0.237654  0.237654  1.615632  0.000000
  0.600000  0.701386  0.486212  0.486212  2.317461  0.000000
  0.800000  0.675943  0.806357  0.806357  3.021170  0.000000
  1.000000  0.657335  1.200018  1.200018  3.767226  0.000000
```

1.200000	0.643844	1.672538	1.672538	4.585066	0.000000
1.400000	0.634212	2.231355	2.231355	5.496721	0.000000
1.600000	0.627568	2.885987	2.885987	6.519416	0.000000
1.800000	0.623321	3.648499	3.648499	7.667450	0.000000
2.000000	0.621071	4.534094	4.534094	8.953387	0.000000
0.200000	0.866122	0.044591	0.023974	0.515656	0.400000
0.400000	0.839261	0.161838	0.084756	0.963529	0.400000
0.600000	0.816877	0.338022	0.174058	1.370144	0.400000
0.800000	0.799520	0.571763	0.293174	1.764183	0.400000
1.000000	0.786220	0.867715	0.448600	2.167054	0.400000
1.200000	0.775991	1.233988	0.650270	2.595698	0.400000
1.400000	0.768076	1.681581	0.911199	3.064986	0.400000
1.600000	0.761933	2.224680	1.247730	3.589180	0.400000
1.800000	0.757180	2.881397	1.680094	4.182772	0.400000
2.000000	0.753549	3.674759	2.233184	4.860866	0.400000

References

- Albano, E. and Rodden, W.P. (1969). "A doublet-lattice method for calculating lift distribution on oscillating surfaces in subsonic flows," *AIAA Journal*, Vol. 7, No. 2, February, pp. 279 – 285.

- Albramowitz M. and Stegun, I.A. (1970). *Handbook of mathematical functions*, Dover publications, Inc., New York,1046 p.

- Amadi, A.R. and Widnall, S.E. (1986). "Energetics and optimum motion of oscillating lifting surfaces of finite span," *J. Fluid Mech.*, vol. 162, pp. 261 – 282.

- Ashley, H. (1968). "Subsonic oscillatory or steady airloads on wings with control surface and other discontinuities," *Dept. of Aeronautics and Astronautics*, Stanford University, *AFOSR* – 68 – 0419, 46 p.

- Bainbrige, R. (1958). "The speed of swimming of fish as related to size and to the frequency and amplitude of the tail beat," *J. Exp. Biol.*, Vol. 35, pp. 109 – 133.

- Brett, J.R. (1964). "The respiratory metabolism and swimming performance of yawing sockege salmon," *J. Fish. Res. Bd. Canada*, Vol. 21, pp. 1183 – 1226.

- Bisplinchoff, R.L., Ashley, H. and Halfman, R.L. (1955). *Aeroelasticity*, Addison-Wesley publishing company, Inc., Reading, Massachusetts, 860 p.

- Bose, N. and Lien, J. (1989). "Propulsion of a fin whale (*Balaenoptera physalus*): why the fin whale is a fast swimmer," *Proc. R. Soc. Lond. B*237, pp. 175–120.

- Bose, N. and Lien, J. (1990). "Energy absorption from ocean waves: a free ride for cetaceans," *Proc. R. Soc. Lond. B*240, pp. 591 – 605.

- Bose, N., Lien, J. and Ahia, J. (1990). "Measurements of the bodies and flukes of several cetacean species: designs for fast and slow swimming," *Proc. R. Soc. Lond.. B*242, pp. 163 – 174.

- Burden, R. L. and Faires, D. J. (1989). *Numerical analysis*, The fourth edition. PWS-KENT publishing company, Boston, 729 p.

- Chopra, M.G. (1974). "Hydromechanics of lunate-tail swimming propulsion. part 1," *J. Fluid Mech.*, Vol. 64, Part 2, pp. 375 – 391.

- Chopra, M.G. (1976). "Large amplitude lunate-tail theory of fish locomotion," *J. Fluid Mech.*, Vol. 74, Part 1, pp. 161 – 182.

- Chopra, M.G. and Kambe, T.K. (1977). "Hydromechanics of lunate-tail swimming propulsion. part 2," *J. Fluid Mech.*, Vol. 79, Part 1, pp. 46 – 69.

- Cheng, H.K. and Murillo, L.E. (1984). "Lunate-tail swimming propulsion as a problem of curved lifting line in unsteady flow, Part 1, Asymptotic theory" *J. Fluid Mech.*, Vol. 143, pp. 327 – 350.

- Dengler, M.A. and Goland, M. (1952). "The subsonic calculation of circulatory spanwise loading for oscillating airfoils by lifting line theory," *J. Aeronautical Sciences*, pp. 751 – 759.

- DeYong, J. (1976). "Historical evolution of vortex-lattice method," *Vortex-lattice Utilization*, NACA *SP* – 405, *N*76 – 28163-*N*76 – 28168, Langley Research Center, Hampton, Vorginia, pp. 1 – 9.

- Davies, D.E. (1963). "Calculation of unsteady generalised airforces on a thin wing oscillating harmonically in subsonic flow," *Aeronautical Research Council*, R. & M., No. 3409, 52 p.

- Falkner, V.M. (1943). "The calculation of aerodynamic load on surface of any shape," *Aeronautical Research Council*, R. & M., No. 1910, 20 p.

- Fung, Y.C. (1969). *An introduction to the theory of aeroelasticity*, Dover publications, Inc., New York, 498 p.

- Garrick, I.E. (1936). "Propulsion of a flapping and oscillating foil," *NACA Report*, No. 576.

- Glauert, H. (1926). *The elements of aerofoil and airscrew theory*, Second edition, reissued in 1983, Cambridge University Press, London, 299*p*

- Guermond, J.L. (1988). "About collocation methods for marine propeller design," *The Society of Naval Architects and Marine Engineers*, Sept., 1988, pp. 8.1 – 8.9.

- Guermond, J.L. and Sellier, A. (1990). "A unified unsteady lifting-line theory," *C. R. Acad. Sci.*, Paris, t. 311, Série ii, pp. 21 – 26.

- Harvald, S.A. (1983). *Resistance and propulsion of ships*, John Wiley & Sons, Inc., New York, 353 p.

- Hertel, H. (1963). *Structure-form-movement*, Reinhold Publishing Co., New York, 251 p.

- Hoar, W.S., and Randall, D.J., (1978). "Fish physiology," Vol. VII, *Locomotion*, Academic Press.

- Houghton, E.L. and Brook, A.E. (1960). *Aerodynamics for engineering students*, Edward Arnold Ltd., London, 458 p.

- Hsu, P.T. (1957). "Calculation of pressure distribution for oscillating wings of arbitrary planform in subsonic flow by the kernel function method," MIT Aeroelastic and Structure Research Laboratory, Report No. 64-1.

- International Business Machines Corporation, (1986, 1987). *Language and library reference*, VS Fortran version 2, 595 p.
- International Business Machines Corporation, (1986, 1987). *Program guide*, VS Fortran version 2, 606 p.
- Jones, R.J. (1940). "The unsteady lift of a wing of finite aspect ratio," *National Advisory Committee for Aeronautics*, Report No. 681, 9 p.
- Jordan, P.F. (1976). "Numerical evaluation of the three-dimensional harmonic kernel," *Z. Flugwiss*, Vol. 24, Heft 4., pp. 205 – 209
- Kálmán, T.P., Giesing, J.P. and Rodden, W.P. (1970). "Spanwise distribution of induced drag in subsonic flow by the vortex lattice method," *J. Aircraft*, Vol. 7, pp. 574 – 576.
- Karpouzian, G., Spedding, G. and Cheng, H.K. (1990). "Lunate-tail swimming propulsion. Part 2. Performance analysis," *J. Fluid Mech.*, vol. 210, pp. 329 – 351.
- Küessner, H.G. (1954). "A general method for solving problems of the unsteady lifting surface theory in the subsonic range," *J. of Aeronautical Science*, pp. 17 – 27.
- Lai, P.S.K., McGregor, R.C. and Bose, N. (1989). "On the flexible fin propeller," *4th International symp. on practical design of ships & mobile units*, Bulgarian Ship Hydrodynamic Center, PRADS, VARNA, 8 p.
- Lai, P.S.K., McGregor, R.C. and Bose, N. (1989). "Experimental investigation of oscillating foil propellers," *22th American towing tank conf.*, ATTC conf., St. John's. Newfoundland, Canada., 7 p.
- Lai, P.S.K. (1990). "Oscillating foil propulsion," *Phd. thesis*, University of Glasgow, 410 p.
- Lan, C.E. (1974). "A quasi-vortex-lattice method in thin wing theory," *J. Aircraft*, Vol. 11, No. 9, pp. 518 – 527.
- Lan, C.E. (1975). "The induce drag of oscillating airofoils in linear subsonic compressible flow," $KU - FRL - 400$, Kansas, 60 p.
- Lan, C.E. (1976). 'Some application of the quasi-vortex-lattice method in steady and unsteady aerodynamics," *Vortex-lattice Utilization*, Langley Research Center, Hampton, Virginia, pp. 385 – 406.
- Lan, C.E. and Lamar, J.E. (1977). "On the logarithmic-singularity correction in the kernel function method of subsonic lifting-surface theory," NASA, TN, $D - 8513, 53$ p.

- Lan, C.E. (1979). "The unsteady quasi-vortex-lattice method with applications to animal propulsion," *J. Fluid Mech.*, Vol. 93, Part 4, pp. 747 – 756.
- Lan, C.E. (1990). Private communications.
- Landhal, M.T. (1966). "Kernel function for nonplanar oscillating surface in a subsonic flow," *AIAA J.*, Vol. 5, No. 5, pp. 1045 – 1046.
- Lawrence, H.R. and Gerber, E.H. (1952). "The aerodynamic forces on low aspect ratio wings oscillating in an incompressible flow," *J. of Aeronautical Science.* pp. 699 – 781.
- Lighthill, M.J. (1969). "Hydrodynamics of aquatic animal propulsion," *Annual Rev. Fluid Mech.*, Vol. 1, pp. 413 – 446.
- Lighthill, M.J. (1970). "Aquatic animal propulsion of high hydromechanical efficiency," *J. Fluid Mech.* Vol. 44, pp. 256 – 301.
- Massachusetts Institute of Technology (1970). *VAX UNIX MACSYMA reference manual*, Version 11, Symbolics, Inc., Printed in the USA.
- Merbt, H. and Landahl, M. (1953). "Aerodynamic forces on oscillating law aspect ratio wing in compressible flow," *Technical Report, Roya Institute of Technology*, Division of Aeronautics, Stockholm 70, Sweden, 30 p.
- Multhopp, H. (1950). "Methods for calculating the lift distribution of wings (subsonic lifting-surface theory)," *Aeronautical Research Council*, R. & M., No. 2884, 96 p.
- Newman, J.N. and Wu, T.Y. (1974). "Hydromechanical aspect of fish swimming," *Swimming and Flying in Nature*, vol. II, ed. T.Y. Wu, J. Brokaw, and C. Brennen, Plenum Press, pp. 615 – 634
- Newman, J.N. (1977). *Marine hydrodynamics*, MIT Press, Cambridge, Mass. 402 p.
- Pistolesi, E. (1937). "Consideration on the mutual interference on airofoil system," *L.G.L. Rep.*, pp. 214 – 219.
- Richardson, J.R. (1955). "A method for calculating the lifting forces on wings (unsteady subsonic and supersonic lifting-surface theory)," *Aeronautical Research Council*, Technical Report, R.& M., No. 3157, London, 30 p.
- Ruyaan, H.L. and Woolston, D.S. (1957). "method for calculating the aerodynamic loading on an oscillating finite wing in subsonic and sonic flow," *National Advisory Committee for Aeronautics*, Report No. 1322, 30 p.
- Spence, D.A. (1958). "The lift on a thin aerofoil with a jet-augmented flap," *The Aeronautical Quarterly*, Vol. 9, pp. 287 – 299.

- Theodorsen, T. (1935). "General theory of aerodynamic instability and the mechanism of flutter," *NACA Report*, No. 496, Washington D.C., pp. 413 – 433.

- von Kármán, T. and Burgers, J.M. (1935). "General aerodynamic theory, perfect fluids," *Aerodynamic theory,* Vol. II, 1976 edition, editor-in-chief Durand, W.K., Peter Smith Publisher, Inc., Gloucester, Mass., 498 p.

- Ward, G.N. (1955). *Linearized theory of steady high-speed flow.* Cambridge University Press, 243 p.

- Watkins, C.E., Runyan, H.L. and Woolston, D.S. (1955). " On the kernel function of the integral equation relating the lift and downwash distributions of oscillating finite wings in subsonic flow," *National Advisory Committee for Aeronautics*, Report No. 1234, 16 p.

- Watkins, C.E., Woolston, D.S. and Cunningham, H.J. (1959). " A systemic kernel function procedure for determining aerodynamic forces on oscillating or steady finite wings at subsonic speed," *National Aeronautics and Space Administration*, Technical Report $R-48$, 21 p.

- Wilmott, P. (1988). "Unsteady lifting-line theory by the method of matched asymptotic expansions," *J. Fluid Mech.*, vol. 186, pp. 303 – 320.

- Woodward, F.A., Tinoco, E.N., and Larsen, J.W. (1967). "Analysis and design of supersonic wing-body combinations, including flow properties in the near field," Part I-theory and application, *NACA* $CR-73106$, pp. 219 – 221.

- Wang, L.X., Fang, Z.D., Zhang, M.Y., Lin, J.B., Gu, L.K., Zhong, T.D., Yong, X.A., Xia, D.P., Luo,Z.H., Xiao, B.Q., Zai, H. and Lin, D.X. (1977). *Handbook of mathematics,* Advanced Education Publishing Services, Beijing, China, 1398 p.

- Wu, T.Y. (1971). "Hydromechanics of swimming propulsion. Part 1. Swimming of a two-dimensional flexible plate at variable forward speeds in an inviscid fluid," *J. Fluid Mech.* Vol. 46, part 2, pp. 337 – 355.

- Wu, T.Y. (1971). "Hydromechanics of swimming propulsion. Part 2. Some optimum shape problems," *J. Fluid Mech.* Vol. 46, part 3, pp. 521 – 544.

- Yates, E.C. (1966). "A kernel function formulation for nonplanar lifting surfaces oscillating in subsonic flow," *AIAA J.*. Vol. 4, No. 8, pp. 1436 – 1488.

- Zartarian, G., Hsu, P.T and Voss, H.M. (1954). "Application of numerical integration techniques to the low-aspect-ratio flutter problem in subsonic and supersonic flows'" *Aeroelastic and Structures Laboratory,* MIT, technical report 52 – 3, for the Bureau of Aeronautics, Department of the Navy, Contact Noa(s) 53 – 564 – *c*, 195 p.

Bibliography

- Ahmad, A. and Windal, S.E. (1985). "Unsteady lifting-line theory as a singular-perturbation problem," *J. Fluid Mech.*, Vol. 153, *pp.*59 – 81.

- Ahmad, A. and Windal, S.E. (1986). "Energetics and optimum motion of oscillating lifting surfaces of finite span," *J. Fluid Mech.*, Vol. 162, *pp.*261–282.

- Atta, E.H., Kandil, O.A., Mook, D.T. and Nayfeh, A.H. (1976). "Unsteady flow past wings having sharp-edge separation," *Vortex-lattice Utilization*, Langley Research Center, Hampton, Virginia, *pp.*407 – 421.

- Beker, J. (1973). "Interfering lifting surfaces in unsteady subsonic flow-comparison between theory and experiment," *AGARD Report No. 614*, North Atlantic Treaty Organization, Advisory Group for Aerospace Research and Development, 37th AGADRD structures and materials panel meeting, The Hague, Netherlands, April 7-12, 1973, 15*P*.

- Destuynder, R. and Tijdeman, H. (1973). "An investigation of different techniques for unsteady pressure measurements in compressible flow and comparison with lifting surface theory," *AGARD Report No. 617*, North Atlantic Treaty Organization, Advisory Group for Aerospace Research and Development, 37th AGADRD structures and materials panel meeting, The Hague, Netherlands, April 7-12, 1973, 29*P*.

- Day, R.A. (1988). *How to write & publish a scientific paper*, second edition, ORYX Press, New York, 211*p*..

- Edwards, J.M. (1988). "Computational unsteady aerodynamics for lifting surfaces," *VKI Lecture Series: Computational Fluid Dynamics*, Vol. 2, von Kármán Institute for Fluid Dynamics, Rhode-Stgenese, Belgium, 119*p*..

- Garner, H.C., Hewitt, B.L. and Labrujere, F.E. (1969). "Comparison of three methods for the evaluation of subsonic lifting-surface theory," *Aeronautical Research Council Report and Memoranda*, No. 3597, Ministry of Technology, London, 41*p*.

- Hedman, S.G. (1965). "Vortex-lattice method for calculation of quasi-steady state loadings on thin elastic wigs in subsonic flow," *Flygtekniska Försöksanstalten*, Meddelande 105, Stockholm, 17*p*.

- Hoerner, Dr.-Ing. S. F. and Borst, H.V. (1985). *Fluid-dynamic lift*, second edition, published by Hoerner, L.A., Albuquerque, N.M. 488*p*.

- Johnston, G.W., Zingg, D.W. and Cameron, P.G. (1985). "An unsteady, nonlinear, finite amplitude analysis procedure for hydrodynamic sections," Defence Research Establishment Atlantic, Contract No. 6*AE*977077 – 4 – 3832, 79*p*.

- Lighthill, M.J. (1960). "Note on the swimming of slender fish," *J. Fluid Mech.*, Vol. 9, *pp.*305 – 317.

- Ohmi, K., Coutanceau, M., Loc, T. and Dulien, A. (1990). "Vortex formation around an oscillating and translating airfoil at large incidences," *J. Fluid Mech.*, Vol. 211, *pp.*37 – 60.

- Lomax, H., Heaslet, A., Fuller, F.B. and Sluder, L. (1952). "Two- and three-dimensional unsteady lift problems in high-speed flight," *National Advisory Committee for Aeronautic,* Report 1077, 55*p.*

- Scherer J.O. (1968). "Experimental and theoretical investigation of large amplitude oscillating foil propulsion systems," U.S. Army Engineering Research and Development Laboratories, $DA - 44 - 009 - amc - 1759(t)$, 56*p.*

- Shen, S.F. (1953). "Effect of strucural flexiblity on aircraft loading, part $X-$A new lefting-line theory for the unsteady lift of a swept or unswept wing in an incompressible fluid ," *U.S. Air Force Material Commend: Air Force Technical Rept.*, No. 6538, 41*p.*

- Wu, T.Y. (1972). "Extraction of flow energy by a wing oscillating in waves," *J. Ship Research,* March, 1972, *pp.*66 – 78